ACTIVE DISTURBANCE ESTIMATION AND COMPENSATION FOR IMPROVING DIESEL AFTERTREATMENT PERFORMANCE

ACTIVE DISTURBANCE ESTIMATION AND COMPENSATION

FOR IMPROVING DIESEL AFTERTREATMENT

PERFORMANCE

BY

JINBIAO NING, B.E., M.E.

A Thesis Submitted to the School of Graduate Studies in Partial Fulfilment of the

Requirements for the Degree of Doctor of Philosophy

Doctor of Philosophy (2017)   McMaster University

(Mechanical Engineering)   Hamilton, Ontario, Canada

TITLE: Active Disturbance Estimation and Compensation for

                     Improving Diesel Aftertreatment Performance

AUTHOR: Jinbiao Ning

                     B.E., M.E., (Tianjin University)

SUPERVISOR: Dr. Fengjun Yan

NUMBER OF PAGES: xxi, 206

Abstract

Diesel engines are widely used in automotive sector due to their high fuel efficiency, distinguished durability and great reliability. However, NO_x and particulate matters (PM) are main concerns of the Diesel engines due to their lean burn conditions. To reduce these emissions, Diesel engines are usually coupled with state-of-the-art Diesel aftertreatment systems including a Diesel Oxidation Catalyst (DOC), a Diesel Particulate Filter (DPF), and a Selective Catalytic Reduction system (SCR). With increasingly stringent regulations, the estimation and control strategies of Diesel after-treatment systems for NO_x and PM reduction are becoming more and more critical and challenging, especially under transient conditions with unknown system dynamics including disturbances and model uncertainties. To address these problems, this thesis focuses on advanced strategies based on disturbance estimation and compensation for improving the performance of Diesel after-treatment systems.

Urea injection and ammonia storage ratio are critical for the SCR system to achieve high NO_x reduction efficiency and low NH_3 slip. Nevertheless, unknown system dynamics including input (urea injection) disturbances and model uncertainties of SCR system make it challenging to achieve high NO_x reduction efficiency and low NH_3 slip. To deal with these obstacles, Paper 1, Paper 2 and Paper 3 (Chapter 2, 3,

and 4 respectively) proposed active disturbance estimation and compensation methods for enhancing the SCR performance. Paper 1 (Chapter 2) introduces two different methods to accurately detect urea injection and correct for urea dosing control. Paper 2 (Chapter 3) depicts a robust Nonlinear Disturbance Observer (robust NDO) to effectively estimate the ammonia storage ratio in a cost-effective way. Paper 3 (Chapter 4) presents a compound control strategies based on active disturbance rejection control (ADRC) to precisely keep NH_3 slip low and achieve high NO_x reduction efficiency.

DOC thermal management is critical to effectively burn the soot during DPF regeneration (PM reduction). But unknown system dynamics including DOC inlet emissions and model uncertainties make it difficult for DOC mean temperature estimation and DOC outlet temperature control during DPF regeneration. To deal with these challenges, Paper 4 and Paper 5 (Chapter 5 and 6 respectively) developed active disturbance estimation and compensation strategies for improving DOC thermal management during DPF regeneration. Paper 4 (Chapter 5) introduces a robust filter based on Smooth Variable Structure Filter (SVSF) with augmented disturbance states to estimate the mean temperature of DOC. Paper 5 (Chapter 6) presents a composite controller combining a feedforward controller and an modified Active Disturbance Rejection Controller (mADRC) with time delay compensation for the DOC outlet temperature control.

The proposed methods in the 5 papers are either validated by the calibrated GT-power model or experiments with Diesel after-treatment systems.

Acknowledgements

Publications

Journal Articles

J1. **Jinbiao Ning**, Fengjun Yan, "Augmented-state Smooth Variable Structure Filter for DOC mean temperature estimation," (submitted)

J2. **Jinbiao Ning**, and Fengjun Yan. "Disturbance rejection in DOC-out temperature control for DPF regeneration." Proceedings of the Institution of Mechanical Engineers, Part D: Journal of Automobile Engineering (2016): 0954407016650782.

J3. **Jinbiao Ning**, and Fengjun Yan. "Robust Nonlinear Disturbance Observer Design for Estimation of Ammonia Storage Ratio in Selective Catalytic Reduction Systems." Journal of Dynamic Systems, Measurement, and Control 137, no. 12 (2015): 121012.

J4. **Jinbiao Ning** and Fengjun Yan, "Compound Control Strategy based on Active Disturbance Rejection for Selective Catalytic Reduction systems," ASME Transactions Journal of Dynamic Systems, Measurement, and Control, Vol. 137 (5), 2015.

Peer-Reviewed Conference Papers

C1. **Jinbiao Ning** and Fengjun Yan, "IMC Based Iterative Learning Control of DOC Temperature during DPF Regeneration," 2016 European Control Conference, Aalborg University, Aalborg, Denmark, 2016.

C2. **Jinbiao Ning** and Fengjun Yan, "Temperature Control of Electrically Heated

Catalyst for Cold-start Emission Improvement," 8th IFAC International Symposium on Advances in Automotive Control, Norrkping , Sweden, 2016.

C3. **Jinbiao Ning** and Fengjun Yan, "Composite Control of DOC-out Temperature for DPF regeneration," 8th IFAC International Symposium on Advances in Automotive Control, Norrkping , Sweden, 2016.

C4. **Jinbiao Ning** and Fengjun Yan, "Nonlinear Disturbance Observer Design for Estimation of Ammonia Storage Ratio in Selective Catalytic Reduction Systems," Proceedings of the American Control Conference, Chicago, USA, 2015.

C5. **Jinbiao Ning** and Fengjun Yan, "Detection of Injected Urea Quantity and Correction for SCR Urea dosing control," No. 2015-01-1038. SAE Technical Paper, Detroit, USA, 2015.

C6. **Jinbiao Ning** and Fengjun Yan, "Active Disturbance Rejection Control of a Selective Catalytic Reduction system for Diesel Engines," 2014 Proceedings of the CSME International Congress, Toronto, Canada, 2014.

Contents

List of Tables

List of Figures

Chapter 1

Introduction

1.1   Background

Diesel engines are widely used in automobile applications due to their great durability
and high fuel efficiency. Nevertheless, their lean-burned combustion profiles lead to
high emissions (e.g. NOx, CO, HC, PM) which have bad impacts on the public
health, the environment and so on. Therefore, regulations on Diesel emissions are
increasingly stringent in recent years all over the world. Figure 1.1 demonstrates the
gradually tightened limits of NO_x and PM on heavy duty Diesel engines introduced
by US EPA (US Environmental Protection Agency). As can be seen in Figure 1.1,
the NO_x limit in 2007 (0.2 $g/bhphr$) is about 50 times stricter than that in 1988 (10.7
$g/bhphr$), and the PM limit in 2007 (0.01 $g/bhphr$) is about 60 times stricter than
that in 1988 (0.6 $g/bhphr$). Similar to US emission standard, Figure 1.2 depicts the
historical view of emission standards for light-duty and heavy-duty Diesel engines in
European Union (EU). Showed in Figure 1.2, the NO_x limit in 2013 (0.40 g/kWh)
is about 20 times lower than that in 1992 (8.0 g/kWh), and the PM limit in 2013

$(0.01 \ g/kWh)$ is about 36 times lower than that in 1992 $(0.36 \ g/kWh)$.
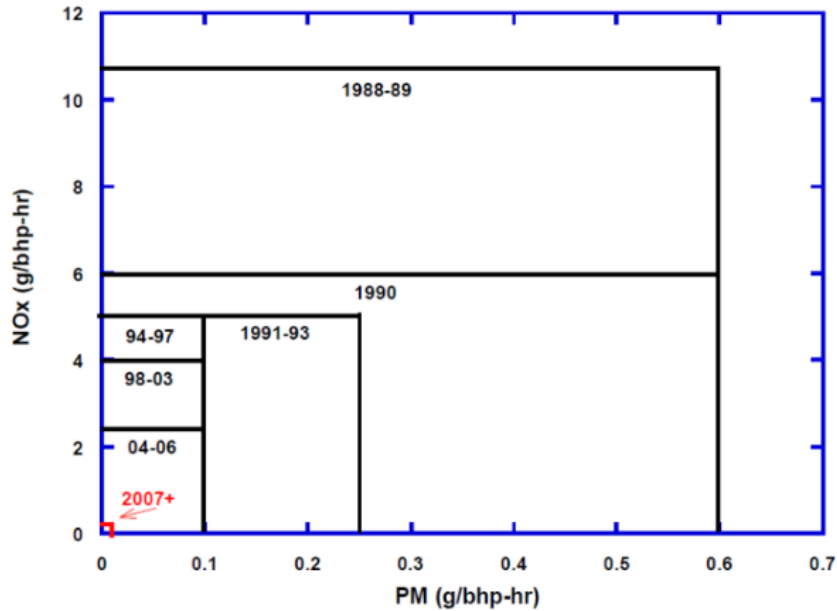
Figure 1.1: Heavy duty Diesel emissions standards since 1988 [1]

It has been studied that after-treatment systems are necessary to further lower the engine-out emissions to meet the emission limits [28], although advanced engine controls and technologies can reduce engine-out emissions. In order to meet stringent emission legislations, modern Diesel engines are equipped with after-treatment systems. The state-of-the-art aftertreatment system includes a Diesel Oxidation Catalyst (DOC), a Diesel Particulate Filters (DPF) and a Selective Catalytic Reduction (SCR) system, as can be seen in Figure 1.3. However, the further strict limits of NO_x and PM on Diesel engines are on the way. An real-driving emissions (RDE) regulatory proposal was signed by EU to reduce in-use emissions since many studies have been reported that in-use emissions from cars are much higher than by certification testing [2, 3]. The challenges for diesel emission reduction are continuing as the Low

(a) Light-duty   (b) Heavy-duty
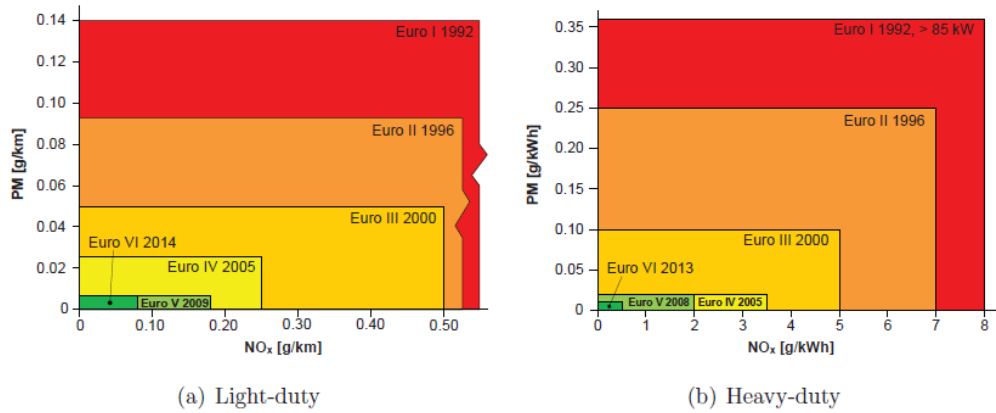
Figure 1.2: EU emission standards for Diesel engines since 1992 [27]

Emission Vehicle III (LEVIII) and US Tier 3 implementation proceeds through 2025, the EU shifts to an emphasis on real-driving emissions (RDE), and the California Heavy Duty (HD) and European Non-Road (NR) sectors tighten further [2, 3]. More efforts are required to improve the performance of Diesel aftertreatment systems so as to comply increasingly stringent emission regulations.
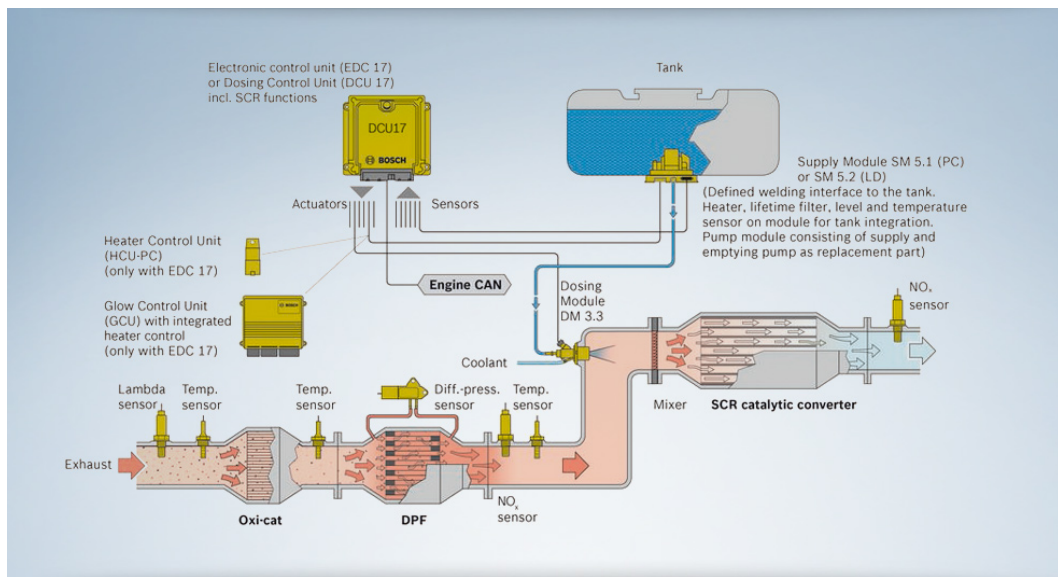
Figure 1.3: Advanced aftertreatment system of Diesel engine [4]

3

1.2   Diesel Aftertreatment Systems

1.2.1   Diesel Oxidation Catalyst (DOC)

Main Functions

The DOC is mainly used to oxidise the CO and unburned HCs to CO_2 and H_2O. In addition, the DOC is able to convert NO to NO_2 for passive regeneration of DPFs and improving the overall NO_x reduction efficiency of SCRs. Furthermore, the DOC is adopted to boost the DOC-out temperature for active regeneration of DPFs. The emission conversation efficiency highly depends on the DOC temperature, so the DOC temperature is critical for fast light-off management to effectively reduce exhaust pipe-out emission, especially during the phase of cold start. Thus, to fast heat up the DOC for light-off management, the DOC is located upstream of the DPF and the SCR (i.e. close to the engine), as can been seen in Figure 1.3.

Physical Structure

The DOC is a flow-through honeycomb monolith structure made of either ceramics or metal, as can be seen in Figure 1.4. Typical cross-section of the DOC is circular or oval. Ceramics substrates are usually square cells, whilst metallic substrates are sinusoidal channels. The number of cells of DOC varies and typical DOC cells are 300-400 cells per square inch (cpsi). Exhaust gases flow through the channels and contact the catalyst on the channel walls.
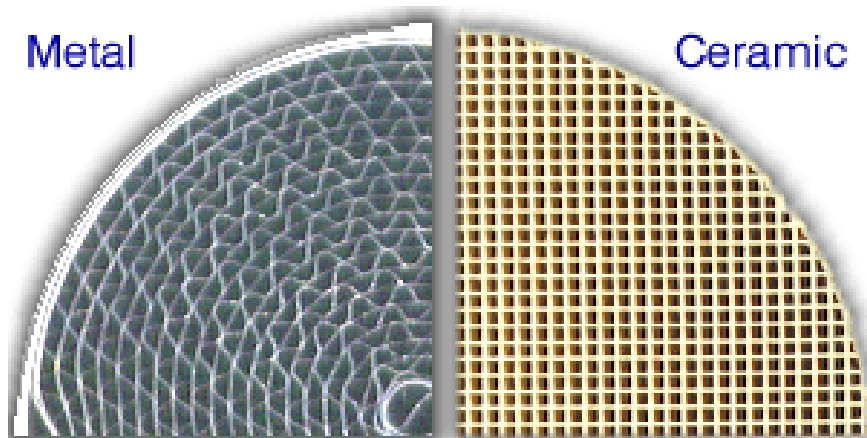
Figure 1.4: The honeycomb monolith structure of DOC [15].

The honeycomb monolith structure of DOC is coated with a catalytic washcoat layer as can be seen in Figure 1.5. The washcoat layer usually consists of inorganic base metal oxides such as alumina, V_2O_5 and zeolites. Also, the precious platinum group metals (PGM) such as platinum itself (Pt), palladium (Pd) and rhodium (Rh) are deposited on the surface and within the pores of the washcoat.
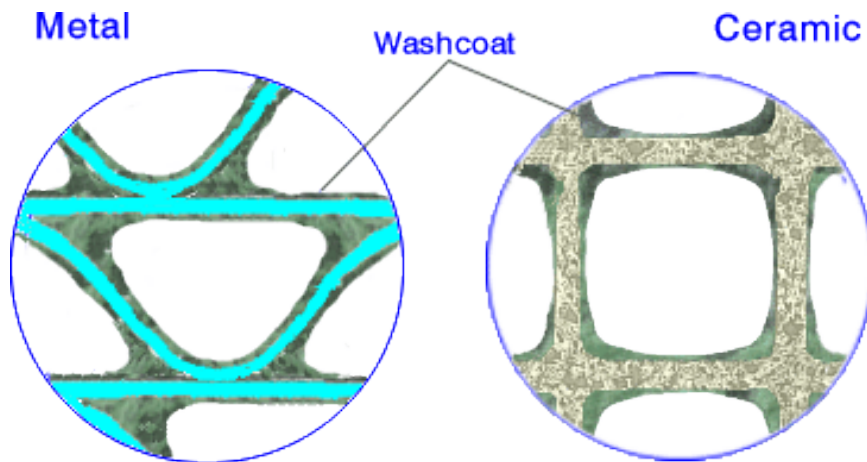
Figure 1.5: The Washcoat of DOC [15].

Chemical Reactions

Chemical reactions in DOC are complex and more details can be seen in [29–33]. The main reactions in DOC include oxidation reactions [29] and Hydrocarbon storage [30], as demonstrated in table 1. In table 1, C_3H_6 and DF (DF_1 and DF_2) represent the partially reacted fuel hydrocarbons and unburned fuel, respectively; DF_1 and DF_2 represent adsorbable slow oxidizing hydrocarbon and non-adsorbable slow oxidizing hydrocarbon, respectively; Z represents Zeolite.

Table 1: Main Reactions in DOC

	Oxidation Reactions
1	$CO + 0.5O_2 \rightarrow CO_2$
2	$C_3H_6 + 4.5O_2 \rightarrow 3CO_2 + 3H_2O$
3	$H_2 + 0.5O_2 \rightarrow H_2O$
4	$NO + 0.5O_2 \rightarrow NO_2$
5	$DF_1 + 19.4O_2 \rightarrow 13.5CO_2 + 11.8H_2O$
6	$DF_2 + 19.4O_2 \rightarrow 13.5CO_2 + 11.8H_2O$
	Hydrocarbon Storage Reactions
7	$Z + DF_1 \rightarrow ZDF_1$
8	$ZDF_1 \rightarrow Z + DF_1$

1.2.2   Diesel Particulate Filter (DPF)

Main Functions

The DPF locates downstream of the DOC, as demonstrated in Figure 1.3. The DPF is a flow-through device for Particulate matter (PM)/ soot reduction. The composition of PM is extremely complex including four main fractions: 1) elemental carbon (i.e. soot), 2) soluble organic fraction, 3)sulfates and 4) ashes (inorganic materials) [34, 35]. As can be seen in Figure 1.6, the PM can be deposited in DPF and the soot can be burned off by using regeneration methods. A platinum-catalyst filter system will passively regenerate from the reaction of NO_2 with carbon under medium- and high-load conditions [36]. Passive regeneration is limited by temperature and by NO_x/C ratios. Active regeneration is required in extended operating conditions since passive regeneration is not enough to keep the filter clean. It has been reported that the approaches of active regeneration have identified common features [37]:

a) Estimation of DPF soot loading using engine and back pressure models, and fuel consumption;

b) Preheating the DOC system to ensure that injected hydrocarbons can ignite and heat up the filter;

c) Increase of exhaust hydrocarbon levels via in cylinder or supplemental fuel injection, for burning on a DOC;

d) Control and monitoring of the regeneration as a function of operating point and conditions;

e) Recalculation of pertinent models to take account of ash build-up.
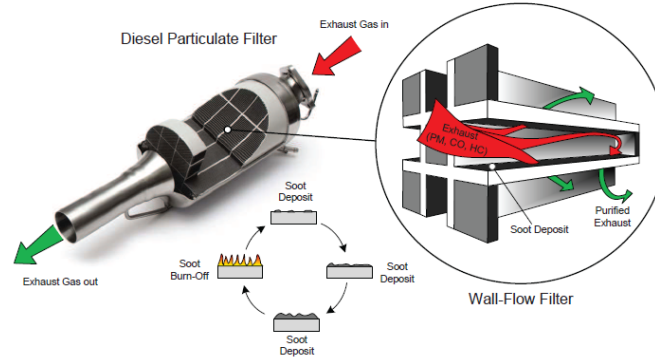
Figure 1.6: The principle of DPF[27].

Chemical Reactions

Main reactions in DPF during passive regeneration and active regeneration are demonstrated in table 2. Reaction 1 and 2 happen during active regeneration when the temperature is in the appropriate temperature range. Reaction 3 and 4 continuously occur during passive regeneration. It has been pointed out that Reaction 2 and 4 can be ignored since O_2 is excessive in Diesel exhaust and NO_2 is a strong oxidizer [16, 17].

Table 2: Regeneration Reactions in DPF [16]

Active Regeneration	
1	$C + O_2 \rightarrow CO_2$
2	$2C + O_2 \rightarrow 2CO$
Passive Regeneration	
3	$2NO_2 + C \rightarrow CO_2 + 2NO$
4	$NO_2 + C \rightarrow CO + NO$

1.2.3   Urea-based Selective Catalytic Reduction (SCR)

Main Functions

The SCR system is a leading and effective aftertreatment technology to reduce nitrogen oxides (NO_x). The SCR system as part of the after-treatment system is located in the downstream of DPF, as can be seen in Figure 1.3.

Physical Structure

The SCR system is composed of a urea dosing system and a SCR catalyst. Urea dosing system contains a urea tank, a urea pump, a pressure line, a urea injector and a dosing control unit (DCU), as depicted in Figure 1.3. The SCR catalyst is a flow-through honeycomb monolith substrate coated with a catalytic layer of precious PGM loading. The 32.5% aqueous urea solution, also called AdBlue or Diesel Exhaust/Emission Fluid (DEF), is used as the source of ammonia for SCR system in vehicle applications. The urea dosing system controls the urea line pressure and injects the DEF into the exhaust pipe upstream of the SCR catalyst.

Chemical Reactions

As can be seen in Figure 1.7, NO_x reduction reactions occur when the exhaust gases flow through the SCR system. From urea injection to NOx reduction reactions in urea-based SCR system, three events are mainly included. Firstly, the AdBlue is injected at upstream of the SCR system by the dosing unit and converted to ammonia. Secondly, when entering the SCR system, the ammonia is partially adsorbed by the substrate of the catalyst. Finally, the ammonia adsorbed on the substrate reacts with NOx and convert them to N_2 and H_2O. Main reactions of SCR are demonstrated in

table 3
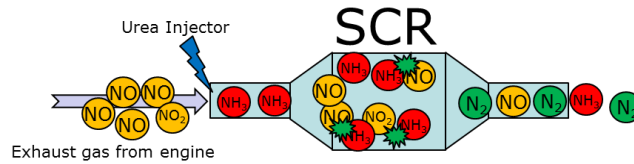
Figure 1.7: Urea based SCR system for Diesel engine.

Table 3: Main Reactions in DOC

	AdBlue to Ammonia
1	$NH_3CONH_3(liquid) \rightarrow NH_2CONH_2* + xH_2O$
2	$NH_2CONH_2* \rightarrow HNCO + NH_3$
3	$HNCO + H_2O \rightarrow CO_2 + NH_3$
	Ammonia Adsorption/Desorption
4	$NH_3 + Z \leftrightarrow ZNH_3$
	Ammonia oxidation
5	$NH_3 + 1.25O_2 \rightarrow NO + 1.5H_2O$
	NO_x Reduction
6	$4NH_3 + 4NO + O_2 \rightarrow 4N_2 + 6H_2O$
7	$2NH_3 + NO + NO_2 \rightarrow 2N_2 + 3H_2O$
8	$4NH_3 + 3NO_2 \rightarrow 3.5N_2 + 6H_2O$

1.3 Literature Review and Challenges

1.3.1 Control and Challenges for NO_x Reduction

The urea is injected into the exhaust pipe and converted to gaseous ammonia. A part of the inlet ammonia is absorbed on the catalytic surface and the remain part of inlet ammonia flows through the SCR system. The ammonia slip is composed of two parts: a part of the inlet ammonia and the ammonia desorption from ammonia storage on SCR surface. A part of inlet NO_x reacts with the ammonia stored on the catalytic surface of the SCR system and the remain part of inlet NO_x flows through the SCR system. Therefore, the urea injection and the ammonia storage ratio play important role in both ammonia slip and NO_x reduction efficiency. However, it is challenging to balance ammonia slip and NO_x reduction efficiency, since both NO_x and NH_3 are toxic and both targets (high NO_x reduction efficiency and low ammonia slip) are conflictive. For one hand, too much urea injection can achieve high NO_x reduction efficiency but cause excessive ammonia slip. On the other hand, less urea injection can have low or no ammonia slip but lead to low NO_x reduction efficiency such that emission regulations cannot be satisfied. To address this challenge, numerous estimation and control strategies have been proposed for urea-based SCR systems. This section summarizes the state-of-the-art estimation and control strategies for SCR NO_x reduction.

Ammonia Storage Ratio Estimation

It has been pointed out that the ammonia storage ratio has critical effect on the ammonia slip and NO_x reduction efficiency in the SCR system. However, the ammonia

storage ratio is difficult to be directly measured due to no available on-board sensors, although some methods and equipment were studied in the laboratory [18]. The estimation of ammonia storage ratio is significant for SCR control but it is challenging due to the high cost of NO_x and NH_3 sensors, cross sensitivity of NO_x sensor to NH_3, the high nonlinearities in chemical reactions [6] and measurement noise. Linear or linearized SCR models were used to design observers for ammonia storage ratio estimation but the performance of these methods are limited due to nonlinearities, model uncertainties and disturbances [19, 20]. Several sliding mode observers were developed in [21] and discrete-time smooth variable structure estimator was proposed in [38] to estimate the ammonia storage ratio in SCR system by using NOx sensors and ammonia sensors. To be noted, ammonia sensors are expensive and not available for mass product after-treatment systems. Sensor reduction is necessary and possible for SCR estimation and feedback control. A cost-effective robust approach was proposed in [39] to estimate the states of SCR system by dual NOx sensors after the SCR system without any ammonia sensors. Furthermore, the NOx sensor is widely used for SCR feedback control [40] and required for OBD regulations. It is worth noting that high-frequency noises are commonly involved in sensor measurements. Robust ammonia storage ratio estimation methods that can attenuate the influence of such noise are therefore desired.

Feedback Control

SCR closed-loop controls were proposed to meet stricter emission regulations since model-based or MAP-based opened-loop control strategies are only sufficient to meet Euro-IV and Euro-V emission standards [5]. Control variables are critical for SCR

closed-loop controls and four potential control variables (i.e. NO_x concentration, NO_x conversion, NH_3 concentration, and NH_3 surface coverage) were discussed in [6]. NO_x concentration and NO_x conversion were reported to be used to compensate the feed-forward control while it can easily lead to high NH_3 slip [41] or unstable problems due to ammonia cross-sensitivity issue [8] of NO_x sensors. Ammonia concentration at downstream of SCR system have been reported to be used for feedback control in [41]. The ammonia surface coverage or the ammonia surface coverage ratio was proposed for feedback control aiming for high NO_x reduction efficiency and low NH_3 slip at the same time [41]. Conventional PID control [6–10] and model-based control strategies [11–14] are reported for SCR feedback control. However, nonlinearities, model uncertainties and disturbances may impair the control performance or cause unstable problems for both conventional PID controllers and model-based controllers. Adaptive controls [22–25] have been developed for SCR control to reduce model mismatch by adapting model parameters. An adaptive model predictive control (MPC) proposed in [26] shows its effectiveness in dealing with both NH_3 slip and NO_x inefficiency issues at the same time, while the adaptive MPC requires relatively high computation effort and a relatively accurate model.

Summary

The high cost of NO_x and NH_3 sensors, cross sensitivity of NO_x sensor to NH_3, the high nonlinearities in chemical reactions [6] and measurement noise are issues for ammonia storage ratio estimation. In addition, nonlinearities, model uncertainties and disturbances are challenges for both conventional PID controllers and model-based controllers. Furthermore, accurate urea injection is critical to achieve high NO_x

reduction efficiency and keep ammonia slip low. Therefore, overdosing or under-dosing of urea injection should be avoided or corrected. Nevertheless, the urea injector may change in lifetime, causing overdosing or under-dosing of urea injection. To address aforementioned problems, Chapter 2, 3 and 4 of this thesis focus on urea injection detection and correction, ammonia storage ratio estimation and ammonia feedback control by proposing robust and cost effective strategies based on active disturbance estimation and compensation.

1.3.2   Control and Challenges for PM Reduction

It has been reported that active regeneration is needed to effectively reduce the PM emission. Based on the principle of DPF, the active regeneration of DPF divides into two stages [42]: 1) close post injection is used to drive the DOC temperature up to light-off temperature for high hydrocarbons (HC) conversion efficiency. 2) far post injection in cylinder or downstream injection in the exhaust pipe is adopted to boost the DOC outlet temperature to satisfy the DPF active regeneration temperature.

For the first stage, the DOC mean temperature is very critical for light off management, whilst the mean temperature of a DOC is not able to be measured directly. Thus, the mean temperature estimation is critical for DOC on-board diagnostic and fast light off management but is challenging due to complex reactions and thermal dynamics in DOC. Mathematical models are required for mean temperature estimation and control of a DOC. Several mathematical models for DOC have been reported in the literature. Detailed kinetic model were proposed for simulation purpose based on first principle [29, 30, 43, 44]. A reduced order model of DOC and an EKF are

proposed for the internal temperature and outlet emissions (e.g. CO, NO, NO_2) prediction in [45]. An control-oriented model with considering its thermal behavior was proposed for DOC control and diagnosis in [46–48]. However, the input disturbance and model uncertainties are not considered for the temperature estimation, leading to great estimation error in the case when model uncertainties and input disturbances exist.

For the second stage, the DOC-out temperature is critical for DPF active regeneration as the DPF inlet temperature should be high enough to effectively burn the accumulated soot in the DPF and should be kept below a certain threshold to prevent damage to the DPF. However, the control of DOC-out temperature is challenging due to several factors including wide-range engine operations, DOC thermal inertia, the complexities of the reactions in DOC, and the physical saturation of the fuel injectors.

Several model-based control strategies [42, 49, 50] were proposed to address this issue. Linear Parameters Varying (LPV) controller was demonstrated in [49] to have better tracking performance for the Diesel Particulate Filter Thermal Management by comparing with model-based PID controller. Model-based temperature control with parameter adaptation by exhaust gas velocity is proposed in [50]. Model Predictive Control (MPC) was proposed in [42] for DOC-out temperature control during DPF regeneration and achieved small temperature error in general but more overshoots than the production controller. There exist several drawbacks in the aforementioned model-based controllers. First of all, these model-based control methods were designed deeply relying on accurate DOC model, while it is difficult to achieve precise model for DOC system since the chemical reactions and thermal dynamics in DOC are complex. Second drawbacks lies in the complexity in design (e.g. LPV) and the

high computational load (e.g. MPC). Furthermore, the above controllers still have nontrivial overshoots that are harmful for the DPF regeneration.

Hence, to enhance active regeneration performance of DPFs and avoid the aforementioned drawbacks, this thesis presents a robust augmented-state smooth variable structure filter (robust SVSF) for DOC mean temperature estimation, and a robust disturbance rejection based control strategy for DOC-out temperature control.

1.4 Outline

To deal with the aforementioned challenges in NO_x reduction and PM reduction, five papers in this thesis present several strategies based on active disturbance estimation and compensation for improving the performance of Diesel aftertreatment systems. The remain parts of this thesis are organized as follows,

Chapter 2 (Paper 1) to Chapter 4 (paper 3) focus on detection and correction of urea injection ,estimation of ammonia storage ratio and ammonia feedback control for SCR NO_x reduction.

In Chapter 2 (Paper 1), a correction factor was defined for detection and correction of under-dosing or overdosing urea injection and two methods were proposed to identify the correction factor. The first method is based on the pump frequency extracted from the frequency analysis of the line pressure. The second method is based on the effective voltage of the motor. The effectiveness of both methods are validated by the experiment of urea dosing system.

In Chapter 3 (Paper 2), two Nonlinear Distrubance Observer based methods were presented to estimate the ammonia storage ratio, aiming for cost reduction. A novel robust Nonlinear Distrubance Observer (robust NDO) was proposed and compared

with the regular NDO. The stability and noise attenuation properties of both observers were theoretically discussed. The effectiveness of both NDOs are validated under FTP-75 test cycle by the full-vehicle GT-power simulation.

In Chapter 4 (Paper 3), a compound control strategy based on active disturbance rejection controller was proposed for SCR ammonia feedback control. The compound control strategy is composed of a active disturbance rejection control, a zero-input controller and a switching mechanism. The proposed control strategy is validated by the high-fidelity GT-power model through steady states and FTP-75 test cycle.

Chapter 5 (Paper 4) and Chapter 6 (paper 5) concentrate on DOC mean temperature estimation and DOC outlet temperature control for PM reduction (DPF active regeneration), respectively.

In Chapter 5 (Paper 4), two estimation methods based on Smooth Variable Structure Filter were proposed to accurately estimate DOC mean temperature. A robust Smooth Variable Structure Filter (robust SVSF) is designed based on the augmented reduced order model of a DOC and compared with regular SVSF. The effectiveness of both methods are validated by the experimentally calibrated DOC model in GT-power environment.

In Chapter 6 (Paper 5), a novel and time-efficient composite controller based on modified Active Disturbance Rejection Control (mADRC) was proposed for DOC-out temperature control during DPF active regeneration. The proposed composite controller is a new combination of a model-based feedforward controller and a mADRC with time delay compensation through the mass flow rate of exhaust gas. The control strategy is validated by the calibrated DOC model in GT-power environment.

Chapter 7 summarises the concluding remarks of this thesis and provides a brief

introduction of further research directions for future work.

Reference

[1] "Current US EPA Regulations, and Engineering Challenges in Automotive Industry — Energy, Technology, & Policy on WordPress.com." [Online]. Available: http://webberenergyblog.wordpress.com/2013/02/02/currentus-epa-regulations-and-engineering-challenges-in-automotive-industry/. [Accessed:04-Sep-2014].

[2] Timothy Johnson. "Vehicular Emissions in Review." SAE International Journal of Engines 9, no. 2016-01-0919 (2016): 1258-1275.

[3] Timothy V Johnson. "Review of vehicular emissions trends." SAE International Journal of Engines 8, no. 2015-01-0993 (2015): 1152-1167.

[4] "Emission Standards on Heavy-Duty Truck and Bus Engines of European Union." [Online]. Available: https://www.dieselnet.com/standards/eu/hd.php. [Accessed:04-Sep-2014].

[5] "Diesel exhaust gas treatment." [Online]. Available: http://products.bosch-mobility-solutions.com/specials/de/abgasnachbehandlung/en/subpage/Denoxtronic-5.html. [Accessed:17-April-2017].

[6] Zakwan Skaf, Timur Aliyev, Leo Shead, and Thomas Steffen. "The state of the art in selective catalytic reduction control." (2014).

[7] John N. Chi. "Control challenges for optimal NO_x conversion efficiency from SCR aftertreatment systems." No. 2009-01-0905. SAE Technical Paper, 2009.

[8] Frank Willems, Robert Cloudt, Edwin Van Den Eijnden, Marcel Van Genderen, Ruud Verbeek, Bram de Jager, Wiebe Boomsma, and Ignace van den Heuvel. "Is closed-loop SCR control required to meet future emission targets?." No. 2007-01-1574. SAE Technical Paper, 2007.

[9] S. M. Zhang, F. Tian, G. F. Ren, and L. Yang. "SCR control strategy based on ANNs and Fuzzy PID in a heavy-duty diesel engine." International Journal of Automotive Technology 13, no. 5 (2012): 693-699.

[10] Chun Ong, Anuradha Annaswamy, Ilya V. Kolmanovsky, Paul Laing, and Dennis Reed. "An adaptive proportional integral control of a urea selective catalytic reduction system based on system identification models." SAE International Journal of Fuels and Lubricants 3, no. 2010-01-1174 (2010): 625-642.

[11] Andrew Herman, Ming-Cheng Wu, David Cabush, and Mark Shost. "Model based control of SCR dosing and OBD strategies with feedback from NH_3 sensors." SAE International Journal of Fuels and Lubricants 2, no. 2009-01-0911 (2009): 375-385.

[12] Ming-Feng Hsieh, and Junmin Wang. "A two-cell backstepping-based control strategy for diesel engine selective catalytic reduction systems." IEEE Transactions on Control Systems Technology 19, no. 6 (2011): 1504-1515.

[13] Binbin Shen, Fangping Yu, Huabiao Jin, Huayu Zhang, and Qidou Wu. "Applied research on diesel engine SCR system with the variable structure control theory." In Electrical and Control Engineering (ICECE), 2011 International Conference on, pp. 4382-4385. IEEE, 2011.

[14] Devesh Upadhyay, and Michiel Van Nieuwstadt. "Model based analysis and control design of a urea-SCR deNOx aftertreatment system." Journal of dynamic systems, measurement, and control 128, no. 3 (2006): 737-741.

[15] "Emission   Aftertreatment   Technologies   [Online]."   Available: https://www.dieselnet.com/tech/cat_ substrate.php. [Accessed:17-April-2017].

[16] Shuzhan Bai, Jiao Tang, Guihua Wang, and Guoxiang Li. "Soot loading estimation model and passive regeneration characteristics of DPF system for heavy-duty engine." Applied Thermal Engineering 100 (2016): 1292-1298.

[17] Messerer, A., R. Niessner, and U. Pöschl. "Comprehensive kinetic characterization of the oxidation and gasification of model and real diesel soot by nitrogen oxides and oxygen under engine exhaust conditions: Measurement, LangmuirHinshelwood, and Arrhenius parameters." Carbon 44, no. 2 (2006): 307-324.

[18] Kubinski, D. J., and J. H. Visser. "Sensor and method for determining the ammonia loading of a zeolite SCR catalyst." Sensors and Actuators B: Chemical 130, no. 1 (2008): 425-429.

[19] Upadhyay, Devesh, and Michiel Van Nieuwstadt. "Model based analysis and control design of a urea-SCR deNOx aftertreatment system." Journal of dynamic systems, measurement, and control 128, no. 3 (2006): 737-741.

[20] Devarakonda, Maruthi, Gordon Parker, and John Johnson. "NOx control systems and methods for controlling NOx emissions." U.S. Patent 8,230,677, issued July 31, 2012.

[21] M. F. Hsieh, and J. Wang. "Observer-based estimation of selective catalytic reduction catalyst ammonia storage." Proceedings of the Institution of Mechanical Engineers, Part D: Journal of Automobile Engineering 224, no. 9 (2010): 1199-1211.

[22] Chi, John N., and Herbert FM DaCosta. Modeling and control of a urea-SCR aftertreatment system. No. 2005-01-0966. SAE Technical Paper, 2005.

[23] Yao, Sheng, Mark Shost, Joon-Ho Yoo, David Cabush, David Racine, Robert Cloudt, and Frank Willems. "Ammonia sensor for closed-loop SCR control." SAE international journal of passenger cars-electronic and electrical systems 1, no. 2008-01-0919 (2008): 323-333.

[24] Hsieh, Ming-Feng, and Junmin Wang. "Adaptive and efficient ammonia storage distribution control for a two-catalyst selective catalytic reduction system." Journal of Dynamic Systems, Measurement, and Control 134, no. 1 (2012): 011012.

[25] Chen, Pingen, and Junmin Wang. "Nonlinear and adaptive control of NO/NO 2 ratio for improving selective catalytic reduction system performance." Journal of the Franklin Institute 350, no. 8 (2013): 1992-2012.

[26] McKinley, Thomas L., and Andrew G. Alleyne. "Adaptive model predictive control of an SCR catalytic converter system for automotive applications." IEEE transactions on control systems technology 20, no. 6 (2012): 1533-1547.

[27] Bc. Vladimír Dvořák. "Modeling and Control of Aftertreatment Systems for Diesel Combustion Engines." Masters thesis, Czech Technical University,2010

[28] Henrik Backman, Kalle Arve, Fredrik Klingstedt, and Dmitry Yu Murzin. "Kinetic considerations of H_2 assisted hydrocarbon selective catalytic reduction of NO over Ag/Al_2O_3: II. Kinetic modelling." Applied Catalysis A: General 304 (2006): 86-92.

[29] Chaitanya S. Sampara, Edward J. Bissett, and Matthew Chmielewski. "Global kinetics for a commercial diesel oxidation catalyst with two exhaust hydrocarbons." Industrial & Engineering Chemistry Research 47, no. 2 (2008): 311-322.

[30] Chaitanya S. Sampara, Edward J. Bissett, and Dennis Assanis. "Hydrocarbon storage modeling for diesel oxidation catalysts." Chemical Engineering Science 63, no. 21 (2008): 5179-5192.

[31] Tae-Joong Wang, Seung Wook Baek, and Je-Hyung Lee. "Kinetic parameter estimation of a diesel oxidation catalyst under actual vehicle operating conditions." Industrial & Engineering Chemistry Research 47, no. 8 (2008): 2528-2537.

[32] Sterling E. Voltz, Charles R. Morgan, David Liederman, and Solomon M. Jacob. "Kinetic study of carbon monoxide and propylene oxidation on platinum catalysts." Industrial & Engineering Chemistry Product Research and Development 12, no. 4 (1973): 294-301.

[33] Xiaobo Song, Harsha Surenahalli, Jeffrey Naber, Gordon Parker, and John H. Johnson. "Experimental and modeling study of a diesel oxidation catalyst (DOC)

under transient and CPF active regeneration conditions." No. 2013-01-1046. SAE Technical Paper, 2013.

[34] Elias Vouitsis, Leonidas Ntziachristos, and Zissis Samaras. "Particulate matter mass measurements for low emitting diesel powered vehicles: what's next?." Progress in Energy and Combustion Science 29, no. 6 (2003): 635-672.

[35] H. Burtscher, "Physical characterization of particulate emissions from diesel engines: a review." Journal of Aerosol Science 36, no. 7 (2005): 896-932.

[36] Gianmarco Boretto, Roberto Imarisio, Pierluigi Rellecati, Enrico Barucchi, and Andrea Sanguedolce. "Serial application of a catalyzed particulate filter on common rail DI diesel engines for passenger cars." In F2004V068, FISITA World Automotive Congress, Barcelona, Spain, pp. 23-27. 2004.

[37] U. H. Zink, and T. V. Johnson. "State-of-the-art filter regeneration managementconcepts realized by LDV companies." In US Dept. of Energy Diesel Engine Emissions Reduction (DEER) Conference, Chicago, IL, USA, 21st25th August. 2005.

[38] Hui Zhang, Junmin Wang, and Yue-Yun Wang. "Robust filtering for ammonia coverage estimation in diesel engine selective catalytic reduction systems." Journal of Dynamic Systems, Measurement, and Control 135, no. 6 (2013): 064504.

[39] Pingen Chen, and Junmin Wang. "A novel cost-effective robust approach for selective catalytic reduction state estimations using dual nitrogen oxide sensors." Proceedings of the Institution of Mechanical Engineers, Part D: Journal of Automobile Engineering 229, no. 1 (2015): 83-96.

[40] Anthony Bonfils, Yann Creff, Olivier Lepreux, and Nicolas Petit. "Closed-loop control of a SCR system using a NO_x sensor cross-sensitive to NH_3." IFAC Proceedings Volumes 45, no. 15 (2012): 738-743.

[41] Ming-Feng Hsieh, and Junmin Wang. "An extended Kalman filter for ammonia coverage ratio and capacity estimations in the application of Diesel engine SCR control and onboard diagnosis." In American Control Conference (ACC), 2010, pp. 5874-5879. IEEE, 2010.

[42] Yong-Wha Kim, Michiel Van Nieuwstadt, Greg Stewart, and Jaroslav Pekar. "Model predictive control of DOC temperature during DPF regeneration." No. 2014-01-1165. SAE Technical Paper, 2014.

[43] K. Hauff, U. Tuttlies, G. Eigenberger, and U. Nieken. "A global description of DOC kinetics for catalysts with different platinum loadings and aging status." Applied Catalysis B: Environmental 100, no. 1 (2010): 10-18.

[44] Chaitanya S. Sampara, Edward J. Bissett, Matthew Chmielewski, and Dennis Assanis. "Global kinetics for platinum diesel oxidation catalysts." Industrial & Engineering Chemistry Research 46, no. 24 (2007): 7993-8003.

[45] Harsha Shankar Surenahalli, Gordon Parker, and John H. Johnson. "Extended Kalman Filter to Estimate NO, NO_2, Hydrocarbon and Temperatures in a DOC during Active Regeneration and Under Steady State Conditions." No. 2015-01-1059. SAE Technical Paper, 2015.

[46] Pingen Chen, and Junmin Wang. "Control-oriented modeling of thermal behaviors for a diesel oxidation catalyst." In American Control Conference (ACC), 2012, pp. 4987-4992. IEEE, 2012.

[47] Pingen Chen, and Junmin Wang. "Control-oriented modeling and observer-based estimation of solid and gas temperatures for a diesel engine aftertreatment system." Journal of Dynamic Systems, Measurement, and Control 134, no. 6 (2012): 061011.

[48] C. Guardiola, B. Pla, J. Mora, and D. Lefebvre. "Control oriented model for diesel oxidation catalyst diagnosis." IFAC-PapersOnLine 48, no. 15 (2015): 427-433.

[49] Karim Bencherif, Fehd Benaicha, Stphane Sadaï, and Michel Sorine. "Diesel particulate filter thermal management using model-based design." No. 2009-01-1082. SAE Technical Paper, 2009.

[50] Olivier Lepreux, Yann Creff, and Nicolas Petit. "Model-based temperature control of a diesel oxidation catalyst." Journal of Process Control 22, no. 1 (2012): 41-50.

Chapter 2

Detection of Injected Urea Quantity and Correction for SCR Urea Dosing Control

2.1 Citation and Main Contributor

Jinbiao Ning, and Fengjun Yan. Detection of injected urea quantity and correction for SCR urea dosing control. No. 2015-01-1038. SAE Technical Paper, 2015.

The main contributor to this paper is the first author-Jinbiao Ning (contributes more than 70%).

2.2   Abstract

Using urea-based Selective Catalytic Reduction (SCR) systems is an effective way in Diesel engine after-treatment systems to meet increasingly stringent emission regulations. The amount of urea injection is critical to achieve high NO_x reduction efficiency and low ammonia slip, and overdosing or under-dosing of urea injection need to be avoided. One of the difficulties in urea injection amount control lies in the accurate measurement/estimation of the urea injection mass. To effectively address this issue, this paper defined a correction factor for under-dosing or overdosing detection and correction, and proposed two methods to identify the correction factor. The first method is based on urea pump model and line pressure. Through frequency analysis, the relation between the urea pump speed and power spectrum characteristics of the line pressure was revealed. The urea pump frequency is extracted from the frequency analysis of the line pressure and used for detecting the urea injection and identifying the correction factor. Second method is based on the effective voltage of the Motor. The relation between urea injection and effective voltage of the Motor was revealed based on the motor dynamic model. The effective voltage of the Motor is used to detect the urea injection and identify the correction factor. The effectiveness of both proposed detection and correction methods are experimentally validated through the urea dosing system.

2.3   Introduction

Diesel engines are major power sources for automobile applications due to their durability and high fuel efficiency. However, the lean burn conditions of Diesel engines

lead to high NO_x emission which contributes to acid rain and smog formation, and have been linked to incidence rates for respiratory tract irritation, infection, asthma [1]. Although some advance engine control technologies can reduce engine-out NO_x, the after-treatment systems are still necessary to further lower the engine NO_x emissions to meet the stringent emission limits [2]. Selective Catalytic Reduction (SCR) system is a promising technique to reduce the NO_x emission and has been adopted by many new production vehicles [3].

In SCR system, the urea (Adblue) is injected and converted to ammonia (NH_3) to reduce NO_x by chemical reaction on a catalytic surface. It is critical to control the amount of urea injection to avoid emission from two aspects. For one aspect, a large amount of ammonia input has a high NO_x reduction efficiency, but it may lead to high ammonia slip that have been considered as emission into Euro VI regulations [4]. For another aspect, less ammonia input leads to lower NO_x reduction efficiency such that the emission regulations cannot be satisfied. Control of the SCR system has become a challenging issue due to future emission legislation and in-use compliance requirement.

To address the issue rose by the degradation of SCR system, feedback control strategies based on ammonia sensor or NO_x sensor were proposed. A model for feedback control and monitoring of urea dosing system utilizing the ammonia sensing was developed in [5]. However, the ammonia sensor is very expensive and unreliable for production SCR system. The feedback and feedforward control were proposed in [6] for urea dosing system based on NO_x sensor. The ammonia cross-sensitivity limits the use of NO_x sensor to detect the catalyst malfunction. Therefore, most of the production SCR systems are open-loop control.

The injector area may change during the lifetime, leading inaccurate urea injection. Overdosing of urea injection may cause the ammonia slip and under-dosing may lower NO_x reduction efficiency. However, it is difficult to measure the urea injection directly by flow sensors due to high cost. Therefore, the estimation of urea injection mass or the effective injector area is very important for urea dosing control. Several studies have demonstrated different methods to estimate the urea injection mass. Signal processing methods included frequency analysis and time domain analysis were adopted to reveal the relation between line pressure and urea injection mass in [7]. However, it only demonstrated the simple relation between the magnitude and injection mass in frequency analysis. Model-based estimation of injected urea quantity and diagnostics for SCR urea system were studied in [8]. However, the return flow was ignored in both methods, which is not suitable for the urea dosing system with large return flow compared to injection mass flow. More efforts are required to estimate the injected urea quantity and compensate for the urea dosing control.

In this paper, a correction factor for detection of under-dosing or overdosing is defined based on the urea flow model. The correction factor can be potentially used for correction in urea dosing control. The contributions of this paper are: 1) a correction factor for detection of under-dosing or overdosing is defined and identified; 2) The pump frequency is extracted for identifying the correction factor by frequency analysis. 3) The effective voltage of motor is used for diagnosis of urea injection by the relation between motor speed and effective voltage of the motor.

The rest of the paper is organized as following. The principle and model of the urea dosing system are demonstrated. The problems and objectives of the detection of urea injection are presented. The first method for detecting urea injection mass and

identifying the correction factor is proposed based on urea pump frequency extracted through frequency analysis of line pressure. Second detection and correction method is based on the effective voltage of motor. The motor dynamic is used to analyze the relation between motor speed and effective voltage of the motor. Both methods are experimentally validated and then conclusions are given.

2.4 Principle and Control of Urea Dosing System

2.4.1 Principle of the Urea Dosing System

This section presents the principle of Urea Dosing System in Figure 2.1. The urea is pumped into the pressure line from the urea tank and the line pressure increases. The pressure sensor in the pressure line is used for feedback control and the controller generates the PWM (Pulse-Width Modulation) signal to control the speed of the Motor. The motor connects to the pump and determine the pump frequency. After the pressure is in steady state, the pumped urea mass equals to the return flow through the throttle based on the mass balance. Urea is injected into the exhaust pipe when the injection command is sent to the injector by the urea Dosing Control Unit (DCU). The urea injection command is PWM signal and the frequency of the PWM is 1 Hz. The urea is converted to ammonia and reacts with NO_x on the substrate of SCR converter. Too much urea injection may cause ammonia slip and too little urea injection may result in low NO_x reduction efficiency. Therefore, the injection is very critical for SCR control.
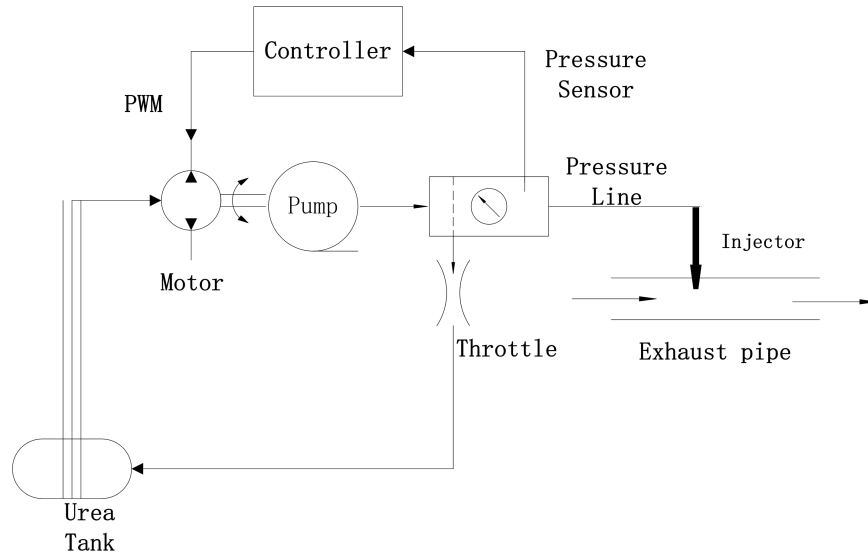
Figure 2.1: The principle of Urea Dosing System.

2.4.2   Control of the Line Pressure

The control scheme of the line pressure is demonstrated in Figure 2.2. The output of the dynamic system is the line pressure and the input for the motor is the PWM signal controlled by the DCU. The controller is a PID controller, when the error between the set-point and the output is larger than a constant , the controller is triggered. Otherwise, the controller outputs last control value. The return flow through the throttle to the urea tank and the injections through the injector to exhaust pipe are treated as two external disturbances. The variation of the line pressure is caused by the pumped urea, return urea, and the urea injection. The pumped urea equals to the return urea when the pressure is at a steady state (5 bar) and there is no urea injection. When the injection starts, the pressure may change. When the error between the set-point and the pressure is lower than Δe, the controller is not triggered, and the pressure drop is fully caused by the urea injection at this condition. However,

when the error between the set-point and output is higher than Δe, the controller is triggered and the pressure drop is caused by the urea injection and pumped urea. When the system is operating on the steady state, the pressure is at 5 bar and the pumped urea equals to the sum of return urea and urea injection.
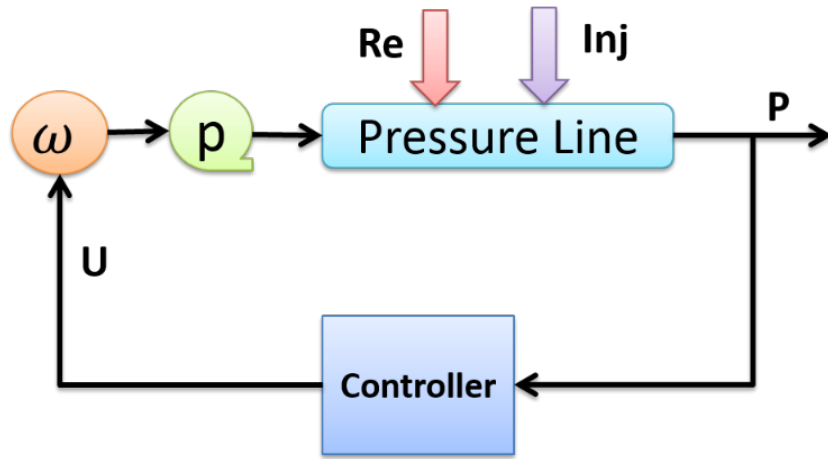
Figure 2.2: Control scheme of the line pressure.

2.4.3   Measurement System

The urea dosing system used for measurement in this paper is Bosch Denoxtronic 2.2 as can be seen from Figure 2.3. The system includes Urea tank, Supply module and Dosing module. The supply module includes the motor and the urea pump. The dosing module is the urea injector. The data was sampled from the supply module and dosing module by the scope.
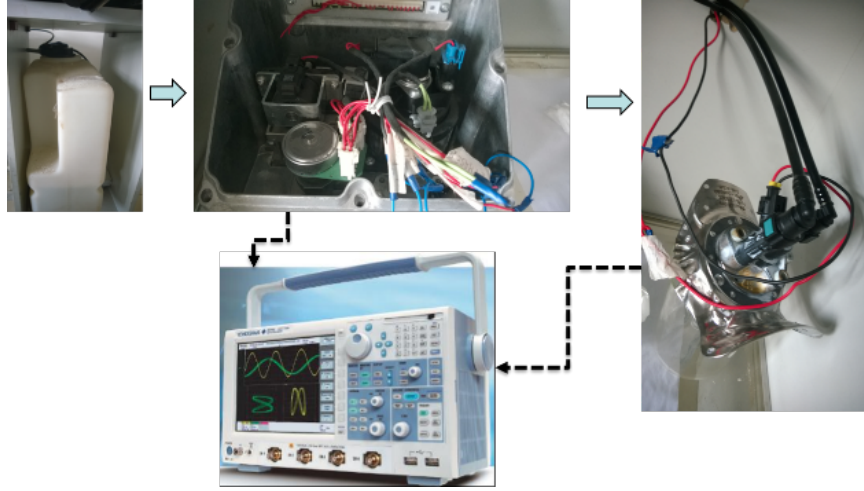
Figure 2.3: The measurement of Urea Dosing System.

2.4.4   Urea Injection Model

Urea injection dynamic can be expressed by the following equation.

$$\dot{U}_{inj} = C_d A \sqrt{2\rho(P - P_{ex})} \tag{2.1}$$

where C_d is injector nozzle discharge coefficient, A the effective area of the urea injector nozzle, ρ the density of urea, P the line pressure (bar), P_{ex} the exhaust gas pressure (bar) in the exhaust pipe, $U_{inj,cyc}$ urea injection mass of every injection period.

The urea injection mass of every control period is the integration of $\dot{U}_{inj}$ in the urea dosing system, which can be expressed by the following equation,

$$U_{inj,cyc} = f(t_{vlv,cyc}, r_{vlv,dyc}, \dot{P}, V_0) = \int_{t_{st}}^{t_{st}+t_{vlv,cyc*r_{vlv,dyc}}} \dot{U}_{inj} \tag{2.2}$$

where V_0 is the voltage of the battery (V), $t_{vlv,cyc}$ the injection period in the DCU,

34

$r_{vlv,dyc}$ the duty cycle of the urea injection.

Based on the principle of the urea injector, the effect of the battery voltage V_0 can be ignored when the variation of battery voltage is very small. When P is a constant, the equation of urea injection can be converted to the following form,

$$U_{inj,cyc} = C_d A \sqrt{2\rho(P - P_{ex})} * r_{vlv,dyc} * t_{vlv,cyc} \qquad (2.3)$$

In the DCU, the injection period is 1 second ($t_{vlv,cyc} = 1s$). Let $K = C_d A \sqrt{2\rho(P - P_{ex})} = U_{inj,cyc}/r_{vlv,dyc}$, which is called injector flow-mass characteristic factor and demonstrated in Figure 2.4.
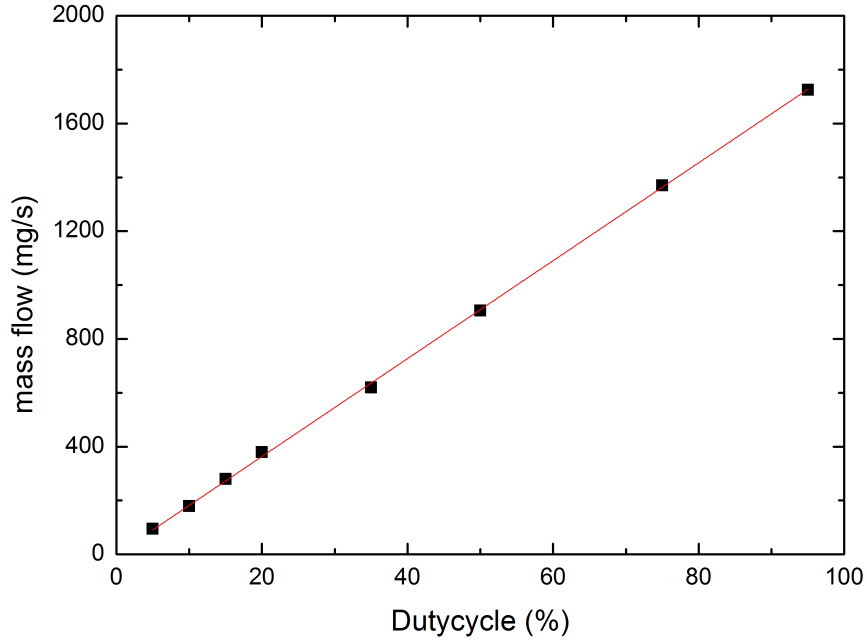
Figure 2.4: Relation between Urea injection mass and duty cycle of injections.

The target urea injection mass $U_{inj,cyc}$ is calculated from SCR control strategy in DCU. Therefore, the injection command (PWM signal) is calculated by the following

equation,

$$r_{vlv,dyc} = U_{inj,cyc}/K_n \tag{2.4}$$

where K_n is the calibrated injector flow mass characteristic factor in DCU by using normal injectors.

2.4.5   Urea Flow Model based on Pump Speed

The pumping urea flow dynamic based on the pump speed is expressed by the following equation.

$$\dot{U}_a = \omega \cdot \rho \cdot D \cdot \eta(P, \omega) \tag{2.5}$$

where U_a is the pumped urea flow mass, ω the motor speed, D the piston displacement of the pump, $\eta(P, \omega)$ the pump volumetric efficiency approximately equal to one, ρ the urea density.

When there is no injection and the urea dosing system is operating on steady state, which is called idle state, the pumped urea flow equals to return flow through the throttle based on the mass balance expressed by the equation below.

$$\dot{U}_{re,idle} = \dot{U}_{a,idle} = \omega_{idle} \cdot \rho \cdot D \cdot \eta(P, \omega) \tag{2.6}$$

where $U_{re,idle}$ is the return urea flow mass at idle state, $U_{a,idle}$ the pumped urea flow mass at idle state, ω_{idle} the motor speed at idle state.

2.4.6   Urea Injection Model based on Urea Flow Model

Based on the mass balance, the pumped urea mass equals to the sum of return urea flow mass and urea injection mass when the urea dosing system operates on the steady state after the injection starts.

$$
\begin{aligned}
\dot{U}_a &= \dot{U}_{re} + \dot{U}_{inj} \\
&= (\omega_{idle} + \Delta\omega) \cdot \rho \cdot D \cdot \eta(P,\omega) \quad = \omega \cdot \rho \cdot D \cdot \eta(P,\omega)
\end{aligned}
\tag{2.7}
$$

where U_{re} is the return urea flow mass when there are urea injections, $\Delta\omega$ the error of motor speed between idle state and the urea injection state. Assuming that U_{re} equals to $U_{re,idle}$ at steady state, the urea injection can be expressed by the following equation,

$$
\dot{U}_{inj} = \Delta\omega \cdot \rho \cdot D \cdot \eta(P,\omega)
\tag{2.8}
$$

Equation (2.8) is the current urea injection during the lifetime. When the injector is normal, the urea injection can be expressed in the following equations,

$$
\dot{U}_{inj,n} = \Delta\omega_n \cdot \rho \cdot D \cdot \eta(P,\omega)
\tag{2.9}
$$

where $U_{inj,n}$ is the urea injection when the injector is normal, $\Delta\omega_n$ error of motor speed between idle state and the urea injection state when the injector is normal. When the injector is new and the calibration is correct, the current urea injection equals to the normal urea injection at the same urea injection command. However, when the injector is old and changes during the lifetime, the current urea injection may not equal to the normal urea injection. Therefore, the under-dosing and overdosing of urea injection should be detected and corrected for urea dosing control.

2.5 Problems and Objective of Detection of Urea Injection

During life time, the effective area of the urea injector nozzle and the factor K may change, leading to inaccurate injection command calculated in DCU. If the injector is blocked, the effective area of the urea injector nozzle turns smaller and the real K is smaller than the K_n in DCU, leading to under-dosing injection. On the other hand, when the effective area of the urea injector nozzle turns larger, the real K is larger than the K_n in DCU, leading to overdosing injection. Therefore, it is necessary to detect under-dosing and overdosing of injection and correct the factor K_n.

2.5.1 Definition of Correction Factor

To detect and correct the inaccuracy of the urea injection, the correction factor needs to be defined. The definition of correction factor k_{cf} can be expressed below,

$$k_{cf} = \frac{\dot{U}_{inj}}{\dot{U}_{inj,n}} = \frac{U_{inj,cyc}/r_{vlv,dyc}}{U_{inj,cyc,n}/r_{vlv,dyc}} = \frac{K}{K_n} \tag{2.10}$$

If the correction factor is identified, the current urea injector flow mass characteristic factor K can be calculated by the following equation,

$$K = k_{cf} * K_n \tag{2.11}$$

According to the definition of the correction factor and the urea injection model based on urea flow model (see equation (2.8), and (2.9)), the expression of correction factor

can be turned into the following equation,

$$k_{cf} = \frac{\dot{U}_{inj}}{\dot{U}_{inj,n}} = \frac{\Delta\omega}{\Delta\omega_n} \tag{2.12}$$

However, there is no speed sensor in the SCR system, making it unfeasible to directly use this equation. In this paper, two different indirect methods are proposed to address this issue.

2.5.2   Objective of Detection and Correction

The objective is to detect the overdosing or under-dosing of urea injection mass and identify the correction factor. It is difficult to calculate the correction factor directly since the flow mass sensor and speed sensors are unavailable to be used in the SCR system. To address this issue, indirect methods are explored to detect the urea injection mass. Based on the principle of urea dosing system, three factors (pumped urea, return urea, and injected urea) cause the variation of the line pressure. Also, the frequency of these three factors are different, referring that signal processing methods can extract useful information to estimate current urea injection mass. The magnitude under fundamental frequency (injection frequency) is used to demonstrate the urea injection mass and detect under-dosing or overdosing in [5]. However, this method cannot satisfy the urea dosing system in this paper based on the experimental analysis demonstrated in Figure 2.5. Therefore, this paper proposed two different methods to detect the urea injection mass indirectly and correct the urea injector flow mass characteristic factor K (the ratio of urea injection mass to injection control duty cycle) in DCU. These two new different methods are proposed based on the pumped urea, which equals to the sum of the return urea and injected urea when the urea
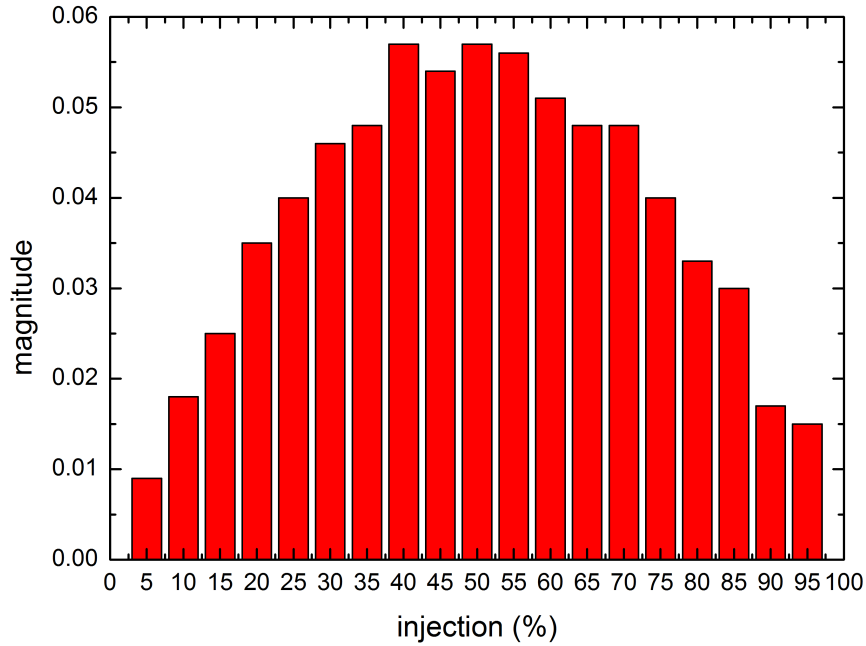
Figure 2.5: Magnitude of line pressure at different injections based on frequency analysis.

dosing system is operating on steady state.

2.6   Detection of Urea Injection Mass based on Urea Pump Frequency

This section proposed a method to detect the urea injection mass based on the urea flow model and urea pump frequency. To address the issue that it cannot directly measure the pump speed, a frequency extraction method is used to extract the urea pump frequency through frequency analysis of line pressure. The detection and correction of urea injection are based on the pump frequency.

2.6.1   Identification of the Correction Factor

In this paper, a frequency extraction method is used to extract the urea pump frequency through frequency analysis of line pressure. Based on the urea pump frequency, the correction factor can be expressed by the following equation,

$$k_{cf} = \frac{\Delta\omega}{\Delta\omega_n} = \frac{\Delta f}{\Delta f_n} = \frac{\Delta f/r_{vlv,dyc}}{\Delta f_n/r_{vlv,dyc}} = \frac{K_\omega}{K_{\omega,n}} \tag{2.13}$$

Where $K_{\omega,n}$ is the linear slope of Δf_n to $r_{vlv,dyc}$ when the injector is normal, K_ω the current slope of Δf to $r_{vlv,dyc}$, Δf_n is the urea pump frequency extracted from the frequency analysis when the injector is normal, Δf the urea pump frequency extracted from the frequency analysis. To eliminate the stochastic error, linear fit method is used.

2.6.2   Extraction of Pump Frequency through Frequency Analysis of Line Pressure
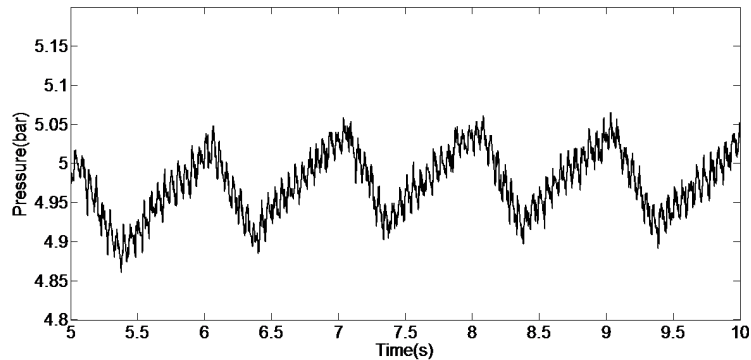
Figure 2.6: Pressure signal sampled from urea dosing system

Figure 2.6 is the line pressure signal through the pressure sensor, which is massively

used in the production SCR systems. To understand the frequency characteristics of
the pressure signal, the Fast Fourier Transform (FFT) method is used. The spec-
trum of the line pressure is demonstrated and different fundamental frequencies can
be seen in Figure 2.7. The fundamental frequency of injection is 1Hz and the urea
pump frequency is from 15 Hz to 30 Hz, depending on the operating conditions. As
can be seen in Figure 2.7, one fundamental frequency is 1Hz and another fundamen-
tal frequency is about 19 Hz. Based on the principle of urea dosing system, 1 Hz
fundamental frequency is caused by the urea injection events and 19 Hz fundamental
frequency is produced by the urea pump events, which can be used to calculate the
urea pump speed. Fundamental frequency of urea pump events can be used to calcu-
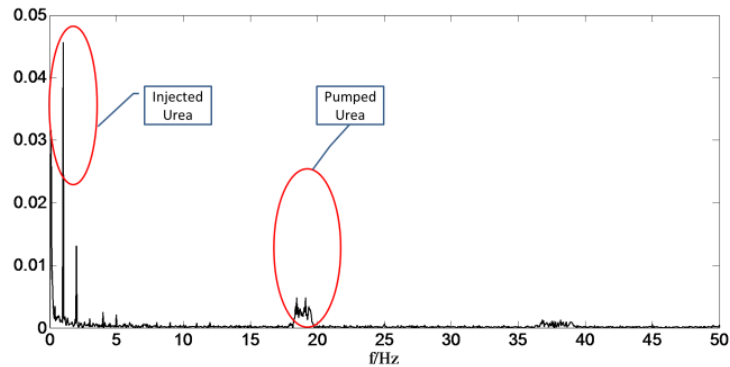
Figure 2.7: The spectrum of line pressure

late the pump speed. Therefore, it is necessary to extract the urea pump frequency
from the spectrum of line pressure. Figure 2.8 demonstrates different urea pump
frequencies over different injection conditions, which are extracted from the spectrum
of line pressure. We can see from Figure 2.8 that frequencies of urea pumping over
different injections (from 5% injection to 95% injection) increase and the increasing
rate is approximately a constant value. Therefore, the frequency of urea pumping

rate can be used to estimate and detect the urea injection mass.
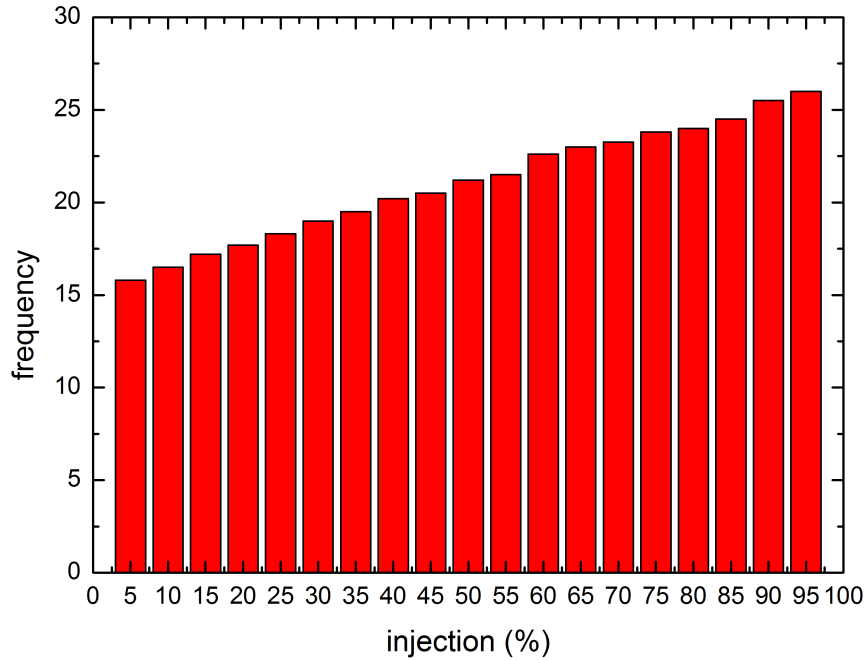
Figure 2.8: The relation between pump frequency and duty cycle of injections

2.6.3 Identification of Correction Factor through the Pump Frequency

Two different experiment cases including normal injector case and blocked injector case were done. The normal injector case is that the injector is normal while the blocked injector case is that the injector is blocked partially. The injection mass in the blocked injector case is lower than that in the normal cases at the same injection command from the DCU. The frequencies of the urea pump event in both cases are demonstrated in Figure 2.9. As can be seen from Figure 2.9, the trends of the frequencies in both cases are the same, while the slope of the normal case is higher than that of the blocked injector case, which means that the frequency of the blocked

injector case is lower than that of normal case due to less urea injection mass at the same injection control command. Through the comparison between the normal case
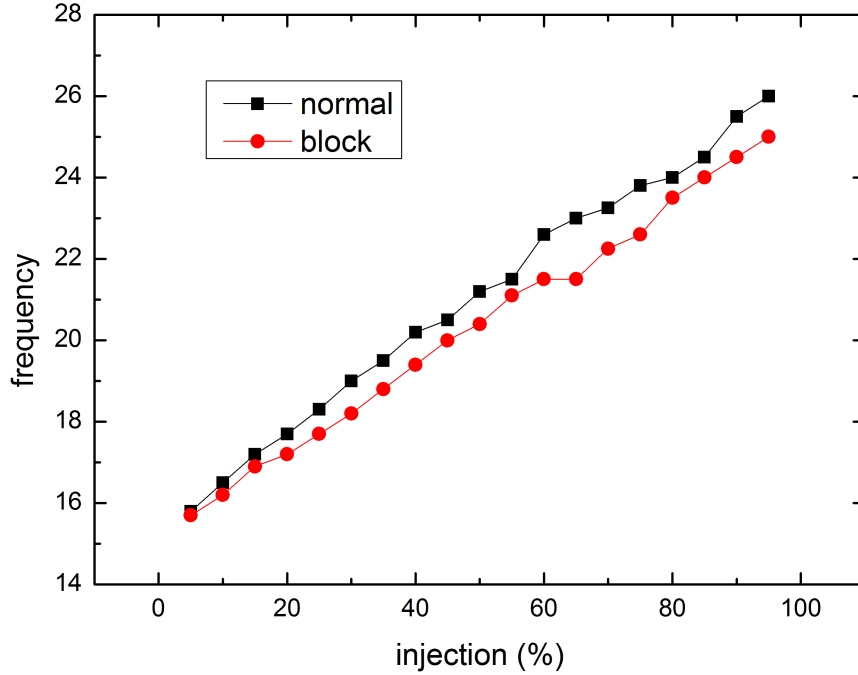
Figure 2.9: The comparison of pump frequency between Block case and Normal case

and block case, the frequencies of the urea pumping rate can be used for diagnosis of urea under-dosing or overdosing, and correction of the injection command. Based on the equation (2.13), the correction factor can be calculated from the linear relation between the frequency differences and the injection duty cycle. From Figure 2.10, the correction factor can be identified through the slope $K_{\omega,n}$ (normal case) and K_ω (blocked case), which can be calculated by using the linear fit method. Furthermore, under-dosing injection is detected since K_ω is lower than $K_{\omega,n}$.
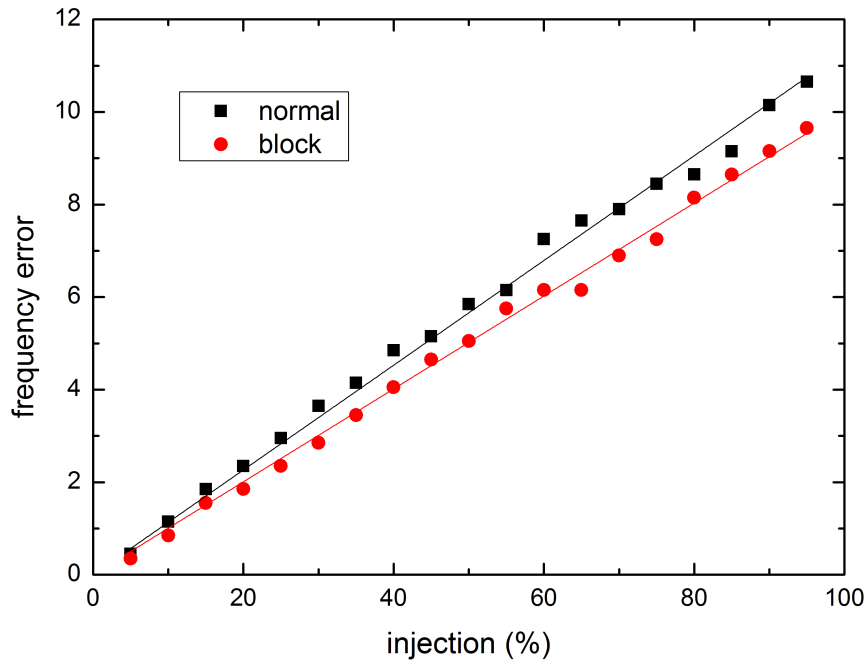
Figure 2.10: The comparison of pump frequency between Block case and Normal case

2.7 Detection of Urea Injection Mass based on Effective Voltage of the Motor

This section proposed another method to estimate the urea injection mass based on the pump model and motor dynamic model. To avoid the impact of variation of the battery voltage, the detection and correction of urea injection is based on the effective voltage of the motor rather than the motor PWM duty cycle.

2.7.1 Pump Model with Motor Dynamics

The motor used in urea dosing system is a brushless DC motor, and can be modeled by using the following equations,

$$
\begin{aligned}
\frac{di}{dt} &= -\frac{R_a}{L_a}i - \frac{K_v}{L_a}\omega + \frac{V_a}{L_a} \\
\frac{d\omega}{dt} &= \frac{K_t}{J}i - \frac{B}{J}\omega - \frac{T_L}{J}
\end{aligned}
\tag{2.14}
$$

Where J is the moment of inertia for the motor load, B the viscous friction, ω the motor speed, L the inductance, V_a is the voltage proportional to motor PWM duty cycle $V_a = V_0 * PWM_{moto,dyc}$, T_L the load for the motor, which is proportional to the line pressure $T_L = f(P) = const$. When the system is operating on the steady state, the motor speed can be expressed in the following equation,

$$
\omega = \frac{V_a K_t - R_a T}{R_a B + K_v K_t}
\tag{2.15}
$$

Then the relation between the motor speed and motor PWM duty cycle can be expressed by the following equation,

$$
\omega = mV_0 * PWM_{moto,dyc} + f_0(P)
\tag{2.16}
$$

where $m = \frac{K_t}{R_a B + K_v K_t}$. When there is no injection, the urea dosing system is operating on idle state and the pump speed can be expressed by the following equations.

$$
\omega_{idle} = mV_0 * PWM_{moto,dyc,idle} + f_0(P)
\tag{2.17}
$$

where $PWM_{moto,dyc,idle}$ is the duty cycle of motor control command when there is no injection. Based on the mass balance, the pumped urea equals to the sum of return flow and urea injection. When the injection starts and it is on the steady state, the urea injection mass can be expressed by the following equations,

$$
\begin{aligned}
\dot{U}_{inj} &= \Delta\omega \cdot \rho \cdot D \cdot \eta(P,\omega) \\
&= mV_0 * \Delta PWM_{moto,dyc} \cdot \rho \cdot D \cdot \eta(P,\omega)
\end{aligned}
\tag{2.18}
$$

2.7.2 Identification of the Correction Factor

According to the definition of the correction factor and the pump model with motor dynamics, when the battery voltage is stable at V_0, the expression of correction factor can be turned into the following equation,

$$
k_{cf} = \frac{\dot{U}_{inj}}{\dot{U}_{inj,c}} = \frac{\Delta PWM_{moto,dyc}}{\Delta PWM_{moto,dyc,n}} = \frac{\Delta PWM_{moto,dyc}/r_{vlv,dyc}}{\Delta PWM_{moto,dyc,n}/r_{vlv,dyc}}
\tag{2.19}
$$

To eliminate the stochastic error, linear fit method is used and the correction factor can be expressed by the following equation,

$$
k_{cf} = \frac{\Delta PWM_{moto,dyc}/r_{vlv,dyc}}{\Delta PWM_{moto,dyc,n}/r_{vlv,dyc}} = \frac{K_{\Delta PWM}}{K_{\Delta PWM,n}}
\tag{2.20}
$$

where $K_{\Delta PWM,n}$ is the linear slope of $\Delta PWM_{moto,dyc}$ to $r_{vlv,dyc}$ when the injector is normal, $K_{\Delta PWM}$ the current slope of $\Delta PWM_{moto,dyc}$ to $r_{vlv,dyc}$.

Through the comparison between the normal case and block case, based on the equation (2.20), the correction factor can be calculated from the linear relation between the duty cycle error of Motor and the injection duty cycle. From Figure 2.11,

the correction factor can be identified through the slope $K_{\Delta PWM,n}$ (normal case) and $K_{\Delta PWM}$ (blocked case), which can be calculated by using the linear fit method. However, the battery voltage always varies in the vehicle. The variation of correction
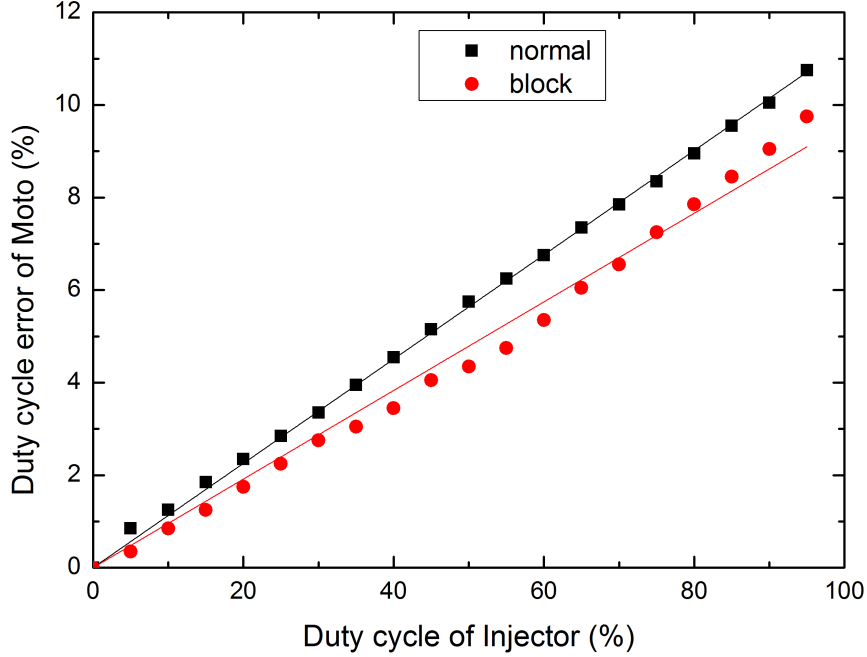
Figure 2.11: The relation between duty cycle of Motor and duty cycle of injection

factor may be very large even though the battery voltage has a small variation. Figure 2.12 demonstrated that the linear slope of $\Delta PWM_{moto,dyc}$ to $r_{vlv,dyc}$ varies when the battery voltage varies. To address the problem that the linear slope of $\Delta PWM_{moto,dyc}$ to $r_{vlv,dyc}$ varies when the battery voltage varies, the battery voltage V_0 requires to be taken into account. If the variation of battery voltage cannot be ignored, the expression of correction factor can be turned into the following equation,

$$
\begin{aligned}
k_{cf} &= \frac{\dot{U}_{inj}}{\dot{U}_{inj,c}} = \frac{V_0 * \Delta PWM_{moto,dyc}}{V_0 * \Delta PWM_{moto,dyc,n}} \\
&= \frac{V_{eff}/r_{vlv,dyc}}{V_{eff,n}/r_{vlv,dyc}}
\end{aligned}
\tag{2.21}
$$
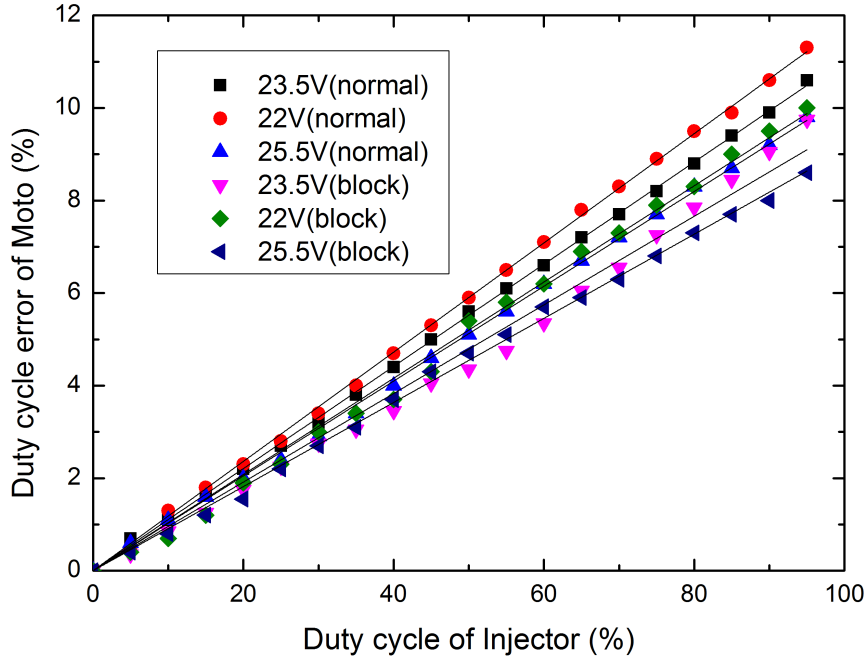
Figure 2.12: The relation between duty cycle of Motor and duty cycle of injection over different battery voltage

To eliminate the stochastic error, linear fit method is used and the correction factor can be expressed by the following equation,

$$k_{cf} = \frac{V_{eff}/r_{vlv,dyc}}{V_{eff,n}/r_{vlv,dyc}} = \frac{K_{V_{eff}}}{K_{V_{eff,n}}} \tag{2.22}$$

where $K_{V_{eff,n}}$ is the linear slope of $V_{eff,n}$ to $r_{vlv,dyc}$ when the injector is normal, $K_{V_{eff}}$ the current slope of V_{eff} to $r_{vlv,dyc}$.

Through the comparison between the normal case and block case, based on the equation (2.22), the correction factor can be calculated from the linear relation between the effective battery voltage and the injection duty cycle. From Figure 2.13, the correction factor can be identified through the slope $K_{V_{eff,n}}$ (normal case) and $K_{V_{eff}}$ (blocked case), which can be calculated by using the linear fit method. Also,

Under-dosing injection is detected since $K_{V_{eff}}$ is lower than $K_{V_{eff},n}$. Although battery voltage varies, the slope of the $K_{V_{eff},n}$ (normal case) among different battery voltages are the same and the $K_{V_{eff}}$ (blocked case) among different battery voltages are almost the same, which means that the identification of the correction factor and the under-dosing detection are more robust than that of PWM duty cycle of motor used only.
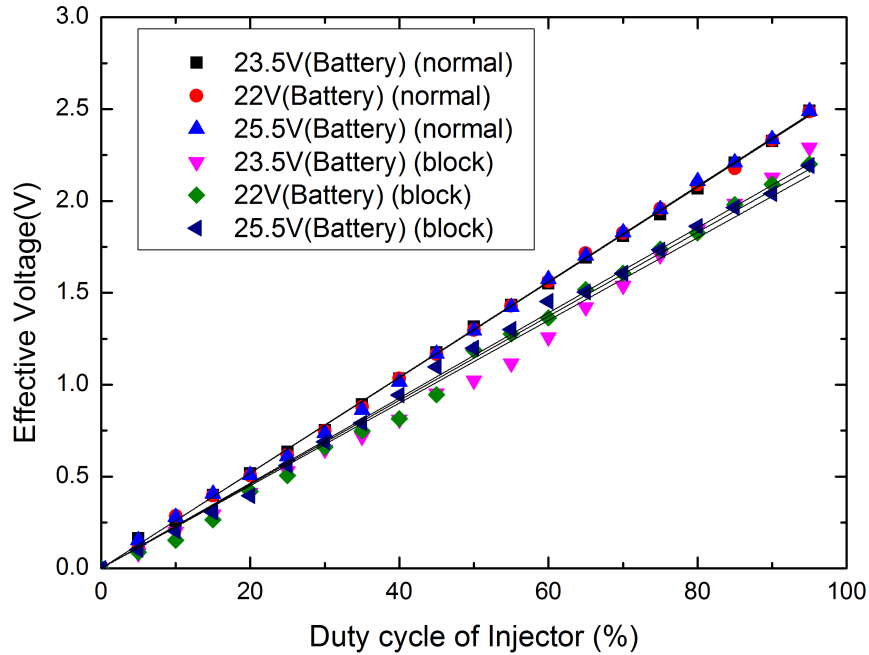
Figure 2.13: The relation between effective voltage and duty cycle of injection

2.8   Summary/Conclusions

Based on the urea injection model and control command in the DCU, a correction factor is defined and identified for the detection and correction of the urea injection. Two different methods are proposed to detect current urea injection mass and identify

the correction factor. First method is based on the pump frequency extracted from the frequency analysis of line pressure by FFT method. Through the comparison between the normal injector case and blocked injector case, the correction factor is identified based on the urea pump frequency by linear fit method. Second method to identify the correction factor is based on the motor dynamic model. The relation between motor speed and effective voltage of motor is revealed when the system is operating on steady state. Through the comparison between the normal injector case and blocked injector case, the correction factor identified by the effective battery voltage is more robust than that of PWM duty cycle used only. Both methods can detect the under-dosing or overdosing injection and identify the correction factor. In the future, the combination of both method will be explored to enhance the robustness of the detection and correction, and implement the algorithm on line in the DCU.

Reference

[1] World Health Organization, WHO Air Quality Guidelines for Particulate Matter, Ozone, Nitrogen Dioxide, and Sulfur Dioxide: Global Update 2005, Geneva, Switzerland: WHO Press, Chap.12, 2006.

[2] Backman, H., Arve, K., Klingstedt, F., and Murzin, D. Y., "Kinetic considerations of H2 assisted hydrocarbon selective catalytic reduction of NO over Ag/Al2O3: II. Kinetic modeling," Applied Catalysis, Vol. 304, pp. 86-92, 2006.

[3] Hsieh, M.F. and Wang, J., "An Extended Kalman Filter for Ammonia Coverage Ratio and Capacity Estimations in the Application of Diesel Engine SCR Control and Onboard Diagnosis." American Control Conference, 2010.

[4] Johnson, T. V., "Review of Diesel emissions and control," SAE Technical paper 2010-01-0301, 2010.

[5] Shost, Mark, Noetzel J., Wu M.C., Sugiarto T., Bordewyk T., Fulks G., and Fisher G. B., "Monitoring, Feedback and Control of Urea SCR Dosing Systems for NOx Reduction: Utilizing an Embedded Model and Ammonia Sensing." No. 2008-01-1325. SAE Technical Paper, 2008.

[6] Hofmann, Lothar, Rusch K., Fischer S., and Lemire B., "Onboard emissions

monitoring on a HD truck with an SCR system using NOx sensors." No. 2004-01-1290. SAE Technical Paper, 2004.

[7] Sun, Y., Wang, Y.Y., Cheng, C. and Levijioki, S., "Detection of Urea Injection System Faults for SCR system," SAE Technical paper 2012-01-0431, 2012.

[8] Wang, Y.Y., Sun, Y. and Gady, K., "Model-Based Estimation of Injected Urea Quantity and Diagnostic for SCR Urea Injection System," American Control Conference, 2012.

Chapter 3

Robust Nonlinear Disturbance Observer Design for Estimation of Ammonia Storage Ratio in Selective Catalytic Reduction Systems

3.1 Citation and Main Contributor

Jinbiao Ning, and Fengjun Yan. "Robust Nonlinear Disturbance Observer Design for Estimation of Ammonia Storage Ratio in Selective Catalytic Reduction Systems." Journal of Dynamic Systems, Measurement, and Control 137, no. 12 (2015): 121012.

The main contributor to this paper is the first author-Jinbiao Ning (contributes

more than 70%).

3.2   Abstract

Urea-based selective catalytic reduction (SCR) system is a promising way to obtain high NO_x reduction and commonly adopted in Diesel engine after-treatment systems. The ammonia storage ratio is critical for SCR feedback control but it is difficult to be directly measured by sensors. This paper aims to effectively estimate the ammonia storage ratio on line and reduce the cost of using ammonia sensors. In the proposed method, the ammonia storage ratio is treated as an external disturbance in the NO_x dynamic model and estimated by the Nonlinear-Disturbance-Observer methods. Furthermore, to reduce estimation errors of ammonia storage ratio caused by the high-frequency measurement noises, a novel robust Nonlinear Disturbance Observer (robust NDO) is proposed and compared with a typical design method (regular NDO). Both the NDOs are developed based on part of the three-state SCR model and cost-effective since NO_x sensors are used only. The stability and noise attenuation properties of both estimations were also analyzed in the paper. The simulation results based on the full-vehicle simulator of FTP-75 test demonstrate that the regular NDO and the robust NDO can effectively estimate the ammonia storage ratio even in cases where ammonia cross-sensitivity affects response. Among the two observers, the robust NDO has better noise attenuation properties.

3.3   Introduction

Due to high fuel efficiency and good durability, Diesel engines are commonly used in automobile applications. However, their lean-burn combustion conditions lead to high NO_x emission which contributes to acid rain and smog formation, and has been linked to incidence rates for respiratory tract irritation, infection, asthma, and so on [1]. Although some advanced engine control technologies can reduce engine-out NO_x, given the tight NO_x emission regulation and the fuel economy impacts NO_x after-treatment systems have, NO_x after-treatment systems play a key role in NO_x control [2]. Selective Catalytic Reduction (SCR) as one of the most promising technologies for NO_x reduction is used by many new production medium- and heavy-duty vehicles [3].

The engine-out NO_x is reduced by chemically reacting with the ammonia on the catalytic surface of SCR system. It is challenging to balance the ammonia slip and NO_x reduction efficiency due to the following two reasons. On one hand, too much ammonia input can obtain high NO_x reduction efficiency but result in high ammonia slip which is limited in the stringent regulations. On the other hand, less ammonia input leads to low NO_x reduction efficiency such that the emission regulations cannot be satisfied. It has been pointed out that the ammonia storage ratio is related to the ammonia slip and NO_x reduction efficiency in the SCR systems. However, it is difficult to be directly measured due to no available on-board sensors, although some methods and equipment were studied in the laboratory [15]. Therefore, the estimation of ammonia storage ratio plays significant role in SCR feedback control.

Several sliding mode observers were developed in [4] and discrete-time smooth variable structure estimator was proposed in [5] to estimate the ammonia storage

ratio in SCR system by using NO_x sensors and ammonia sensors. However, ammonia sensors are very expensive and not available for mass product after-treatment systems. Sensor reduction is necessary and possible for SCR estimation and feedback control. A cost-effective robust approach was proposed in [6] to estimate the states of SCR system by dual NO_x sensors after the SCR system without any ammonia sensors. Furthermore, the NO_x sensor is widely used for SCR feedback control [14] and required for OBD regulations. However, the high-frequency noises are commonly involved in the sensor measurement. Robust ammonia storage ratio estimation methods that can attenuate the influence of such noise are therefore desired.

In this paper, a robust Nonlinear Disturbance Observer is proposed for ammonia storage ratio estimation and compared with a regular Nonlinear Disturbance Observer. The novel method is motivated by the robust disturbance observer techniques in [7, 8] and improved from the regular Nonlinear Disturbance Observer (regular NDO) design [9, 10]. Nonlinear Disturbance Observer is widely used in Disturbance Observer Based Control (DOBC) [9–11, 20, 21]. The contributions of this paper are: 1) The ammonia storage ratio is treated as an external disturbance and estimated by the proposed novel robust Nonlinear Disturbance Observer based on part of the three-state SCR model. 2) The stability analysis of the robust estimation approach based on the nonlinear disturbance observer is demonstrated. 3) It is a potential cost-effective approach to estimate the ammonia storage ratio since the NO_x sensor is used only, avoiding the use of expensive and unreliable ammonia sensors.

The rest of the paper is organized as follows. The SCR principle, the three-state SCR model, and the problem formulation are demonstrated in section 3.4. Two different Nonlinear Disturbance Observer design for estimating the ammonia storage

ratio are presented in section 3.5. The effectiveness of the estimation methods are validated through high-fidelity full-vehicle simulator in section 3.6. Conclusion is given in section 3.7.

3.4 The Modeling of SCR System and Problem Formulation

This section presents the brief introduction of the principle of the SCR system and the problem formulation.

The SCR system as part of the after-treatment system is located in the exhaust gas pipe of Diesel engines. As can be seen from Figure 3.1, NO_x reduction reactions occur when the exhaust gas of the engine goes through the SCR system. The 32.5% aqueous urea solution, also called AdBlue, is used as the source of ammonia for SCR system in vehicle applications. From urea injection to NO_x reduction reactions in urea-based SCR system, three events are mainly included. Firstly, the AdBlue is injected at upstream of the SCR system by the dosing unit and converted to ammonia. Secondly, when entering the SCR system, the ammonia is partially adsorbed by the substrate of the catalyst. Finally, the ammonia adsorbed on the substrate reacts with NO_x and convert them to N_2 and H_2O.
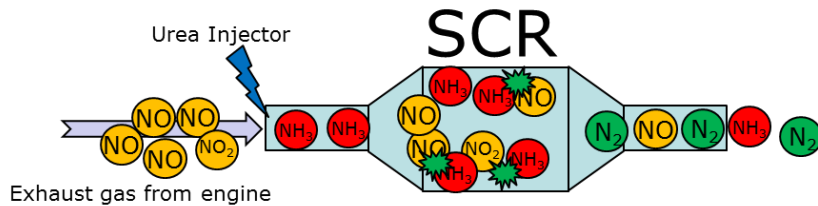
Figure 3.1: Urea base SCR system for Diesel engines

3.4.1   The Principle of Selective Catalytic Reduction System

AdBlue to Ammonia

AdBlue is injected into the exhaust pipe and converted to ammonia if the conditions satisfy the conversion requirement. The conversion from AdBlue to ammonia includes mainly three steps: evaporation, decomposition, and hydrolyzation [16]. The reactions are shown in (3.1), (3.2), (3.3), respectively.

a) AdBlue evaporation:

$$NH_3CONH_3(liquid) \rightarrow NH_2CONH_2* + xH_2O \tag{3.1}$$

b) Urea decomposition:

$$NH_2CONH_2* \rightarrow HNCO + NH_3 \tag{3.2}$$

c) Isocyanic acid (HNCO) hydrolyzation:

$$HNCO + H_2O \rightarrow CO_2 + NH_3 \tag{3.3}$$

It has been demonstrated that the above reactions generally start if the exhaust gas temperature is above 200 $°C$ and reach a maximum reaction rate around 350 $°C$ [17]. When the exhaust gas temperature is less than 200 $°C$, several byproducts such as cyanuric acid, biuret, melamine, ammelide and ammeline as deposits on pipe wall can be generated by the urea decomposition reaction [18], which is a main issue that affects the low temperature performance of SCR system. The concentration of ammonia into the SCR system can be measured by an ammonia sensor or predicted

by the AdBlue injection rate.

Ammonia Adsorption/Desorption

When the ammonia enters the SCR system, it can be adsorbed on the catalyst substrate and the adsorbed ammonia can be desorbed from the substrate, which can be expressed by the following reaction [3].

$$NH_3 + \theta \leftrightarrow NH_3{}^* \tag{3.4}$$

where θ is the free SCR substrate site (not covered by NH_3). The reaction rates of the ammonia adsorption and desorption can be expressed as below [12].

$$R_{ads} = k_{ads} \exp(-\frac{E_{ads}}{RT}) C_{NH_3} (1 - \theta_{NH_3}) \tag{3.5}$$

$$R_{des} = k_{des} \exp(-\frac{E_{des}}{RT}) \theta_{NH_3} \tag{3.6}$$

where R_{ads} and R_{des} represent the chemical reaction rate (mole/sec); T is temperature (K); k_{ads}, k_{des}, E_{ads}, E_{des} and R are constants; C_{NH_3} is the concentration of NH_3 $(mole/m^3)$; and θ_{NH_3} is the ammonia surface coverage ratio [3] defined by,

$$\theta_{NH_3} = \frac{M_{NH_3}{}^*}{\Theta} \tag{3.7}$$

where $M_{NH_3}{}^*$ is the mole number of ammonia stored in the SCR substrate and Θ is the ammonia storage capacity (mole) which is temperature dependent, $\Theta = S_1 e^{-S_2 T}$. This means that less ammonia can be stored in the catalyst if temperature is higher and less ammonia can react with NO_x, which will easily lead to higher NH_3 slip.

Importantly, the adsorbed ammonia can be oxidized to NO when the temperature is higher than 450 $°C$. Based on the assumptions that reaction rates of SCR system are assumed to be a function of the gas phase concentration of NO_x and ammonia storage [22], the ammonia oxidation can be described by the following expressions [3].

$$NH_3 + 1.25O_2 \rightarrow NO + 1.5H_2O \tag{3.8}$$
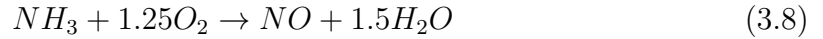
$$R_{oxi} = k_{oxi} \exp(-\frac{E_{oxi}}{RT})\theta_{NH_3} \tag{3.9}$$

NO_x Reduction

NO_x reduction reactions are the main reactions in the SCR system. When entering the SCR converter, the NO_x can catalytically react with the adsorbed ammonia and be converted to N_2 according to the following reactions [3, 22].

$$4NH_3 + 4NO + O_2 \rightarrow 4N_2 + 6H_2O \tag{3.10}$$

$$2NH_3 + NO + NO_2 \rightarrow 2N_2 + 3H_2O \tag{3.11}$$

$$4NH_3 + 3NO_2 \rightarrow 3.5N_2 + 6H_2O \tag{3.12}$$
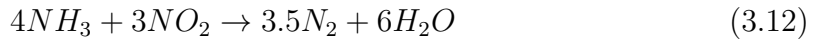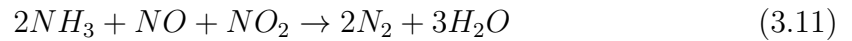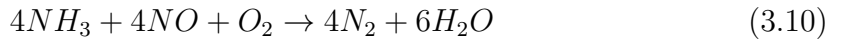
Since more than 90% of the engine-out NO_x is usually NO [12], the reaction (3.10) is considered as the dominant reaction in NO_x reduction and called "standard SCR". Similarly, the reaction (3.11) and (3.12) are called "fast SCR" and "slow SCR", respectively according to their reaction rates. The NO_x reaction rate is showed in

the following reaction,

$$R_{red} = k_{red} \exp(-\frac{E_{red}}{RT}) C_{NO} \theta_{NH_3} \tag{3.13}$$

3.4.2 Three-state SCR Model

Based on the molar balance, the main SCR dynamics can be described by the following equations [12],

$$\begin{cases} \dot{C}_{NO} = \Theta(R_{oxi} - R_{red}) \\ \dot{\theta}_{NH_3} = R_{ads} - R_{des} - R_{red} - R_{oxi} \\ \dot{C}_{NH_3} = \Theta(R_{des} - R_{ads}) \end{cases} \tag{3.14}$$

Based on Continuous Stirred Tank Reactor (CSTR) approach and mass conservation law, the SCR model is developed by using the above dynamic equations. A simple but sufficient accurate model presented and validated in [12] was adopted and expressed by the following equations.

$$\begin{cases} \dot{C}_{NO} = -C_{NO}\left(\Theta r_{red}\theta_{NH_3} + \frac{F}{V}\right) + \theta_{NH_3}\Theta r_{oxi} + \frac{F}{V}C_{NO,in} \\ \dot{\theta}_{NH_3} = -\theta_{NH_3}\left(r_{ads}C_{NH_3} + r_{des} + r_{red}C_{NO} + r_{oxi}\right) + r_{ads}C_{NH_3} \\ \dot{C}_{NH_3} = -C_{NH_3}\left(\Theta r_{red}\theta_{NH_3} + \frac{F}{V}\right) + \theta_{NH_3}\Theta r_{oxi} + \frac{F}{V}C_{NH_3,in} \end{cases} \tag{3.15}$$

where $r_x = k_x \exp(-\frac{E_x}{RT})$, $x = red, oxi, ads, des$; C_{NO}, C_{NH_3} are the tailpipe NO_x and ammonia concentrations; $C_{NH_3,in}$ is the pre-SCR ammonia concentration; U_{Adblue} is the input of AdBlue controlled by the SCR controller; $C_{NO,in}$ is the engine exhaust NO_x concentration; F is exhaust volume flow rate; and V is SCR catalyst volume.

3.4.3   Problem Formulation and Design Objective

Full-state estimation of the SCR system in [19] was designed based on the equations (3.15). However, four sensors (two ammonia sensors and two NO_x sensors) are required to sense the concentration of NO_x and ammonia before and after the SCR system, as can be seen in Figure 3.2. The high cost makes it unpractical for mass production uses. To reduce the use of the NO_x sensors and improve the robustness of the
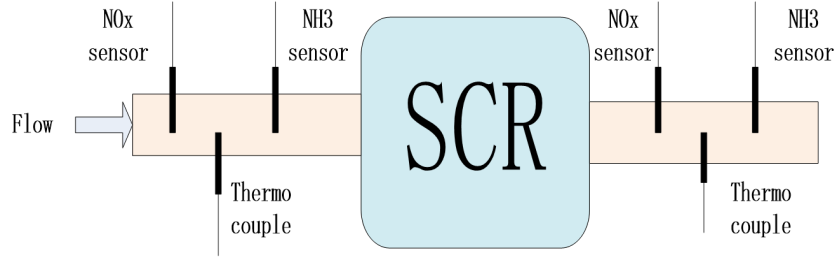
Figure 3.2: Sensors for SCR system

estimation, the sliding mode observer [4] and discrete-time smooth variable structure estimator [5] were proposed based on part of the three-state model as below,

$$
\begin{cases}
\dot{\theta}_{NH_3} = -\theta_{NH_3}\left(r_{ads}C_{NH_3} + r_{des} + r_{red}C_{NO} + r_{oxi}\right) + r_{ads}C_{NH_3} \\
\dot{C}_{NH_3} = -C_{NH_3}\left(\Theta r_{red}\theta_{NH_3} + \frac{F}{V}\right) + \theta_{NH_3}\Theta r_{oxi} + \frac{F}{V}C_{NH_3,in}
\end{cases}
\tag{3.16}
$$

However, the ammonia sensors are still used in both methods, which are very expensive and unavailable to use in production after-treatment systems. To reduce exhaust gas sensors and avoid using ammonia sensors, in Figure 3.3, one NO_x sensor before the SCR system and one or two different NO_x sensors after the SCR system are applied to estimate the ammonia storage ratio. Also, the objective of this approach is to estimate the ammonia storage ratio by using NO_x sensor only. Therefore, partial three-state model is required to estimate the ammonia storage ratio based on the
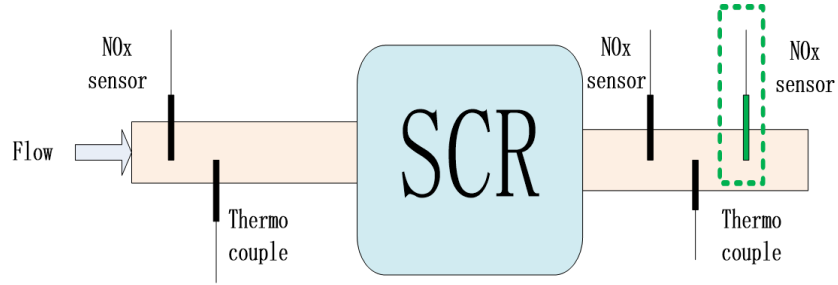
Figure 3.3: NO_x Sensors only for SCR system

NO_x dynamic model in the following,

$$\dot{C}_{NO} = -C_{NO} \left(\Theta r_{red}\theta_{NH_3} + \frac{F}{V} \right) + \theta_{NH_3}\Theta r_{oxi} + \frac{F}{V}C_{NO,in} \qquad (3.17)$$

Equation (3.17) shows that the NO_x sensor is required only to measure the NO_x concentration before and after the SCR system. However, it is very difficult to estimate the ammonia storage ratio directly by (3.17) since the ammonia storage ratio is not a state. Equation (3.17) can be converted to the following form,

$$\dot{x} = f(x) + g_1(x)u + g_2(x)d \qquad (3.18)$$

where $\begin{cases} x = C_{NO} \\ f(x) = -ax \\ g_1(x)u = au \\ g_2(x) = (b - cx) \\ d = \theta_{NH_3} \\ u = C_{NO,in} \\ a = \dfrac{F}{V}, b = r_{oxi}\Theta, c = \Theta r_{red} \end{cases}$, in which a, b, c are positive parameters. There-

fore, the ammonia storage ratio estimation is transformed into a NDO problem.

3.5 Nonlinear Disturbance Observer based Estimation of Ammonia Storage Ratio

The ammonia storage ratio estimation methods based on the nonlinear function of NO_x dynamic equation (3.18) are proposed in this section. In this section, two different nonlinear-disturbance-observer-based design methods are presented and their stability and noise attenuation properties are analyzed in details.

3.5.1 Regular Nonlinear Disturbance Observer

Design of Regular NDO

In the subsection, the design principle of the regular Nonlinear Disturbance Observer [9–11] is introduced.

Assumption 1: There exists a positive constant $\bar{d}$ such that the variation of the

disturbance is bounded as expressed below [10],

$$\left| \dot{d} \right| \leq \bar{d} \tag{3.19}$$

where $\bar{d}$ is an unknown positive constant.

Assumption 2: It is assumed that a smooth function $h(x)$ exists such that the relative degree from d to $h(x)$, r, is uniform well-defined for all x and t [10].

For a system in the following form [9–11], with **assumption 1** and **assumption 2**,

$$\begin{cases} \dot{x} = f(x) + g_1(x)u + g_2(x)d \\ y = h(x) \end{cases} \tag{3.20}$$

where $f(x)$, $g_1(x)$, $g_2(x)$, $h(x)$ are known functions, u is the input of the dynamic model, y is the measurement output, d is and unknown, time-varying disturbance, the regular Nonlinear Disturbance Observer can be designed by the following equations,

$$\begin{cases} \dot{z} = -l(x)g_2(x)z - l(x)(g_2(x)p(x) + f(x) + g_1(x)u) \\ \hat{d} = z + p(x) \end{cases} \tag{3.21}$$

where $p(x)$ and $l(x)$ are chosen as following equations,

$$\begin{cases} p(x) = K L_f^{r-1} h(x) \\ l(x) = \dfrac{\partial p(x)}{\partial x} \end{cases} \tag{3.22}$$

where r is the relative degree from the disturbance d to the output , $L_f^{r-1}h(x)$ is Lie derivatives [13].

Lemma 1: With **assumption 1** and **assumption 2**, there always exists an observer gain K so that the observer of equation (3.21) can be bounded-input-bounded-output (BIBO) stable.

Proof of **Lemma 1** can be seen in Appendix A of Ref. [10].

Remark 1: Let $n(x)$ denotes $L_{g_2} L_f^{r-1} h(x)$. The observer gain K should be determined to be positive when $n(x) > 0$ and to be negative when $n(x) < 0$; The disturbance estimation error can be bounded by choosing the observer gain K and the estimation error can be bounded in steady state as below,

$$\left| \frac{\bar{d}}{K * n_0} \right| \tag{3.23}$$

where $n_0 = \min_x |n(x)|$, is a positive scalar.

The Stability Analysis for Ammonia Storage Ratio Estimation

The ammonia storage ratio is treated as the external disturbance and estimated by the nonlinear disturbance observer. To guarantee that the estimation of ammonia storage ratio can converge to the real ammonia storage ratio in the SCR system, the **assumption 1**, **assumption 2**, and **remark 1** are required to be satisfied. In SCR system, the disturbance is the ammonia storage ratio and its dynamic is expressed below,

$$\dot{\theta}_{NH_3} = -\theta_{NH_3} \left(r_{ads} C_{NH_3} + r_{des} + r_{red} C_{NO} + r_{oxi} \right) + r_{ads} C_{NH_3} \tag{3.24}$$

where $r_{ads}, r_{des}, r_{red}, r_{oxi}$ are constants in SCR systems. θ_{NH_3} is the ammonia storage ratio and between 0 and 1 ($0 \leq \theta_{NH_3} \leq 1$) in SCR systems. C_{NH_3}, C_{NO} are the concentration of ammonia and NO_x measured by sensors and they are bounded in

SCR systems as expressed below,

$$\begin{cases} 0 < C_{NH_3} < \bar{C}_{NH_3} \\ 0 < C_{NO} < \bar{C}_{NO} \end{cases} \tag{3.25}$$

where $\bar{C}_{NH_3}$ and $\bar{C}_{NO}$ are positive values. Thus, the ammonia storage ratio is bounded as below,

$$\left| \dot{d} \right| = \left| \dot{\theta} \right| \leq \bar{d} \tag{3.26}$$

Therefore, it can be concluded the dynamic of the ammonia storage ratio in SCR systems can satisfy the **assumption 1**. In SCR systems, the measurement dynamic can be expressed by the following form,

$$y = h(x) = x \tag{3.27}$$

The relative degree can be calculated by equation (3.27) and $r = 1$, which satisfies the **assumption 2**. According to the regular nonlinear disturbance observer design, $n(x)$, $p(x)$ and $l(x)$ can be obtained by the following equations,

$$\begin{cases} n(x) = L_{g_2} L_f^{r-1} h(x) = g_2(x)x \\ p(x) = K L_f^{r-1} h(x) = Kx \\ l(x) = \dfrac{\partial p(x)}{\partial x} = K \end{cases} \tag{3.28}$$

To satisfy the **remark 1**, the observer gain K is chosen by the following equation,

$$K = k * sign(g_2(x)x), k > 0 \tag{3.29}$$

Therefore, the observer gain K is positive when $g_2(x)x > 0$ and negative when $g_2(x)x < 0$, which meets the **remark 1**. After all three conditions are satisfied, the observer error dynamics is BIBO (input-bounded-output-bounded) stable [10]. Thus, the parameter can be manually adjusted for the estimation of ammonia storage ratio.

Noise Attenuation Properties

In the SCR system, the measurement noise is common in the NO_x sensors. The measured state can be denoted by,

$$x_n = x + n \tag{3.30}$$

where n is the measurement noise. Based on equation (3.21) and (3.28), the estimated disturbance can be expressed as below,

$$\hat{d} = z + p(x_n) = z + K(x + n) \tag{3.31}$$

This means that the disturbance $\hat{d}$ estimated in equation (3.31) is contaminated by the high-frequency measurement noise, due to the term $K(x + n)$.

3.5.2   Robust Nonlinear Disturbance Observer

To address the noise attenuation problem in regular Nonlinear Disturbance Observer, a robust Nonlinear Disturbance Observer design is proposed, motivated by the robust design techniques in [7] and [8].

Design of Robust NDO

For the nonlinear system (3.18), with the assumptions that the disturbance d, 1st order derivative $\dot{d}$ and 2nd order derivative $\ddot{d}$ are bounded, the robust Nonlinear Disturbance Observer can be designed as following,

$$
\begin{cases}
\hat{d} = z + K\hat{x} \\
\dot{z} = -Kg_2(\hat{x})(z + K\hat{x}) - K(f(\hat{x}) + g_1(\hat{x})u) \\
\dot{\hat{x}} = g_2(\hat{x})\hat{d} + f(\hat{x}) + g_1(\hat{x})u - L(\hat{x} - x)
\end{cases}
\tag{3.32}
$$

where K, L are observer gains that we can choose to guarantee the estimated disturbance $\hat{d}$ can converge to d.

The Stability Analysis for Ammonia Storage Ratio Estimation

To guarantee the estimation of the ammonia storage ratio in the reasonable range, the estimation disturbance $\hat{d}$ is limited in the boundedness region. Based on the equation (3.18), the observer for SCR system can be transformed to the following form,

$$
\begin{cases}
\hat{d} = z + K\hat{x} \\
\dot{z} = -K(b - c\hat{x})(z + K\hat{x}) - K(-a\hat{x} + au) \\
\dot{\hat{x}} = (b - c\hat{x})\hat{d} - a\hat{x} + au - L(\hat{x} - x) \\
0 \leq \hat{d} \leq 1
\end{cases}
\tag{3.33}
$$

Denoting the estimation error of the disturbance as d_e, the 1st order derivative of d_e can be obtained by the following expression,

$$
\begin{aligned}
\dot{d}_e &= \dot{d} - \dot{\hat{d}} = \dot{d} - \dot{z} - K\dot{\hat{x}} \\
&= \dot{d} + Kg_2(\hat{x})z + K(Kg_2(\hat{x})\hat{x} + f(\hat{x}) + g_1(\hat{x})u) \\
&\quad - Kg_2(\hat{x})\hat{d} - Kf(\hat{x}) - Kg_1(\hat{x})u + KL(\hat{x} - x) \\
&= \dot{d} - KL\tilde{x}
\end{aligned}
\tag{3.34}
$$

where $\tilde{x}$ refers to $x - \hat{x}$, d_e refers to $d - \hat{d}$, $\dot{d}$ is the 1st order derivative of d. The 2nd order derivative of d_e can be obtained by the following expression,

$$
\begin{aligned}
\ddot{d}_e &= \ddot{d} - KL\dot{\tilde{x}} \\
&= \ddot{d} - KL(f(x) + g_1(x)u + g_2(x)d - g_2(\hat{x})\hat{d} - f(\hat{x}) - g_1(\hat{x})u + L(\hat{x} - x)) \\
&= \ddot{d} - KL(-(a + L + c(d - d_e))\tilde{x} + (b - cx)d_e)
\end{aligned}
\tag{3.35}
$$

where $\ddot{d}$ is the 2nd order derivative of d. Therefore, the following equation can be obtained by eliminating the $\tilde{x}$ through equation (3.34) and (3.35),

$$
\ddot{d}_e + (a + L + cd)\dot{d}_e - cd_e\dot{d}_e + (c\dot{d} + KL(b - cx))d_e = \ddot{d} + (a + L + cd)\dot{d}
\tag{3.36}
$$

The observer gain is $K = ksgn(b - cx), k > 0, L > 0$. Therefore,

$$
\ddot{d}_e + (a + L + cd)\dot{d}_e - cd_e\dot{d}_e + (c\dot{d} + kL\,|b - cx|)d_e = \ddot{d} + (a + L + cd)\dot{d}
\tag{3.37}
$$

Let $e_1 = d_e, \dot{e}_1 = \dot{d}_e = e_2$, the equation (3.37) can be transformed to the following form,

$$\begin{cases} \dot{e}_1 = e_2 \\ \dot{e}_2 = D + ce_1e_2 - Me_2 - Ne_1 \end{cases} \tag{3.38}$$

where $D = \ddot{d} + (a + L + cd)\dot{d}$, $M = (a + L + cd)$, $N = (c\dot{d} + kL|b - cx|)$. D, M and N are bounded based on the SCR system and the observer gains k and L. Let $\eta = \begin{bmatrix} e_1 \\ e_2 \end{bmatrix}$, then equation (3.38) can be transformed to the following form,

$$\dot{\eta} = A\eta + h_D \tag{3.39}$$

where $A = \begin{bmatrix} 0 & 1 \\ -N & ce_1 - M \end{bmatrix}$, $h_D = \begin{bmatrix} 0 \\ D \end{bmatrix}$. h_D is bounded.

Based on the SCR system ($0 \leq d \leq 1$) and the limitation ($0 \leq \hat{d} \leq 1$) of the robust nonlinear disturbance observer, we can know that,

$$0 \leq |d_e| \leq 1 \tag{3.40}$$

Therefore, the observer gain k and L can be chosen so that A is Hurwitz.

Lemma 2: With the assumption that A is Hurwitz, the observer state η for equation (3.39) is bounded for any bounded h_D. The proof is given in Appendix A.

Noise Attenuation Properties

Given the measurement noise of equation (3.30), the estimated disturbance is expressed by the following equation,

$$
\begin{aligned}
\hat{d} &= z + K\hat{x} \\
&= z + K \int_0^t \{g_2(\hat{x})\hat{d} + f(\hat{x}) + g_1(\hat{x})u - L(\hat{x} - x_n)\}dt \\
&= z + K \int_0^t \{g_2(\hat{x})\hat{d} + f(\hat{x}) + g_1(\hat{x})u - L(\hat{x} - x))\}dt + KL \int_0^t n\,dt
\end{aligned}
\tag{3.41}
$$

Compared with regular NDO, the robust NDO eliminate the noise effect by integration as demonstrated in equation (3.41).

3.6   Simulation Results

The performances of the robust NDO and regular NDO were demonstrated through the full-vehicle simulation of the FTP-75 test cycle in Simulink environment. Through the simulation, the following performances of both proposed nonlinear disturbance observers are illustrated: 1) the effectiveness of both estimation approaches; 2) the noise attenuation properties of the robust NDO and the regular NDO. Since both regular NDO and robust NDO are BIBO stable and subjected to measurement noise, the tuning principle of the observer parameter k and L is to balance the estimation performance and the noise tolerance. In this simulation, the parameters of k and L were selected as $k = 20$, $L = 20$.

3.6.1   Main Variables during FTP-75 test

To test the robust NDO and regular NDO, the light-duty vehicle model built in GT-Power environment is used. The engine model of the light-duty vehicle model is a map-based model based on a 3 L turbocharged Diesel engine. The FTP-75 (Federal Test Procedure) has been used for emission certification and fuel economy testing for light-duty vehicles in the United States. The mole fraction of NO_x, the exhaust gas flow rate before SCR, SCR temperature, and vehicle speed during the FTP-75 test are demonstrated in Figure 3.4.
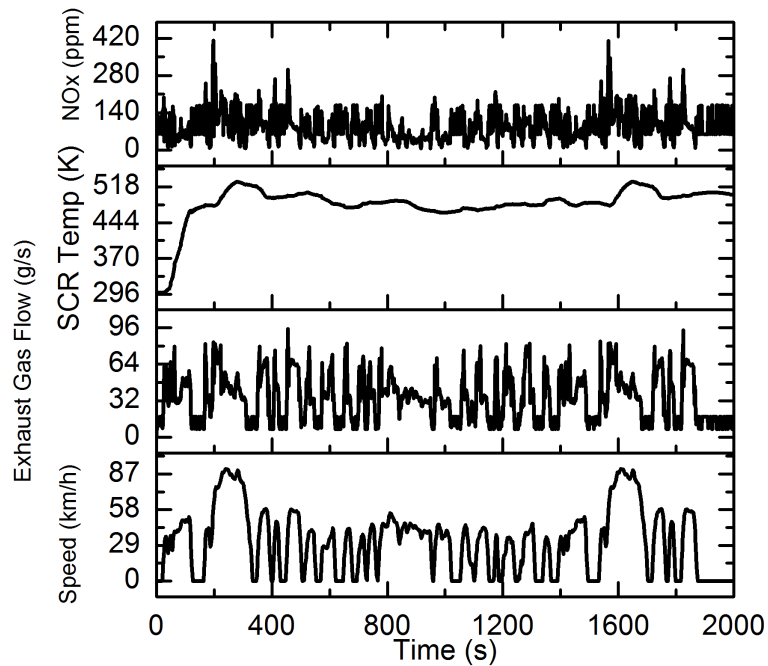
Figure 3.4: The temperature and total NO_x out of the engine

3.6.2   Performance of both NDOs when NO_x Sensor without Ammonia Cross-sensitivity

In this scenario, it is assumed that the NO_x sensor can get accurate value, although the NO_x sensor would have ammonia cross-sensitivity. In fact, two different NO_x sensors are used in [6] to eliminate the ammonia cross-sensitivity, avoiding the use of expensive ammonia sensor. Two different NO_x sensors (see Figure 3.3) are used to estimate the accurate NO_x concentration and sensor reading values can be expressed in the following [6],

$$\begin{cases} C_{NO_x,sen1} = C_{NO_x} + K_{cs1} * C_{NH_3} \\ C_{NO_x,sen1} = C_{NO_x} + K_{cs2} * C_{NH_3} \end{cases} \tag{3.42}$$

According to equation (3.42) the NO_x concentration can be calculated by the following expression,

$$C_{NO_x} = \frac{K_{cs2} * C_{NO_x,sen1} - K_{cs1} * C_{NO_x,sen2}}{K_{cs2} - K_{cs1}} \tag{3.43}$$

Therefore, it is feasible to eliminate the ammonia cross-sensitivity without using ammonia sensors.
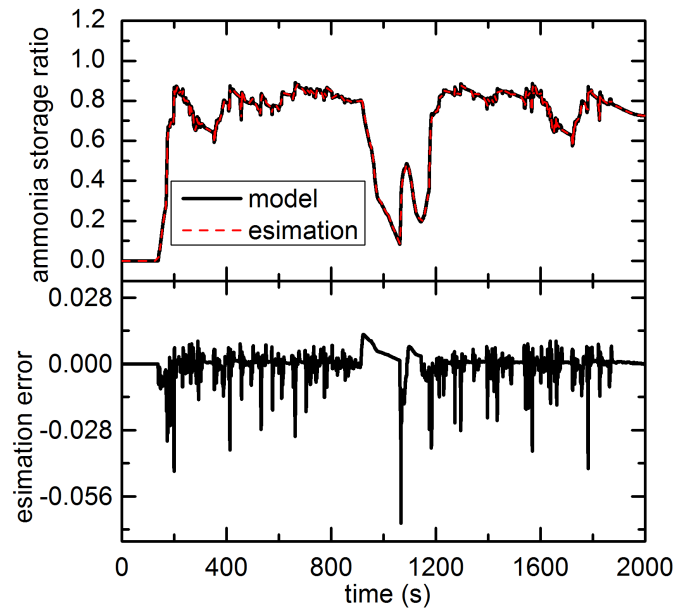
Figure 3.5: Estimation performance of regular NDO without measurement noise
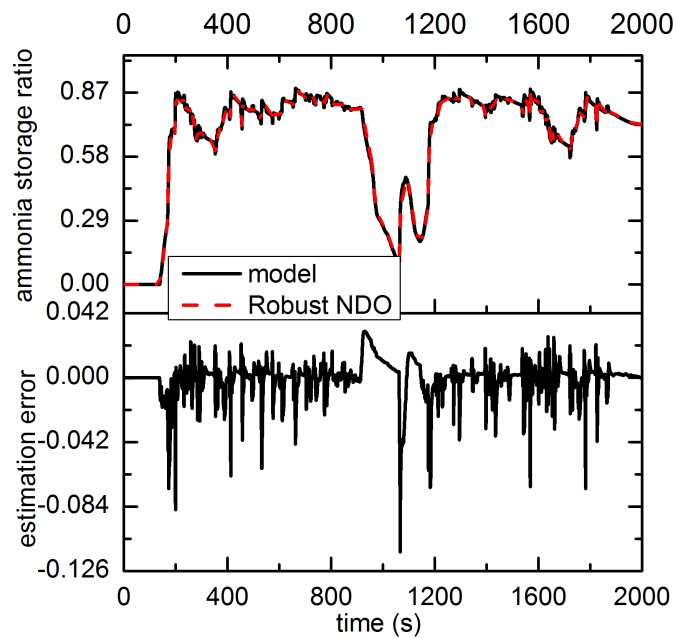
Figure 3.6: Estimation performance of robust NDO without measurement noise

In Figure 3.5, most of the estimation errors are lower than 0.05, which shows good performance of the regular NDO (NDO in all the figures refers to the regular NDO) to estimate the ammonia storage ratio. In Figure 3.6, most of the estimation errors are lower than 0.084, which demonstrated that the robust NDO can also effectively estimate the ammonia storage ratio. To further discuss the noise attenuation abilities of both nonlinear disturbance observer, high-frequency white noise was added to the NO_x measurement. The measurement noises are uniformly distributed in the range [-10 10] ppm based on the NO_x sensor characteristics. In Figure 3.7, the estimation errors have high-frequency errors due to the measurement noise. Furthermore, the estimation errors reach 0.4 at some points. Although there are also high-frequency errors, the estimation errors are almost half of that of regular NDO, as can be seen in Figure 3.8. Thus, compared with regular NDO, robust NDO has better noise attenuation performance. This is due to the difference between their noise attenuation properties analyzed in Section 3.5.1 and Section 3.5.2.
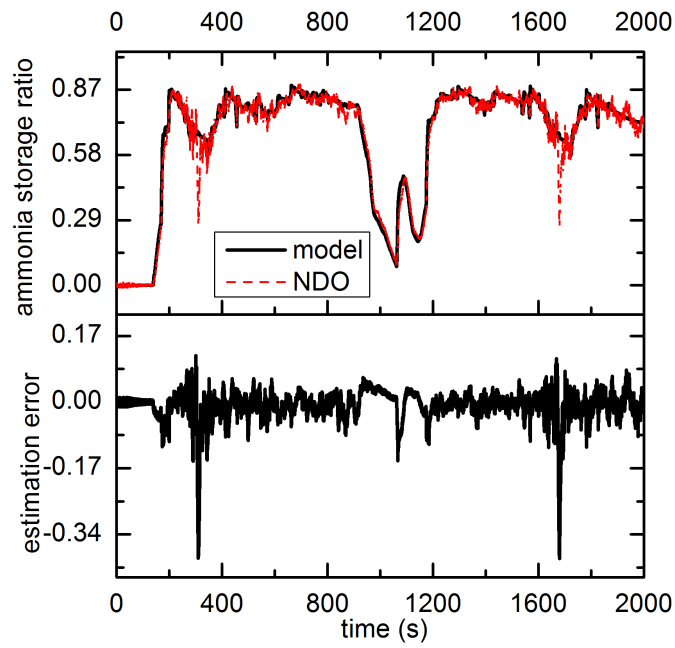
Figure 3.7: Estimation performance of regular NDO with measurement noise
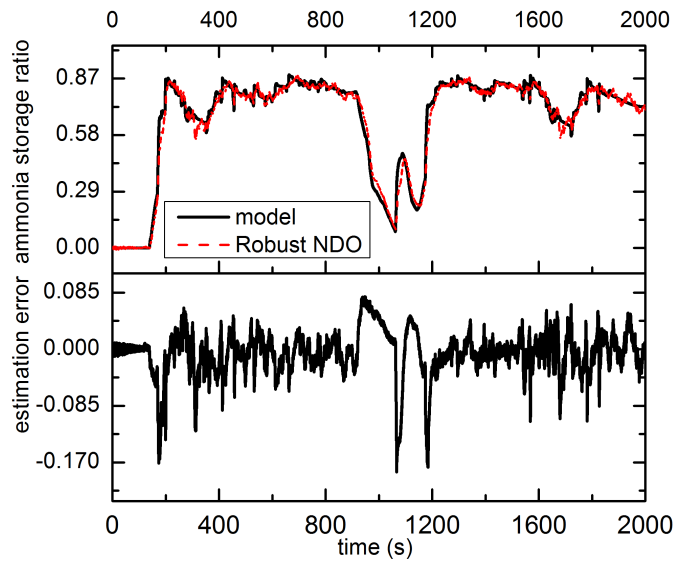
Figure 3.8: Estimation performance of robust NDO with measurement noise

3.6.3   Performance of both NDOs when NO_x Sensor with Ammonia Cross-sensitivity

In this scenario, one NO_x sensor after the SCR system is used and has ammonia cross-sensitivity issue. The NO_x slip and ammonia slip are demonstrated in Figure 3.9. K_{cs} is assumed as a constant and $K_{cs} = 0.5$. Then the NO_x sensor reading value can be expressed in the following [3],
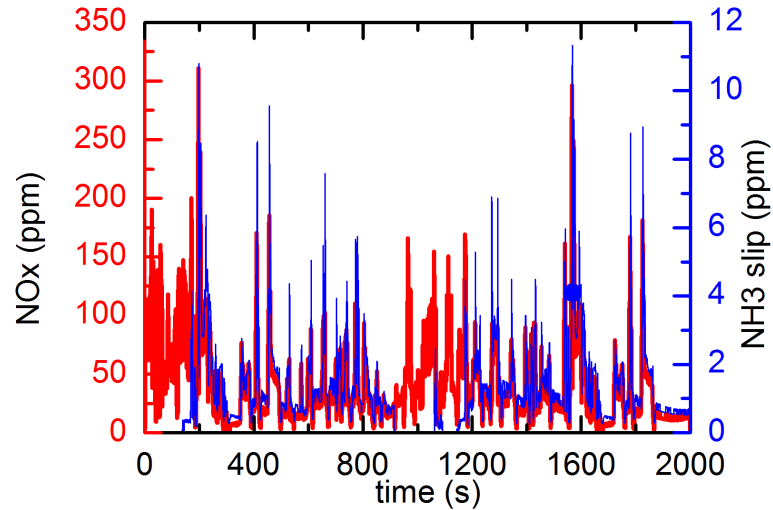
Figure 3.9: NO_x slip and NH_3 slip

$$C_{NO_x,sen} = C_{NO_x} + K_{cs} * C_{NH_3} \tag{3.44}$$

As can be seen in Figure 3.10 and Figure 3.11, when there exists ammonia slip, the estimation of ammonia storage ratio will be lower than that of model prediction. However, when there is no ammonia slip, the estimation of ammonia storage ratio can converge to that of model prediction very fast. Although some peak estimation errors are as high as 0.2 due to the peak value of ammonia slip, most estimation errors are

lower than 0.074. Since the ammonia slip is limited in the stringent regulations, the SCR system is required to have very low ammonia slip, even close to zero. Therefore, both regular NDO and robust NDO can effectively estimate the ammonia storage ratio and have similar performance when there is no measurement noise.
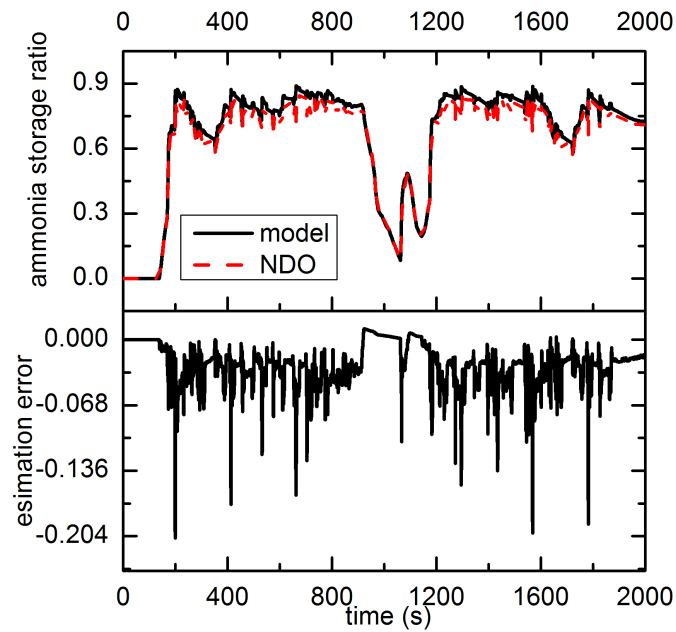
Figure 3.10: Estimation performance of regular NDO with ammonia cross-sensitivity
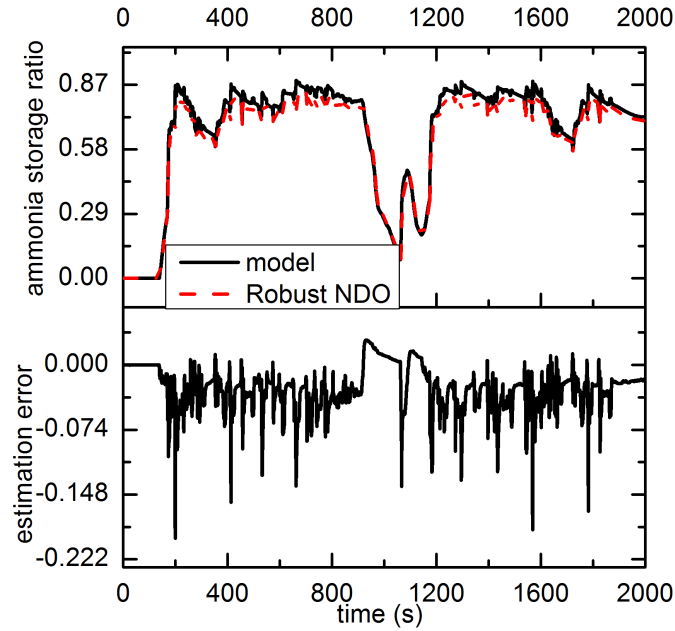
Figure 3.11: Estimation performance of robust NDO with ammonia cross-sensitivity

In this scenario, the measurement noises are also uniformly distributed in the range [-10 10] ppm. In Figure 3.12, the estimation errors of regular NDO have high frequency errors due to the measurement noise. Furthermore, the estimation errors can be as high as 0.4 at some points. From Figure 3.13, although high frequency errors exist, the estimation errors are lower than that of regular NDO. Compared Figure 3.12 with Figure 3.13, the robust NDO has a better noise attenuation properties than the regular NDO. This consistently matches the noise abilities as investigated in Section 3.5.
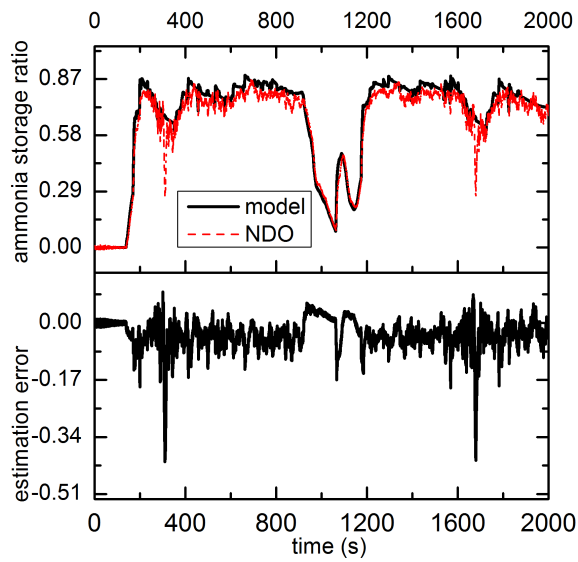
Figure 3.12: Estimation performance of regular NDO with ammonia cross-sensitivity and measurement noise
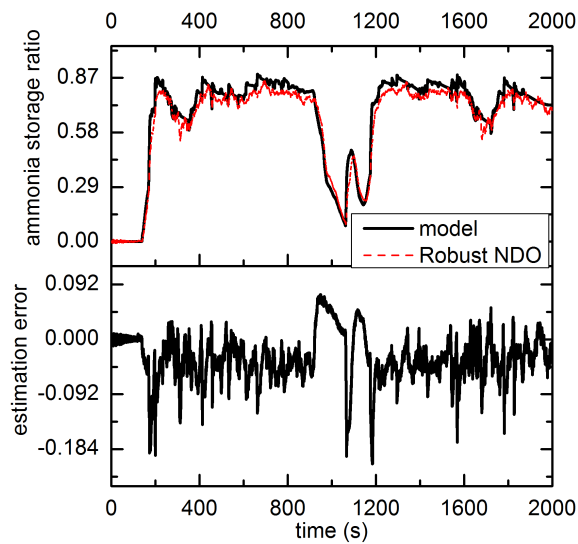
Figure 3.13: Estimation performance of routbust NDO with ammonia cross-sensitivity and measurement noise

3.7   Conclusion

In this work, two different observer-based approaches are proposed to estimate the ammonia storage ratio. The ammonia storage ratio is treated as an external disturbance and estimated by the Nonlinear Disturbance Observer based on the NO_x dynamic model. The stabilities and noise attenuation abilities of both observers are demonstrated to guarantee the convergence of the ammonia storage ratio. To improve the performance of the observer against to the high-frequency measurement noise, a robust NDO was designed, motivated from the robust estimation technique and specially improved from the regular NDO. The stability of the robust NDO was also analyzed in details. The simulation results demonstrated that both NDO (regular NDO and robust NDO) can effectively estimate the ammonia storage even in cases where ammonia cross-sensitivity affects response. However, the robust NDO has better noise attenuation performance by comparing with the regular NDO.

Reference

[1] World Health Organization, 2006, WHO Air Quality Guidelines for Particulate Matter, Ozone, Nitrogen Dioxide, and Sulfur Dioxide: Global Update 2005, WHO Press, Geneva, Switzerland, Chap. XII.

[2] Johnson, T. V., 2006, "Diesel emission control in review," SAE Technical Paper, No. 2006-01-0030.

[3] Hsieh, M.-F., and Wang, J., 2010, "An extended Kalman filter for ammonia coverage ratio and capacity estimations in the application of Diesel engine SCR control and onboard diagnosis," American Control Conference (ACC), pp. 5874-5879.

[4] Hsieh, M.-F., and Wang, J., 2010, "Observer-Based Estimation of Selective Catalytic Reduction Catalyst Ammonia Storage," Proceedings of the Institution of Mechanical Engineers, Part D: Journal of Automobile Engineering, 224(9), pp. 11991211.

[5] Zhang, H., Wang, J., and Wang, Y.-Y., 2013, "Robust Filtering for Ammonia Coverage Estimation in Diesel Engine Selective Catalytic Reduction Systems," Journal of Dynamic Systems, Measurement, and Control, 135(6), 064504.

[6] Chen P., and Wang J., 2014, "A novel cost-effective robust approach for selective catalytic reduction state estimations using dual nitrogen oxide sensors," Proceedings of the Institution of Mechanical Engineers, Part D: Journal of Automobile Engineering, 229(1), pp. 83-96.

[7] Kim, K. S., Rew, K. H., and Kim, S., 2010, "Disturbance Observer for Estimating Higher Order Disturbances in Time Series Expansion," IEEE Transactions on Automatic Control, 55(8), pp. 19051911.

[8] Yan, F., and Wang, J., 2012, "Engine cycle-by-cycle cylinder wall temperature observer-based estimation through cylinder pressure signals," Journal of Dynamic Systems, Measurement, and Control, 134(6), 061014.

[9] Chen, W.-H., 2004, "Disturbance Observer Based Control for Nonliear Systems," IEEE/ASME Transaction on mechatronics, 9(4), pp. 706-710.

[10] Chen, W. H., and Guo, L., 2004, "Analysis of disturbance observer based control for nonlinear systems under disturbances with bounded variation," Proceedings of International Conference on Control.

[11] Chen, W.-H., Donald J. B., Peter J. G., and John O., 2000, "A nonlinear disturbance observer for robotic manipulators," IEEE Transactions on Industrial Electronics, 47(4), pp. 932-938.

[12] Upadhyay, D., and Michiel, V. N., 2002, "Modeling of a urea SCR catalyst with automotive applications," ASME 2002 international mechanical engineering congress and exposition, pp. 707-713.

[13] Isidori, A.,1995, Nonlinear Control System: An Introduction, 3rd ed. New York:Springer-Verlag

[14] Bonfils, A., Yann C., Olivier L., and Nicolas P., 2012, "Closed-loop control of a SCR system using a NOx sensor cross-sensitive to NH_3," Advanced Control of Chemical Processes, 8(1), pp. 738-743.

[15] Kubinski, D. J., and Visser, J. H., 2008, "Sensor and method for determining the ammonia loading of a zeolite SCR catalyst," Sensors and Actuators B: Chemical, 130(1), pp. 425-429..

[16] Piazzesi, G., Devadas, M., Krcher, O., Elsener, M., and Wokaun, A., 2006, "Iso-cyanic acid hydrolysis over Fe-ZSM5 in urea-SCR," Catalysis Communications, 7(8), 600-603.

[17] Strots, V. O., Santhanam, S., Adelman, B. J., Griffin, G. A., and Derybowski, E. M., 2009, "Deposit formation in urea-SCR systems," SAE Technical Paper, No. 2009-01-2780.

[18] Schaber, P. M., Colson, J., Higgins, S., Thielen, D., Anspach, B., and Brauer, J., 2004, "Thermal decomposition (pyrolysis) of urea in an open reaction vessel," Thermochimica acta, 424(1), 131-142.

[19] Zhou, G., Jrgensen, J. B., Duwig, C., & Huusom, J. K., 2012, "State estimation in the automotive SCR deNOx process," Proceedings of 8th IFAC Symposium on Advanced Control of Chemical Processes, pp. 501-506.

[20] Yang, J., Chen, W.-H., and Li, S., 2011, "Non-linear disturbance observer-based

robust control for systems with mismatched disturbances/uncertainties," IET control theory & applications, 5(18), pp. 2053-2062.

[21] Yang, J., Li, S. and Chen, W.-H., 2012, "Nonlinear disturbance observer-based control for multi-input multi-output nonlinear systems subject to mismatching condition," International Journal of Control, 85(8), pp. 1071-1082.

[22] Devarakonda, M., Parker, G., Johnson, J. H., Strots, V., and Santhanam, S., 2008, "Adequacy of reduced order models for model-based control in a urea-SCR aftertreatment system," SAE Technical Paper, No.2008-01-0617.

Chapter 4

Compound Control Strategy based on Active Disturbance Rejection for Selective Catalytic Reduction systems

4.1 Citation and Main Contributor

Jinbiao Ning, and Fengjun Yan. "Compound Control Strategy Based on Active Disturbance Rejection for Selective Catalytic Reduction systems." Journal of Dynamic Systems, Measurement, and Control 137, no. 5 (2015): 051008.

The main contributor to this paper is the first author-Jinbiao Ning (contributes more than 70%).

4.2   Abstract

Urea-based Selective Catalytic Reduction (SCR) systems are effective ways in Diesel engine after-treatment systems to meet increasingly stringent emission regulations. To achieve high NO_x reduction efficiency and low NH_3 slip, the control of the SCR system becomes more challenging, especially in transient operating conditions with model uncertainties. To effectively address this issue, this paper proposed a compound control strategy with a switching mechanism between an Active Disturbance Rejection (ADR) controller and a zero-input controller. The ADR controller estimates and rejects the total (internal and external) disturbances from the SCR system when the exhaust gas temperature is high and its variation is small. The zero-input controller is used to lower ammonia surface coverage ratio to avoid high ammonia slip when exhaust gas temperature suddenly rises. The proposed control strategy is validated through a high-fidelity GT-Power simulation for a light-duty Diesel engine over steady states and FTP-75 test cycle. Its effectiveness is demonstrated especially in rapidly transient conditions with model uncertainties.

4.3   Introduction

Diesel engines are major power sources for automobile applications due to their durability and high fuel efficiency. However, the lean burn conditions of Diesel engines lead to high NO_x emission which contributes to acid rain and smog formation, and have been linked to incidence rates for respiratory tract irritation, infection, asthma [1]. Although some advance engine control technologies can reduce engine-out NO_x,

the after-treatment systems are still necessary to further lower the engine NO_x emissions to meet the stringent emission limits [2]. Selective catalytic reduction (SCR) system is a promising after-treatment technique to reduce the NO_x emission and has been adopted by many new production vehicles [3].

In SCR system, the urea (Adblue) is injected and converted to ammonia (NH_3) to reduce NO_x by chemical reaction on the catalytic surface. It is critical to control the amount of urea injection to avoid emission from two aspects. For one aspect, a large amount of ammonia input has a high NO_x reduction efficiency, but it may leads to high ammonia slip that have been considered as emission into Euro VI regulations [4]. For another aspect, less ammonia input leads to lower NO_x reduction efficiency such that the emission regulations cannot be satisfied. Control of the SCR system has become a challenging issue due to future emission legislation and in-use compliance requirement. Several control methods [5–10] were proposed to address this issue.

Model-based or MAP-based Feed-forward control strategies are sufficient to meet Euro-IV and Euro-V emission standards [5]. However, to meet future emission and in-use compliance requirements, closed-loop SCR control is required [6].

To achieve close-loop SCR control, NO_x sensors and ammonia sensors are used. NO_x (NO/NO_2) can be measured by NO_x sensors, so that it can be used to compensate the feed-forward control. But it can easily lead to high NH_3 slip [5] and NO_x sensor has ammonia cross-sensitivity issue [7]. Ammonia concentration at downstream of SCR system have been reported to be used for feedback control in [5]. Ammonia surface coverage or ammonia surface coverage ratio feedback control was proposed because it can achieve high NO_x reduction efficiency and low NH_3 slip at the same time [5]. The ammonia surface coverage cannot be directly measured but

can be estimated by observer [5, 6, 8], which requires accurate control-oriented models. Several studies [4–9] proposed three-state SCR models, assuming that all NO_x are only NO in the exhaust gas. However, high rate of production for NO_2 in modern DOC based after-treatment systems yields four-state models [10] including both NO and NO_2 reactions. An adaptive model predictive control (MPC) proposed in [9] shows its effectiveness in dealing with both NH_3 slip and NO_x inefficiency issues at the same time. However, the adaptive MPC requires relatively high computation effort and a relatively accurate model.

Although control oriented and lumped parameter models can be used to estimate states of SCR dynamic system, there exist some problems in model-based control. The main challenges in model-based control are the system disturbances and model uncertainties. The disturbances consist of both internal disturbances and external disturbances. The aging and system degradation of SCR application, urea injection inaccuracy, urea injection constrain, the ammonia buffering in the SCR catalyst are referred to as the internal disturbances. External disturbances include the exhaust gas flow mass ratio, the exhaust gas temperature, the ratio of NO/ NO_2, NO_x sensor cross-sensitivity, measurement noise and etc. The model uncertainties include parameter uncertainties, state estimation errors and so on. To deal with these issues, an ammonia surface storage feedback adaptive control integrated with ammonia feedback PI controller was proposed to compensate and adapt the ammonia storage ratio control [5]. To make the control effective in [5], proper PI parameters need to be selected and therefore calibration efforts are still required.

In this paper, a novel NH_3 feedback compound control strategy based on the active disturbance rejection control (ADRC) concept [11–14] is proposed to avoid the

aforementioned problems in model-based control. The contributions of this paper are: 1) a novel, model-free Active Disturbance Rejection (ADR) controller is proposed to reject total (internal and external) disturbances. 2) A switching mechanism with ADR controller and a zero-input controller is designed to avoid high ammonia slip when exhaust gas temperature suddenly rises. 3) The estimation of ammonia surface storage ratio is by-passed to avoid the inaccuracy from model uncertainties and disturbances.

The rest of the paper is organized as following. The principle and modeling of the SCR system are demonstrated in section 4.4. The compound control strategy with a switching mechanism between an ADR controller and a zero-input controller is presented in section 4.5. In section 4.6, high-fidelity simulations based on experimentally-validated light-duty vehicle in GT-Power software are performed to verify the proposed approach. The conclusion is given in section 4.7.

4.4   The Principle and Modeling of the SCR system
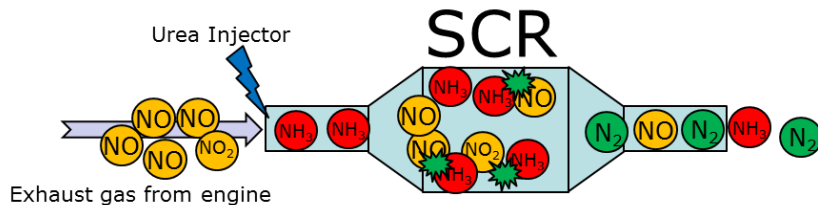
Figure 4.1: Urea based SCR system for Diesel engines

This section presents the principle and modeling of the SCR system, and describes

potential uncertainties and disturbances therein. The SCR system as part of the after-treatment system is located in the exhaust gas pipe of Diesel engines. As can be seen from Figure 4.1, NO_x reduction occurs when the exhaust gas of the engine goes through the SCR system. In SCR system, three events are mainly included: 1) The AdBlue is injected at upstream of the SCR system by the dosing unit and converted to ammonia. 2) When entering the SCR system, the ammonia is adsorbed by the substrate of the catalyst. 3) The ammonia adsorbed on the substrate reacts with NO_x and convert them to N_2.

4.4.1   Principle of Selective Catalytic Reduction system

Adblue to ammonia

The demand amount of Urea is injected into the SCR system by dosing control. The 32.5% aqueous urea solution (AdBlue) is used as the source of ammonia for SCR system in vehicle applications because it is less hazardous, easier to handle and safer to transport. AdBlue is converted to ammonia mainly by three processes: evaporation, decomposition, and hydrolyzation [15], as shown in following equations.

$$NH_2CONH_2(liquid) \rightarrow NH_2CONH_2 * + \xi H_2O \tag{4.1}$$

$$NH_2CONH_2* \rightarrow HNCO + NH_3 \tag{4.2}$$

$$HNCO + H_2O \rightarrow +NH_3 + CO_2 \tag{4.3}$$

Factors that affect Adblue evaporation are spatial droplet size and temperature [16]. So, the reaction rate depends on different Adblue injector designs and engine exhaust

gas temperature. It has been reported that the above reaction generally starts from 200 °C and reaches a maximum reaction rate around 350 °C [17]. When the exhaust gas temperature is less than 200 °C, the urea decomposition reaction can generate byproducts such as cyanuric acid, biuret, melamine, ammelide and ammeline as deposits on pipe wall [18], which is the direct issue that affects the low temperature performance of SCR system. In this paper, a compound control strategy is designed to avoid this problem. The hydrolyzation process is inactive under temperature of 400 °C. But it is reported that the reaction rate is faster than the SCR DeNOx reaction rate in zeolite based SCR system [19]. Therefore, the concentration of ammonia is very difficult to precisely predict by the AdBlue injection rate due to disturbances and uncertainties such that the concentration of ammonia is typically modeled by the following nonlinear and time-variant function,

$$C_{NH_3,in} = f_1(F, U_{Adblue}, T, t) \tag{4.4}$$

where $C_{NH_3,in}$ is the concentration of ammonia ($mole/m^3$), the exhaust gas temperature (K), t the time (s), F the exhaust gas flow rate (kg/s) and U_{Adblue} the injection rate of AdBlue at upstream of the SCR system (g/s).

Ammonia Adsorption/Desorption

The reaction is a modified version in [20]. When the NH_3 entered the SCR system, it can be adsorbed on the catalyst substrate and desorbed from the substrate, which can be expressed [3].

$$NH_3 + Z \leftrightarrow ZNH_3 \tag{4.5}$$

where Z is the free SCR substrate site (not covered by NH_3). The calculation of ammonia adsorption rate assumes non-activated energy with adsorption process, while the calculation of ammonia desorption rate accounts for activation energies associated with desorption process [20]. The rate of ammonia adsorption and desorption can be expressed by the following equations,

$$R_{ads} = k_{ads}C_{NH_3}(1 - \theta_{NH_3}) \tag{4.6}$$

$$R_{des} = k_{des}\exp[-\frac{E_{des}}{RT}(1 - \gamma\theta_{NH_3})]\theta_{NH_3} \tag{4.7}$$

where R_{ads}, R_{des} represent the chemical reaction rate (mole/sec), T the temperature (K), k_{ads}, k_{des}, E_{des} and R constants, C_{NH_3} the concentration of NH_3 $(mole/m^3)$, and θ_{NH_3} the ammonia surface coverage ratio [3] defined by:

$$\theta_{NH_3} = \frac{M^*_{NH_3}}{\Theta} \tag{4.8}$$

where $M^*_{NH_3}$ is the mole number of ammonia stored in the SCR substrate, Θ the ammonia storage capacity (mole) which is temperature dependent, $\Theta = S_1 e^{-S_2 T}$. This means that less NH_3 can be stored in the catalyst and less NH_3 can react with NO_x if the temperature is higher.

Ammonia and NO oxidation

Oxidation reactions have been studied to be more favored to happen on Zeolite based catalysts than Vanadium based catalysts [21]. Specificaly, the adsorbed NH_3 can be oxidized to NO at temperature higher than 450 $°C$ [3]. Although the NO oxidation reaction is not commonly mentioned, it was demonstrated by [21] of being present in

Fe-Zeolite based SCR system. The reaction, the reaction rate of ammonia, and NO oxidation can be described by following equations,

$$ZNH_3 + 1.5O_2 \rightarrow NO + 1.5H_2O \tag{4.9}$$
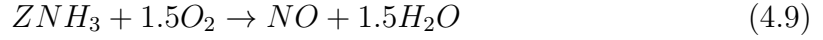
$$R_{oxi} = k_{oxi} \exp(-\frac{E_{oxi}}{RT})\theta_{NH_3} \tag{4.10}$$

$$0.5O_2 + NO \rightarrow NO_2 \tag{4.11}$$

$$R_{NO_{oxi}} = k_{NO_{oxi}} \exp(-\frac{E_{NO_{oxi}}}{RT})(C_{NO}\sqrt{P_{O_2}} - \frac{C_{NO_2}}{k_{eq}}) \tag{4.12}$$

where R_{oxi}, $R_{NO_{oxi}}$ represents the chemical reaction rate (mole/sec), k_{oxi}, $k_{NO_{oxi}}$, E_{oxi}, $E_{NO_{oxi}}$, and k_{eq} constants, C_{NO}, C_{NO_2} the concentration of NO, NO_2 ($mole/m^3$), P_{O_2} the mole fraction of O_2.

NO_x Reduction

After the ammonia is adsorbed by SCR system, it can then catalytically react with NO_x and convert them to N_2. The main reactions in the SCR system are listed below,

$$4ZNH_3 + 4NO + O_2 \rightarrow 4N_2 + 6H_2O \tag{4.13}$$

$$2ZNH_3 + NO + NO_2 \rightarrow 2N_2 + 3H_2O \tag{4.14}$$

$$4ZNH_3 + 3NO_2 \rightarrow 3.5N_2 + 6H_2O \tag{4.15}$$
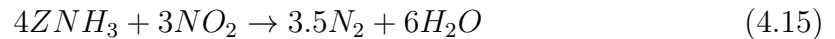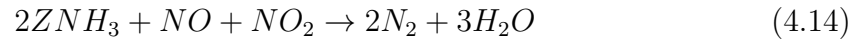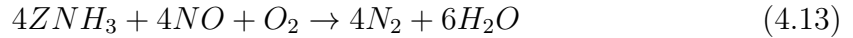
The equation (4.13) is called "standard SCR", because more than 90% of the Diesel-exhaust NO_x is usually composed of NO [22] and the reaction rate is fast. The equation (4.14) is known as "fast SCR", since its reaction rate can be one order

of magnitude faster than the standard SCR reaction in [25]. The equation (4.15) in commonly called "slow SCR" in Vanadium based SCR system. However it is reported that this reaction can even faster than the "standard SCR" in Fe-Zeolite based SCR catalyst. The reaction rate is showed in the following equations,

$$R_{NO} = k_{NO} \exp(-\frac{E_{NO}}{R}(\frac{1}{T} - \frac{1}{473}))\frac{C_{NO}\theta_{NH_3}}{1 + K_{LH}\frac{\theta_{NH_3}}{1-\theta_{NH_3}}}(\frac{P_{O_2}}{0.02})^{\beta} \qquad (4.16)$$

$$R_{Fast} = k_{Fast} \exp(-\frac{E_{Fast}}{R}(\frac{1}{T} - \frac{1}{473}))\frac{C_{NO_2}}{\varepsilon + C_{NO_2}}C_{NO}\theta_{NH_3} \qquad (4.17)$$

$$R_{Slow} = k_{Slowt} \exp(-\frac{E_{Slow}}{R}(\frac{1}{T} - \frac{1}{473}))C_{NO_2}\theta_{NH_3} \qquad (4.18)$$

where R_{NO}, R_{Fast}, R_{Slow} represents the chemical reaction rate (mole/sec), k_{NO}, k_{Fast}, k_{Slow}, E_{NO}, E_{Fast}, E_{Slow}, K_{LH}, β,and ε the constants.

4.4.2   Model of Selective Catalytic Reduction system

There are several three-state [5–9], [22–24] and four-state [10] control-oriented models of SCR system based on Continuous Stirred Tank Reactor (CSTR) approach and mass conservation law. However, these models are based on some simple assumptions (e.g. SCR system as a CSTR, urea can be fully converted into ammonia, engine-out NO_x are fully NO) and lose much information. Moreover, several parameters are needed to be identified and these parameters may change during the lifetime of the SCR system. In conclusion, the SCR model is expressed by following nonlinear and time

variant functions.

$$
\begin{cases}
\dot{C}_{NO} = f_2(C_{NO}, C_{NO_2}, \theta_{NH_3}, C_{NH_3}, C_{O_2}, T, t) + \frac{F}{V}C_{NO,in} \\[6pt]
\dot{C}_{NO_2} = f_3(C_{NO}, C_{NO_2}, \theta_{NH_3}, C_{NH_3}, C_{O_2}, T, t) + \frac{F}{V}C_{NO_2,in} \\[6pt]
\dot{\theta}_{NH_3} = f_4(C_{NO}, C_{NO_2}, \theta_{NH_3}, C_{NH_3}, C_{O_2}, T, t) \\[6pt]
\dot{C}_{NH_3} = f_5(C_{NO}, C_{NO_2}, \theta_{NH_3}, C_{NH_3}, C_{O_2}, T, t) + \frac{F}{V}f_1(F, U_{Adblue}, T, t)
\end{cases}
\tag{4.19}
$$

where V is the SCR catalyst volume(m^3), f_1 to f_5 the nonlinear and time variant functions which are very difficult to get exact expression.

4.5 Compound Controller Design

Typically, the major factors related to NO_x conversion efficiency of SCR system are the NO_2/NO ratio, the exhaust gas temperature and the ammonia storage ratio. To enhance the NO_2/NO ratio, it requires a pre-oxidation catalyst. Controlling the exhaust gas temperature requires after-treatment thermal management by controlling EGR or injection timing of the engine, which is out of the scope of this paper. Since ammonia storage ratio cannot be measured, the objective of this paper is to explore indirect method, maintaining the ammonia slip lower than 10 ppm on average and 25 ppm at peak, to regulate the ammonia coverage ratio for enhancing NO_x reduction. The ammonia emission is regulated in UERO VI and the ammonia slip limit of 10 ppm on average and 25 ppm at peak is applied [24].

Specifically, three major factors lead to the ammonia slip: temperature rise, ammonia overdosing and ammonia precursor [27]. There are different measures (e.g. SCR+AMOX [27], two-cell SCR [28], advanced dosing strategy [5, 9, 28]) to account

for ammonia slip. Advance dosing strategy is another method besides Ammonia oxidation catalyst (AMOX) and two-cell SCR to limit the ammonia slip. In this paper, the ammonia precursor is ignored in the model and an advanced ammonia feedback dosing strategy is designed to regulate ammonia slip and ammonia coverage ratio.

According to the nonlinear and time-variant model of SCR system in Section 4.4, it is challenging to get an exact model and design a robust model-based controller. A compound control strategy with a switching mechanism between an Active Disturbance Rejection controller and a zero-input controller is developed to achieve the control target. Figure 4.2 shows the structure of the compound control strategy. Based on the profile of the SCR system, the zero-input controller is designed by setting the input to zero. The switching mechanism is designed to avoid the high ammonia slip when the temperature rises, and the ADR controller is designed to avoid overdosing. To make average ammonia slip lower than 10 ppm, the desired value of the ammonia slip is set to 8 ppm.
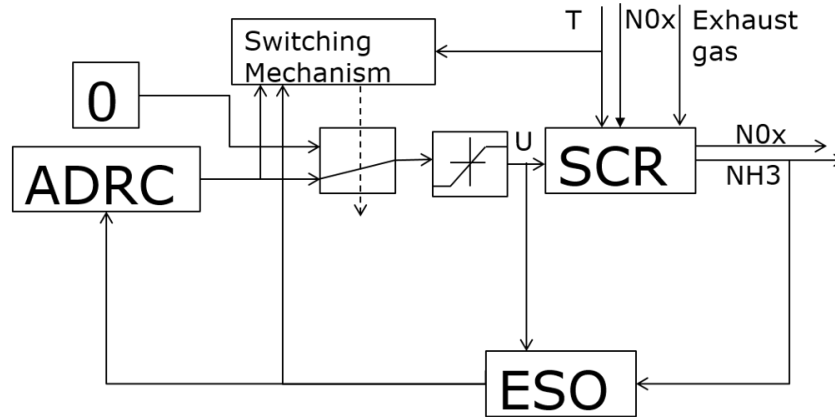
Figure 4.2: ADRC combined with a switch controller

4.5.1   ADR Controller design

The ADR controller consists of an Extended State Observer and a Disturbance Rejection Controller. Figure 4.3 is the structure of ADR controller for SCR system.
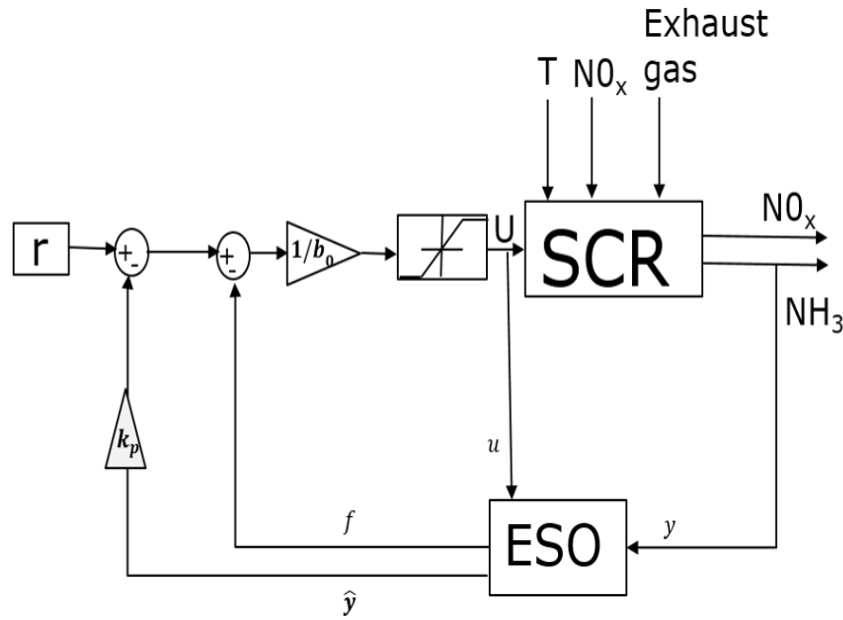
Figure 4.3: ADRC controller design for SCR system

Extended state observer(ESO) design

Different from building the exact model and identifying the parameters of the dynamic system, the method of ESO is to treat the total disturbance of the system as an extended state of the system and to estimate it in real time. Based on the concept of

ESO, Let $x_1 = C_{NH_3}$, then the model (equation (4.19)) can be transformed to below,

$$
\begin{cases}
\dot{x}_1 = f + b_0 u \\
y_1 = x_1
\end{cases}
\tag{4.20}
$$

where $f = f_5(C_{NO}, C_{NO_2}, \theta_{NH_3}, C_{NH_3}, C_{O_2}, T, t) + \frac{F}{V} f_1(F, U_{Adblue}, T, t) - b_0 u$, $u = U_{Adblue}$, $y_1 = x_1 = C_{NH_3}$. Here, f contains model mismatch and total disturbances including external disturbances and internal disturbances of SCR system. So f is the total disturbance that we need to reject in the controller; Assuming f is differentiable such that equation (4.20) can be rewritten in the following state space form,

$$
\begin{cases}
\dot{x}_1 = x_2 + b_0 u \\
\dot{x}_2 = \dot{f} = h \\
y_1 = x_1
\end{cases}
\tag{4.21}
$$

where the state is augmented with $x_2 = f$. Basing on the SCR system, we can know that h is bounded. Then, the ESO can be designed in the following form,

$$
\begin{cases}
\dot{\hat{x}}_1 = \hat{x}_2 + b_0 u + l_1(y_1 - \hat{y}_1) \\
\dot{\hat{x}}_2 = l_2(y_1 - \hat{y}_1) \\
\hat{y}_1 = \hat{x}_1
\end{cases}
\tag{4.22}
$$

where $\hat{x} = [\hat{x}_1, \hat{x}_2]^T \in R^2$, and $l = [l_1, l_2]^T$ are the observer gain vector, which can be calculated by the pole placement method. According to [26], the observer gain vector can be easily tuned after parameterization in the following form,

$$
[l_1, l_2]^T = [2\omega_0, \omega_0^2]^T
\tag{4.23}
$$

Then, the ESO has two parameters to specify: b_0 and ω_0. According to the profile of the process converting Urea injection to ammonia, we let $b_0 = 1$. The latter is a tuning parameter which amounts to the bandwidth of the observer. For adjusting ω_0, the trade-off can be easily made between estimation performance and noise-sensitivity. In generally, the larger ω_0, the more accurate the estimation is, but also be more sensitive to the noise. In this paper, we set $\omega_0 = 100$ to achieve good estimation performance.

Disturbance Rejction Controller design

With the extended state observer, the augmented state $x_2 = f$ can be estimated in real-time. Then, the controller can be designed to compensate the total disturbance in real-time, which can convert equation (4.20) to 1st Order Integrate Cascade form. And a Proportional controller is designed to control the 1st order Integrate Cascade system. Then, the controller designed can be expressed by the following form,

$$u = \frac{k_p(r - x_1) - x_2}{b_0} \tag{4.24}$$

where k_p is a tuning parameter, r the desired trajectory. Then, the system (3.1) can be turned into the following form,

$$\dot{x}_1 = f - \hat{x}_2 + k_p(r - \hat{x}_1) \tag{4.25}$$

For a well-turned ESO, $\hat{x}_2$ can track f closely. The term $f - \hat{x}_2$ in (4.25) can be turned into a little bounded error, which makes equation (4.25) become a bounded input and bounded output (BIBO) stable by tuning the parameter k_p.

4.5.2   Switching Mechanism Design
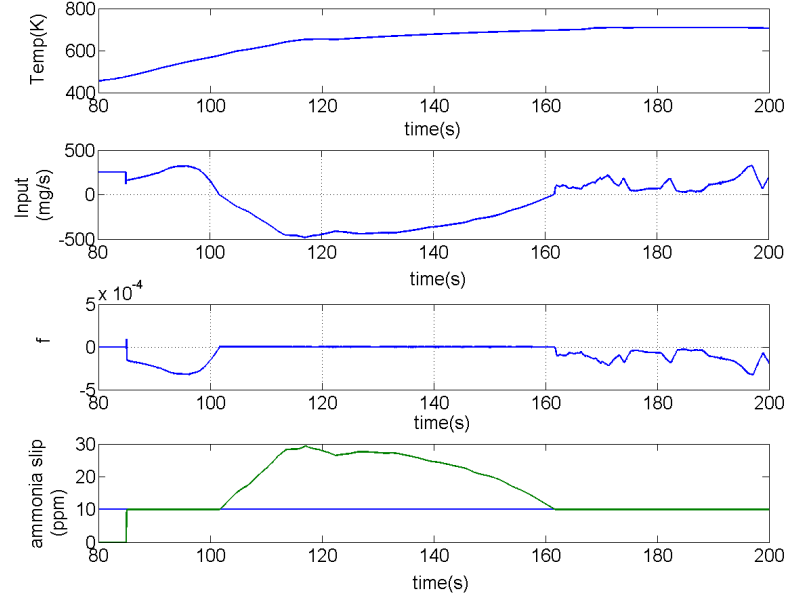
Figure 4.4: The conditions before and after the input hits zero

The phenomena that the SCR system can store more ammonia in the catalyst at low temperature than high temperature and that the sharply rising temperature can lead to high NH_3 slip from the catalyst are demonstrated in section 4.4. On the control point of view, because of the saturation of the input, the disturbance cannot be rejected after the input hits zero, which leads to high ammonia slip when the temperature rise up rapidly from low temperature (see Figure 4.4). To avoid high NH_3 slip at downstream of the SCR system, the controller should be set to zero before the input hits zero. To address this issue, the compound control strategy is designed with a zero-input controller and a switching mechanism (see Figure 4.2). In the switching mechanism, the temperature, the increasing rate of the temperature, the input of the controller and the increasing rate of f observed by the ESO are

detected. The compound controller will be switched to zero-input controller when the following conditions meet. 1) The temperature should be lower than a threshold; 2) The increasing rate of the temperature is greater than a threshold; 3) The input is lower than a threshold related to temperature; 4) The rate of total disturbance f is increasing.

4.6   Simulation Results

The compound strategy was validated over steady-state operating conditions and FTP-75 test cycle in co-simulation between GT-Power and Matlab/Simulink environment.

4.6.1   Light-duty Vehicle Model

To test the compound control strategy, the light-duty vehicle model is used. Figure 4.5 shows a 1-D vehicle model built in GT-power environment with 5 different components: Driver, ECU, Engine, Vehicle and After-treatment systems. Driver Model is to track the test cycle to make the Engine and After-treatment system operate in different operation conditions. The parameters can be changed in the after-treatment system for simulating different aging problems such as injector inaccuracy and ammonia surface storage capacity reduction. This particular Engine is based on a 3-liter turbo-charged Diesel engine and the SCR system is about 5 liters. The engine model is a map-based model and the SCR model is a modified version referenced from [20].
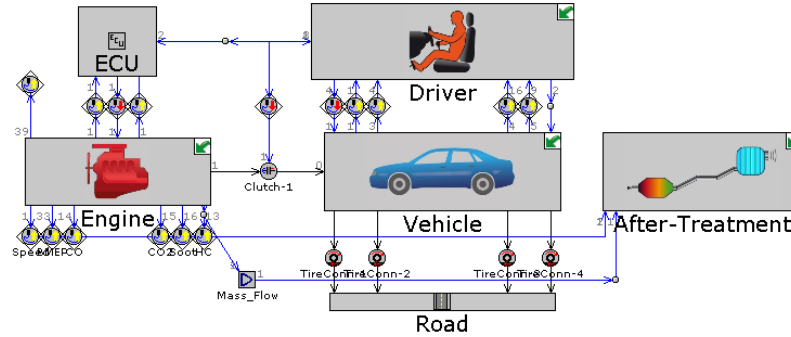
Figure 4.5: The light-duty vehicle model built in GT-POWER

4.6.2   Steady State test

When the engine is on steady state, the mole fraction of NO_x, the exhaust gas temperature and the exhaust gas flow rate out of engine are constant values. But for the SCR system and the compound controller, these conditions are unknown disturbances. The objective of the compound control strategy is to regulate the ammonia storage by ammonia feedback control and make the ammonia slip near 10 ppm as much as possible to have a high NO_x reduction efficiency. Therefore, the 8 ppm is selected as the control set-point to make the control output near 10 ppm as much as possible and make the average ammonia slip lower than 10 ppm but very close to 10 ppm. Based on this control target, the control output should not be strictly tracking the 8 ppm and it is acceptable if the control output is close to 10 ppm. So, the compound controller can fulfil the target in Figure 4.6. And Figure 4.7 demonstrates that the compound control strategy can have a high NO_x reduction efficiency about 82%.
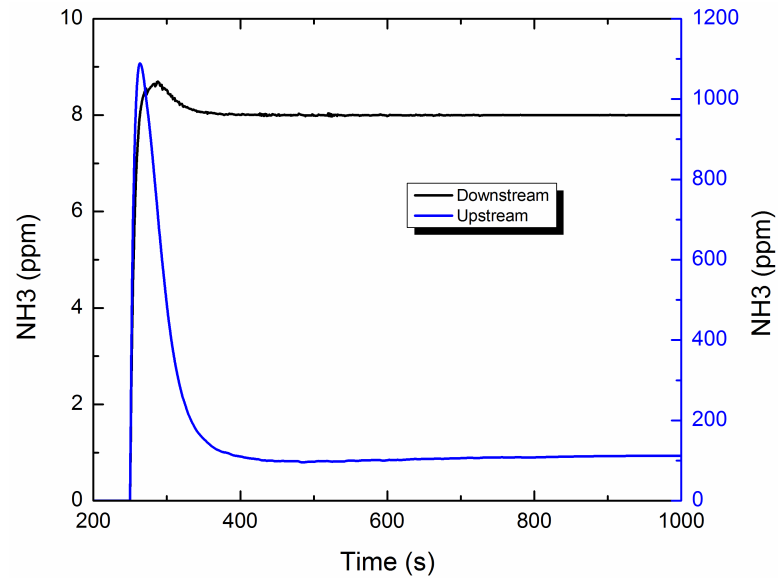
Figure 4.6: Ammonia input and output of compound control strategy when engine on Steady state
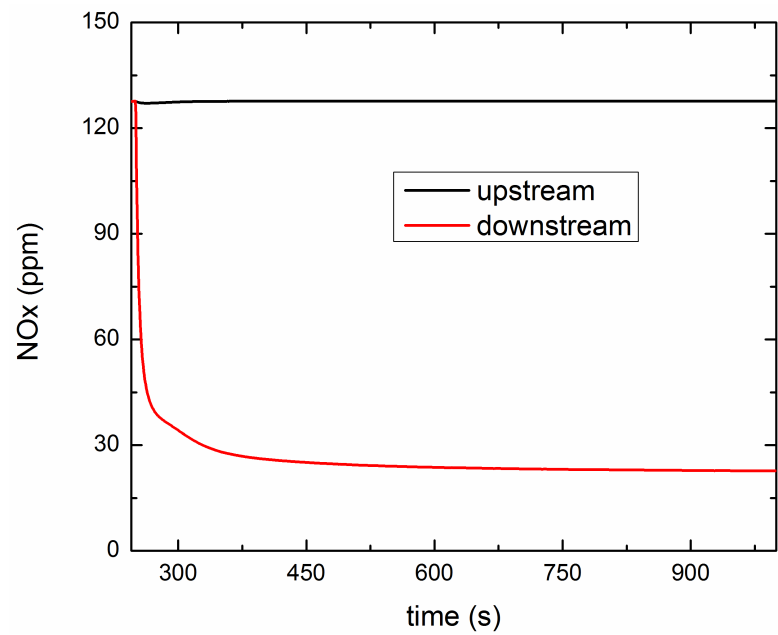
Figure 4.7: NO_x redution of compound control strategy when engine on Steady state

4.6.3   FTP-75 cycle

The FTP-75 (Federal Test Procedure) has been used for emission certification and fuel economy testing of light-duty vehicles in the United States. As can be seen from Figure 4.8, the FTP-75 test cycle is highly transient and the vehicle speed can track the reference speed well.
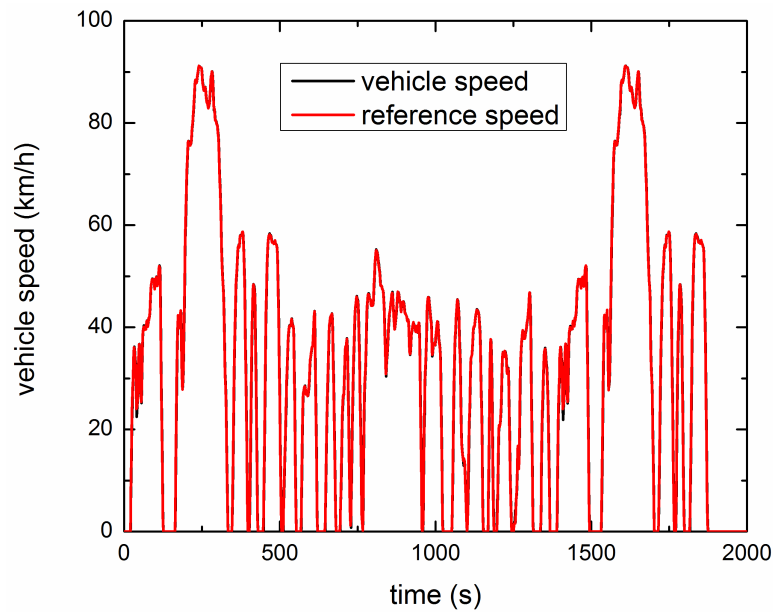
Figure 4.8: The speed tracking in the FTP-75 test

4.6.4   The Outlet Conditions during the FTP-75 test cycle

The exhaust gas temperature, the mole fraction of NO_x and the exhaust gas flow rate are external disturbances of SCR system and vastly varied over FTP-75 test cycle. From Figure 4.9 we can see the profile of temperature during the FTP-75 test. To guarantee that the injected urea can be fully converted into NH_3, the compound control strategy can shut down injection when temperature is lower than 473K. It

can be seen from Figure 4.10 that the mole fraction of NO and NO_2 are different. However, it is difficult to measure the exact amount of NO and NO_2 by NO_x sensor. In Figure 4.11, the variation of exhaust gas flow rate is demonstrated. It can be seen from these two figures that the external disturbances change rapidly, which makes it challenging for the SCR control.
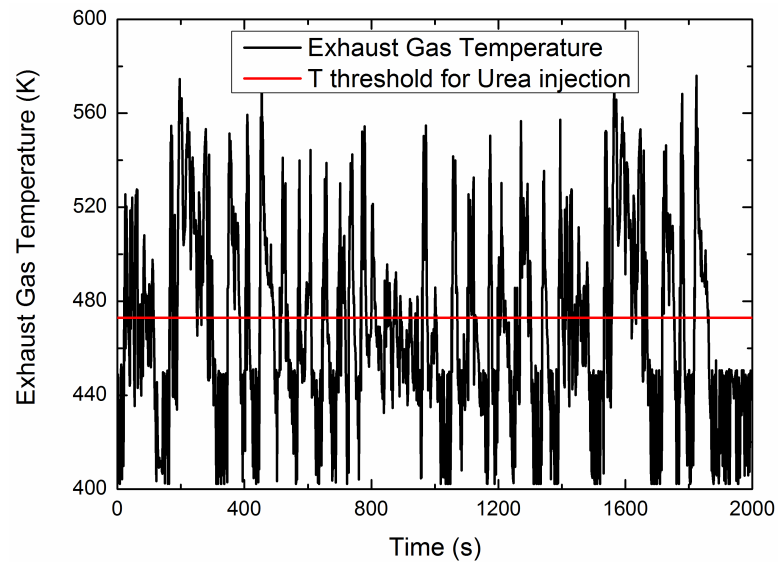
Figure 4.9: The temperature out of the engine
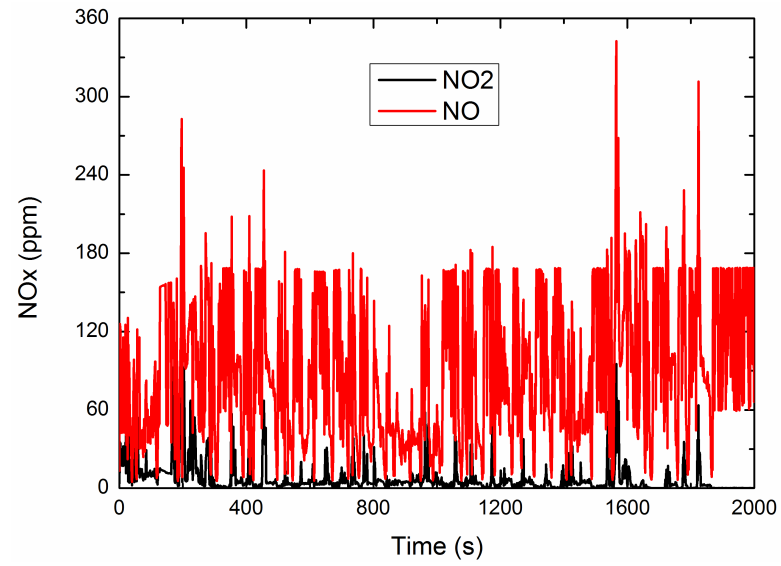
Figure 4.10: The mole fraction of the NO and NO_2 at upstream of the SCR system
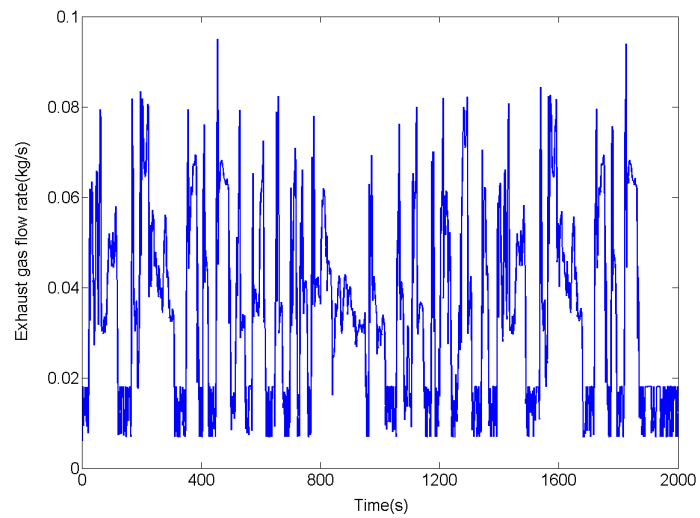
Figure 4.11: The flow mass rate of the exhaust gas out of engine

4.6.5   The Internal Conditions of SCR system during the FTP-75 test cycle

Several parameters and states of the SCR system play important role in the reaction rate. Some parameters and states cannot be measured, for example the ammonia surface coverage ratio. From Figure 4.12, we can see that the profile of ammonia surface coverage ratio, which varied greatly during FTP-75 test. Some reaction parameters Θ, k_x and r_x ($x = ads, des, oxi$) can be identified by using the experiment data. However, the accurate values cannot be obtained because they will change during life time. These variable dynamics are treated as internal disturbances of the SCR system and be rejected by the compound control strategy.
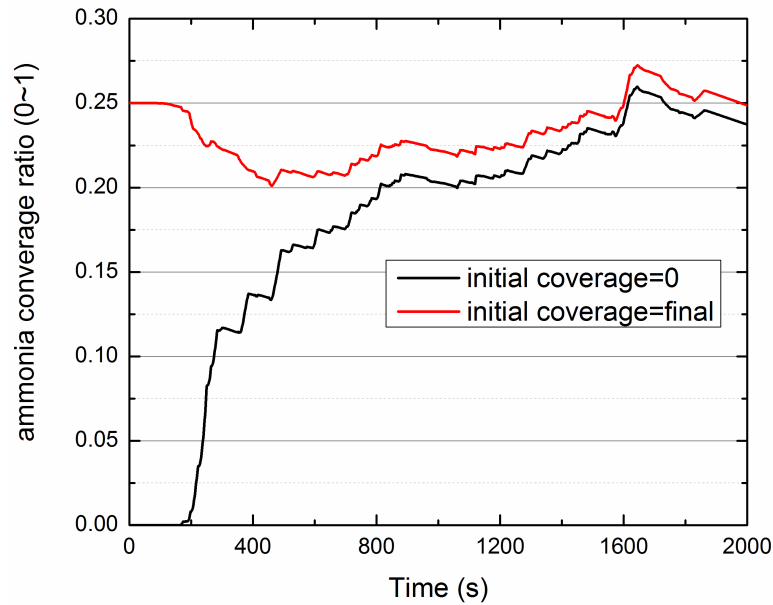
Figure 4.12: The variation of the ammonia surface storage ratio

4.6.6 The Results of the Control Strategy without the Switching Mechanism

The control strategy without the switching mechanism is an ADR controller only, which will lead to high ammonia slip when exhaust gas temperature change rapidly. As can be seen in Figure 4.13, the amount of upstream ammonia (input) is large while that of downstream ammonia (output) is small and the temperature is low, following which the amount of downstream ammonia (output) is high while there is no upstream ammonia (input) and the temperature rises sharply. From Figure 4.14, it can be seen that the ammonia surface storage ratio dramatically rises when the amount of upstream ammonia (input) is large, which means that when the temperature is low, more ammonia can be stored in the SCR but when the temperature suddenly rises, the stored ammonia desorbs and leads to high ammonia slip.
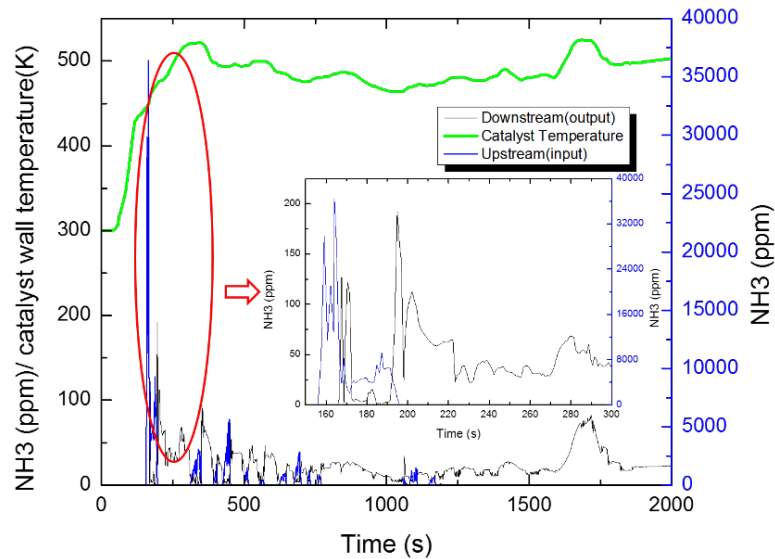
Figure 4.13: The ammonia input and downstream ammonia of the SCR system
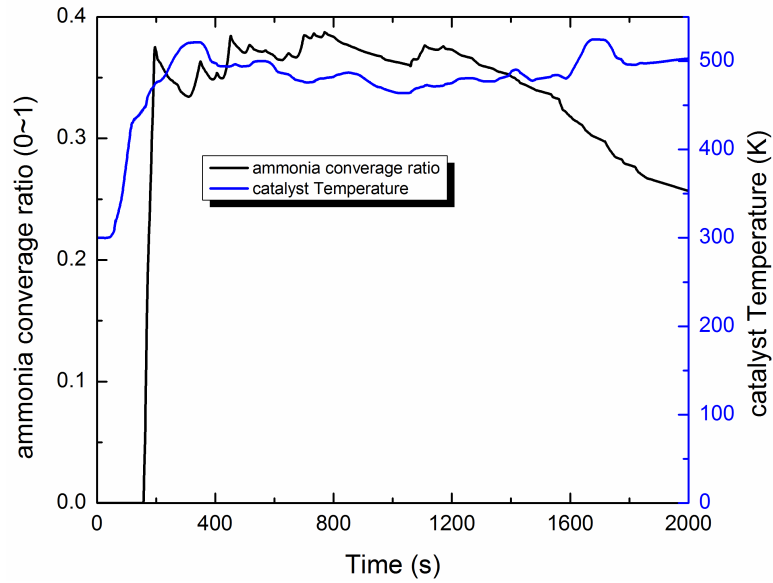
Figure 4.14: The variation of the ammonia surface storage ratio

4.6.7 The Results of Compound Control Strategy over FTP-75 test cycle

Figure 4.15 and Figure 4.16 are the results of the compound controller over FTP-75 test. The objective of the compound control strategy is to deliver the maximum NO_x efficiency consistent with NH_3 slip constraints. The compound control strategy regulates the ammonia storage by ammonia feedback control and make the ammonia slip near 10 ppm as much as possible to have a high NO_x reduction efficiency. From Figure 4.15, we can see that the average mole fraction of ammonia slip can satisfy the control target (lower than 10 ppm but very close to 10 ppm on average and 25 ppm at peak) during the FTP-75 test. As can be seen clearly from Figure 4.16, a relative high NO_x reduction efficiency is obtained during the FTP-75 test (low temperature test cycle). These results demonstrate that the compound control strategy with the

switching mechanism can reject total disturbances and fulfil the control target during the FTP-75 test. Figure 4.17 is the ammonia input of the SCR system.
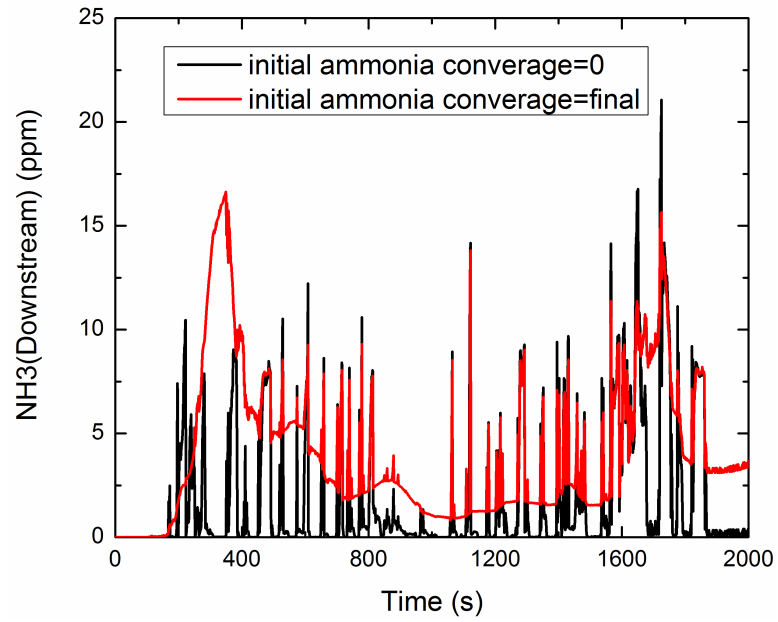
Figure 4.15: Ammonia slip after SCR system
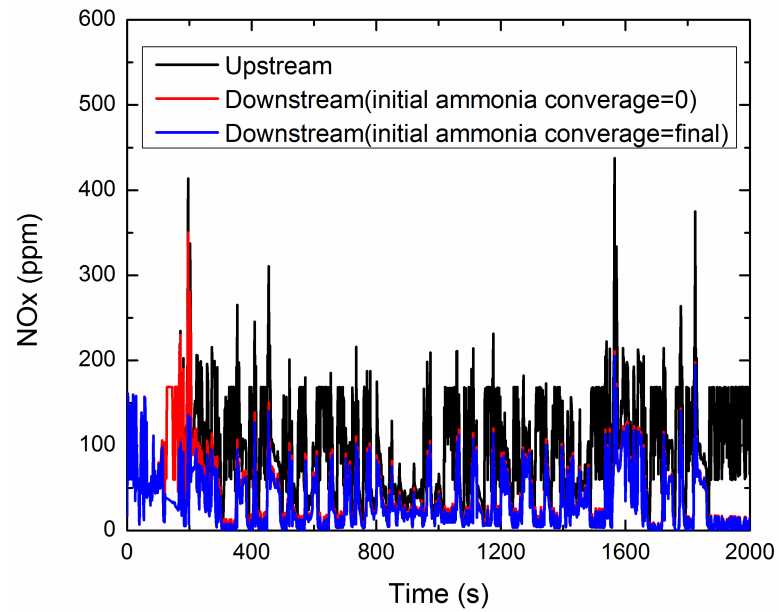
Figure 4.16: NO_x reduction after SCR system
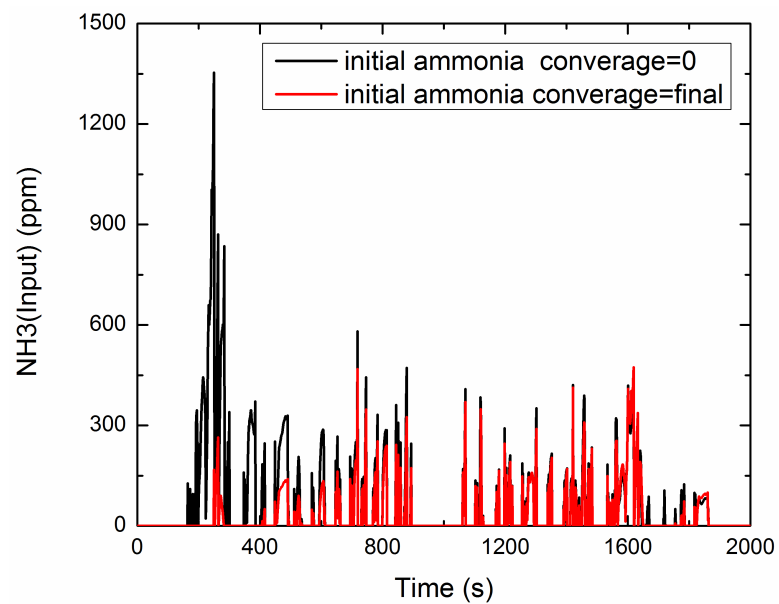
Figure 4.17: Ammonia input at the upstearm of SCR system

4.6.8 The Comparison of NO_x Reduction Efficiency

The feed-forward open-loop controller is targeting a NH_3/NO_x ratio of 1.0. Urea injection does not occur until the inlet gas temperature exceeds the injector controller threshold temperature of 200 $°C$. Figure 4.18 demonstrates the cumulative NO_x mass before and after the SCR system under FTP-75 test. The NO_x conversion efficiency of compound control strategy is higher than that of feed-forward controller in Figure 4.18. Therefore, the compound controller can improve the NO_x conversion efficiency and make the NH_3 slip within the regulation bounds.
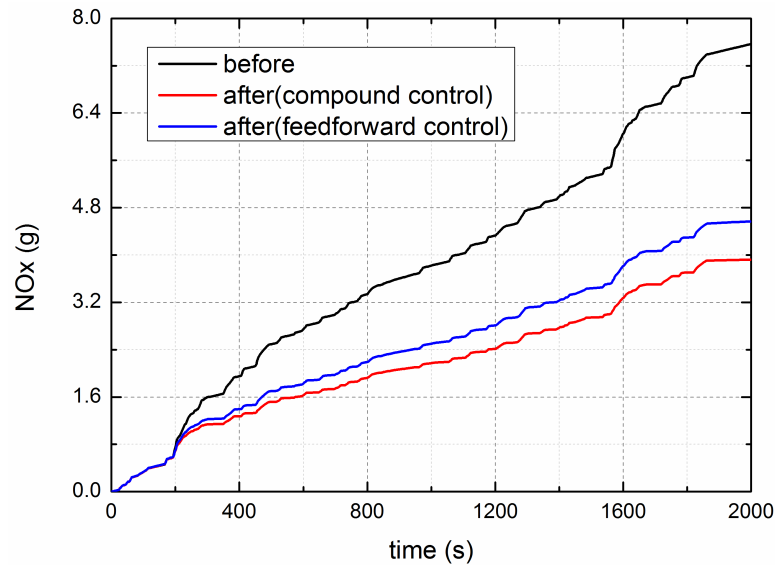
Figure 4.18: Comparison between compound control and feed-forward control

4.6.9 Controller Performance over Aging Cases

This section is to test two different uncertainties in the SCR system: difference between desired ammonia concentration and real ammonia concentration, the difference between design ammonia surface storage capacity and real ammonia surface storage

capacity. The assumption in this paper is that the urea-to-ammonia concentration is complete and the difference between desired ammonia concentration and real ammonia concentration fully comes from urea injection inaccuracy. Urea injection inaccuracy and ammonia surface storage capacity reduction are common aging problems during the use of SCR system. Also, production variations in Urea Injectors and/or real ammonia surface storage capacities commonly exist. These factors will affect the performance of the controller. Three aging cases (+10% and -10% variations for the Urea Injector, and 10% decrease for ammonia surface storage capacity) are adjusted in the GT-power SCR model. Figure 4.19 and Figure 4.20 are the results of the compound control strategy over the FTP-75 test in different aging cases. As can be seen in Figure 4.19, although there are variations among different aging cases, the mole fraction of downstream NH_3 in three cases satisfied the target (lower than 10 ppm on average and 25 ppm at peak). As can be seen in Figure 4.20, the SCR-out NO_x concentration is almost the same among different cases. These results demonstrated that the controller can keep good performance during lifetime.
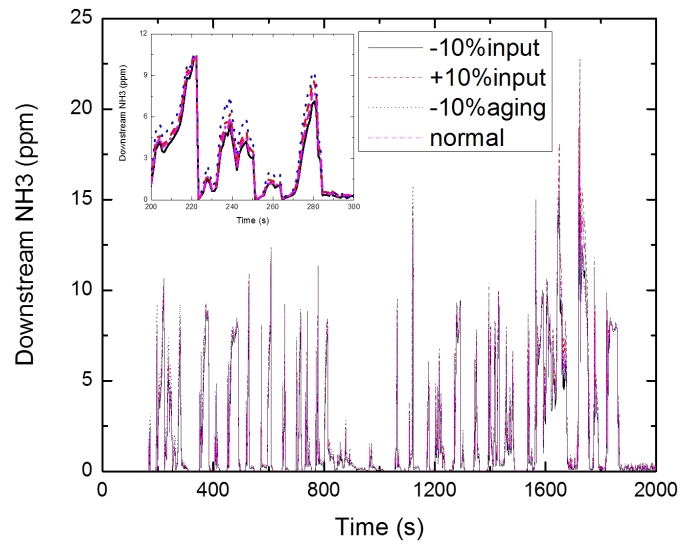
Figure 4.19: Ammonia slip of Urea injection inaccuracy and ammonia storage decrease due to aging
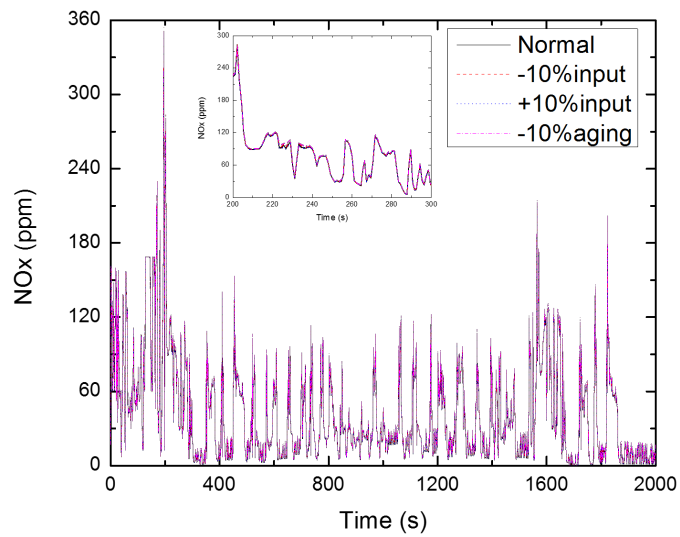
Figure 4.20: SCR-out NO_x of Urea injection inaccuracy and ammonia storage decrease due to aging

4.7   Conclusion

A novel compound control strategy with a switching mechanism between an Active Disturbance Rejection Controller and a zero-input controller has been presented, which uses downstream NH_3 mole fraction as feedback signal. Basing on the principle of SCR system, the compound control strategy is designed to reject the total disturbance of the SCR system and to avoid high ammonia slip at downstream of SCR system when temperature suddenly rises. The compound control strategy was tested over the steady state and FTP-75 cycle test. The result shows that the compound control strategy can achieve the control target (lower than 10 ppm on average and 25 ppm at peak). The potential of the compound control strategy was validated in three different aging issues: +10% and -10% variations for the Urea injector and 10% decrease for ammonia surface storage capacity. The proposed control strategy offered significant robustness over FTP-75 test in these cases. It is clear that the proposed control strategy can address problems rose by transient operation states and aging conditions.

Reference

[1] World Health Organization, 2006, WHO Air Quality Guidelines for Particulate Matter, Ozone, Nitrogen Dioxide, and Sulfur Dioxide: Global Update 2005, WHO Press, Geneva, Switzerland, Chap. 12.

[2] Backman, H., Arve, K., Klingstedt, F., and Murzin, D. Y., 2006, "Kinetic Considerations of H2 Assisted Hydrocarbon Selective Catalytic Reduction of NO over Ag/Al2O3: II. Kinetic Modeling," Applied Catalysis, Vol. 304, pp. 86-92.

[3] Hsieh, M.-F. and Wang, J., 2010, "An Extended Kalman Filter for Ammonia Coverage Ratio and Capacity Estimations in the Application of Diesel Engine SCR Control and Onboard Diagnosis," Proceedings of American Control Conference, Baltimore, Maryland.

[4] Johnson, T. V., 2010, "Review of Diesel Emissions and Control," SAE World Congress, SAE Technical Paper No. 2010-01-0301.

[5] Willems, F. and Cloudt, R., 2011, "Experimental Demonstration of a New Model-Based SCR Control Strategy for Cleaner Heavy-Duty Diesel Engines," IEEE Transaction on Control Systems Technology, Vol. 19, No. 5.

[6] Willems, F., Cloudt, R., Eijnden, E. v. d., Genderen, M. v., Verbeek, R., Jager

B. d., Boomsma, W., Heuvel, I. v. d., 2007, Is Closed-loop SCR Control Required to Meet Future Emission Targets?," SAE World Congress, SAE Technical Paper No. 2007-01-1574.

[7] Hsieh, M.-F. and Wang, J., 2011, "Design and Experimental Validation of An Extended Kalman Filter-Based NO_x Concentration Estimator in Selective Catalytic Reduction System Applications," Control Engineering Practice, 19 (2011), pp. 346353.

[8] Hsieh, M.-F. and Wang, J., 2010, "Observer-Based Estimation of Selective Catalytic Reduction Catalyst Ammonia Storage, Proceedings of the Institution of Mechanical Engineers, Part D: Journal of Automobile Engineering, No. 224: 1199.

[9] McKinley, T. L. and Alleyne, A. G., 2012, "Adaptive Model Predictive Control of an SCR Catalytic Converter System for Automotive Applications," IEEE Transaction on Control Systems Technology, Vol. 20, No. 6.

[10] Devarakonda, M., Parker, G., Johnson, J., Strots, V. and Santhaam, S., 2008, "Model-Based Estimation and Control System Development in a Urea-SCR After-Treatment System," SAE World Congress, SAE Technical Paper No. 2008-01-1324.

[11] Gao, Z., Huang, Y., Han, J., 2001, "An Alternative Paradigm for Control System Design," Proceedings of IEEE Conference on Decision and Control, No. 5:457885.

[12] Han, J., 2009, "From PID to Active Disturbance Rejection Control," IEEE Transaction on Industrial Informatics Vol. 56, No. 3:9006.

[13] Gao, Z., 2006, "Active Disturbance Rejection Control: a Paradigm Shift in Feedback Control System Design," Proceedings of the American Control Conference, Minneapolis, MN, Vol.2, pp. 399405.

[14] Zheng, Q., Chen, Z., Gao, Z., 2009, "A Practical Approach to Disturbance Decoupling Control," Control Engineering Practice, Vol.17, No. 9:101625.

[15] Piazzesi, G., Devadas, M., Krocher, O., Elsener, M., and Wokaun, A., 2006, "Isocyanic Acid Hydrolysis Over Fe-ZAM5 in Urea SCR," Catalysis Communications, Vol. 7, pp. 600-602.

[16] Kim, J. Y., Ryu, S.H., and Ha, J. S., 2004"Numerical Prediction on the Characteristics of Spray-Induced Mixing and Thermal Decomposition of Urea Solution in SCR System," Proceeding of ASME Internal Combustion Engine Division, No. ICEF2004-0889, pp. 165-170.

[17] Strots, V. O., Santhanam, S., Adelman, B. J., Griffin, G. A., and Derybowski, E. M., 2009, "Deposit Formation in Urea-SCR Systems," SAE World Congress, SAE Technical Paper No. 2009-01-2780.

[18] Schaber, P., Colson, J., Higgins, S., Thielen, D., Anspach, B., and Brauer, J., 2004, "Thermal Decomposition (Pyrolysis) of Urea in an Open Reaction Vessel," Thermochimica Acta, Vol. 424, pp. 131-142.

[19] Yim, S. D., Kim, S. J., Baik, J. H., Nam, I., Mok, Y. S., Lee, J. H., Cho, B. K., and Oh, S. H., 2004, "Decomposition of Urea into NH_3 for the SCR Process," Industrial & Engineering Chemistry Research, Vol. 43, pp. 4856-4862.

[20] Chatterjee, D., Burkhardt, T., Webel, M., Nova, I., Grossale, A. and Tronconi, E., 2007, "Numerical simulation of Zeolite- and V-based SCR Catalyst Converters," SAE World Congress, SAE Technical Paper No. 2007-01-1136.

[21] Grossale, A., Nova, I., and Tronconi, E., 2008, "Study of a Fe-zeolite-based System as NH_3-SCR Catalyst for Diesel Exhaust Aftertreatment," Catalysis Today, Vol.136, pp.18-27.

[22] Upadhyay, D. and Nieuwstadt, M. V., 2002, "Modeling of a Urea SCR Catalyst with Automotive Applications," ASME International Mechanical Engineering Congress and Exposition, IMECE2002-32104.

[23] Upadhyay, D. and Nieuwstadt, M. V., 2006, "Model Based Analysis and Control Design of a Urea-SCR DeNOx Aftertreatment System," ASME Journal of Dynamic Systems, Measurement, and Control, Vol. 128, pp. 737-741.

[24] Schr, C. M., Onder, C. H., Elsener, M. and Geering, H. P., 2004, "Model-based Control of an SCR System for a Mobile Application," SAE World Congress, SAE Technical Paper No. 2004-05-0412.

[25] Grossale, A., Nova, I., Tronconi, E., Chatterjee, D., and Weibel, M., 2008, "The Chemistry of Reaction Analysis," Journal of Catalysts,Vol.256, pp.312-322.

[26] Gao, Z., 2003, "Scaling and Bandwidth-Parameterization Based Controller Tuning," Proceedings of the American Control Conference, Denver, Colorado.

[27] Hunnekes, E.V., Heijden, P. and Patchett, J. A., 2006, "Ammonia Oxidation Catalysts for Mobile SCR System," SAE World Congress, SAE Technical Paper No. 2006-01-0640.

[28] Hsieh, M.-F. and Wang, J., 2011, "A Two-cell Backstepping-based Control Strategy for Diesel Engine Selective Catalystic Reduction Systems," IEEE Transactions on Control Systems Technology, Vol.19,NO.6.

Chapter 5

Augmented-state Smooth Variable Structure Filter for Mean Temperature Estimation of a Diesel Oxidation Catalyst

5.1 Citation and Main Contributor

Jinbiao Ning and Fengjun Yan, "Augmented-state Smooth Variable Structure Filter for Mean Temperature Estimation of a Diesel Oxidation Catalyst", (submitted)

The main contributor to this paper is the first author-Jinbiao Ning (contributes more than 70%).

5.2 Abstract

The mean temperature of Diesel Oxidation Catalyst (DOC) is critical for on-board diagnostics and light off management. However, the mean temperature is difficult to be measured in production aftertreatment systems. To effectively estimate the mean temperature of a DOC, this paper presents two different filtering methods to compensate model uncertainties and disturbances. In the proposed method, a regular Smooth Variable Structure Filter (regular SVSF) was designed based on the reduced order model of a DOC. The reduced order model was calibrated and validated by the experimentally calibrated GT-power DOC model. Furthermore, to reduce estimation errors of mean temperature caused by disturbances and model uncertainties, a state disturbance was augmented to the reduced order model and the robust SVSF was designed based on the augmented model. Experiments were conducted on the chassis dyno with a Jetta Car for calibration and validation of the high-fidelity GT-power DOC model. The effectiveness of both regular SVSF and roubust SVSF were verified by high-fidelity GT-power DOC model. Simulation results based on the high-fidelity GT-power DOC model exhibit that the robust SVSF with augmented disturbance states can effectively estimate the mean temperature and has better estimation performance than regular SVSF in the case where HC concentration for both filters is much larger or smaller than real HC concentration.

5.3 Introduction

With increasingly stringent emission regulations, advanced diesel after-treatment systems are playing more and more important role in satisfying the current and coming

legislations. The state-of-the-art Diesel after-treatment system usually consists of a Diesel Oxidation Catalyst (DOC), a Diesel Particulate Filter (DPF) and a Selective Catalytic Reduction system (SCR) or a NO_x storage catalyst (also called Lean NOx Trap, abbr. LNT), as can be seen in Figure 5.1. The DOC is mainly used to oxidise the CO and HCs to CO_2 and H_2O and to convert NO to NO_2 for passive regeneration of DPFs and fast reactions of SCRs. In addition, the DOC is adopted to boost the DOC-out temperature for active regeneration of DPFs. The emission conversation efficiency of DOC highly depends on the mean temperature of a DOC, so the mean temperature of a DOC is critical for fast light off management to reduce exhaust pipe out emission, especially during the phase of cold start. However, the mean temperature of a DOC is not able to be directly measured. Therefore, the mean temperature estimation is critical for DOC on-board diagnostics and fast light off management but is challenging due to complex reactions and thermal dynamics in DOC.
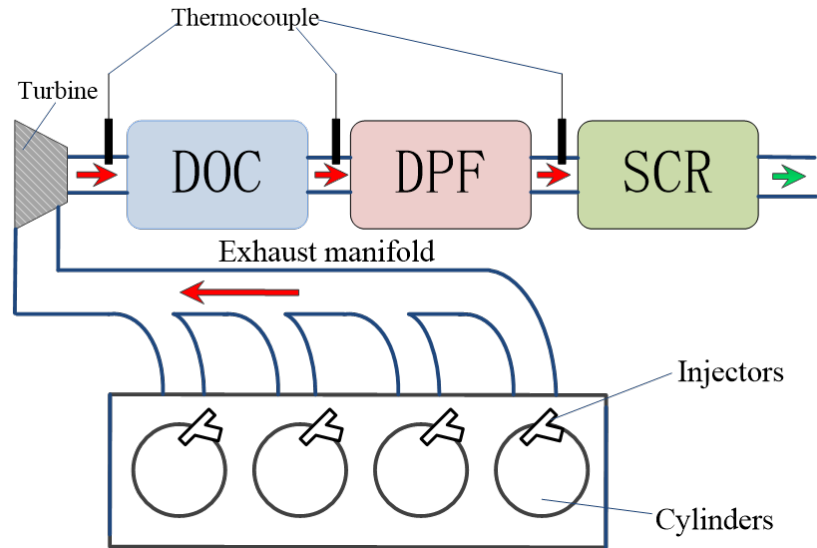
Figure 5.1: Aftertreatment system configuration

Mathematical models are required for mean temperature estimation and control of

a DOC. Several mathematical models for DOC have been reported in the literature. The effectiveness of one-dimensional (1D) automotive catalyst models have been reviewed in [1]. Detailed kinetic 1D models were proposed for simulation purpose based on first principle [3–6]. A reduced order 1D model of DOC and an Extended Kalman Filter (EKF) were proposed for the internal temperature and outlet emissions (e.g. CO, NO, NO_2) prediction in [2]. An control-oriented model with considering its thermal behavior was proposed for DOC control and diagnosis in [7–9]. However, the input disturbance and model uncertainties are not considered for the temperature estimation, leading to great estimation error in the case when model uncertainties and input disturbances exist. In particular, engine-out HCs are difficult to be accurate since the composition of HCs are very complex. It has been reported that there are about 80 $C_1 - C_{18}$ hydrocarbon species in engine-out and DOC-out exhaust gases [6]. Therefore, more efforts are required to deal with problems rose by model uncertainties and disturbances, especially in the case where HC is inaccurate for the mean temperature estimation.

In this paper, two smooth variable structure filter (SVSF) based filtering methods were proposed for the mean temperature estimation. The reduced order 1D model proposed in [2] was adopted for the SVSF based mean temperature estimators due to its relative low computational load and sufficient accuracy of thermal dynamics. A novel augmented state based smooth variable structure filter (robust SVSF) was proposed for mean temperature estimation of a DOC and compared with the regular SVSF. The novel robust SVSF is modified from regular SVSF and motivated from augmented states or extended states to timely estimate and compensate the disturbances, aiming to improve the estimation accuracy and robustness. The

SVSF is widely used in different areas such as trapped unburned fuel estimation for a Turbocharged Diesel Engine [20], battery parameters estimation such as capacitance, hysteresis, and state of charge (SOC) [21], ammonia storage ratio estimation in diesel after-treatment systems [22], and fault detection and diagnosis [23–26]. The augmented state or extended state is adopted in offset free model predictive control (offset-free MPC) [11–13] and extended state observer (ESO) based control [14–19].

The main contributions of this paper are: 1) The regular SVSF was designed based on a reduced ordered model to estimate the mean temperature of a DOC; 2) Augmented states were added to the reduced order model of a DOC and a robust SVSF was designed based on the augmented model; 3) The convergence of the robust SVSF is theoretically analysed; 4) Both regular SVSF and robust SVSF were compared under steady state and highly transient new European dynamic cycle (NEDC).

The rest of the paper is organized as follows. The experimental facility is demonstrated in section 5.4. A brief introduction of the principle and modeling of a DOC is demonstrated in section 5.5. The design of robust SVSF based on augmented states is presented in section 5.6. Experimental calibration and validation of a 1-D high-fidelity GT-power DOC model and simulations based on the 1-D high-fidelity GT-power DOC model are introduced to verify the proposed approaches in section 5.7. At the end of the chapter, the conclusion is given.

5.4   Experimental Facility

In this study, the experiments were done on the chassis dyno test platform with a Jetta Car. The Jetta car has a 2.0 Liter Turbocharged Direct Injection (TDI) Diesel engine equipped with high pressure common-rail fuel injection system, a dual-loop

Exhaust Gas Recirculation (High and Low Pressure EGR) and a Variable Turbine Geometry (VTG) turbocharger. The exhaust system consists of a DOC, a DPF, and a NO_x storage catalyst. The actual chassis dyno setup and measurements of DOC is demonstrated in Figure 5.2. The experimental instruments contain a OBD link SX which provides an access to the engine control unit (ECU) variables such as exhaust gas flow rate, engine speed, vehicle speed and so on. A Nova gas analyzer model 4000 is available to measure NO_x, CO, CO_2, O_2 and HC concentrations. Two thermocouples were installed at DOC inlet and DPF outlet. Two exhaust gas sample hoses were connected to the DOC inlet and DPF outlet. Physical parameters of the
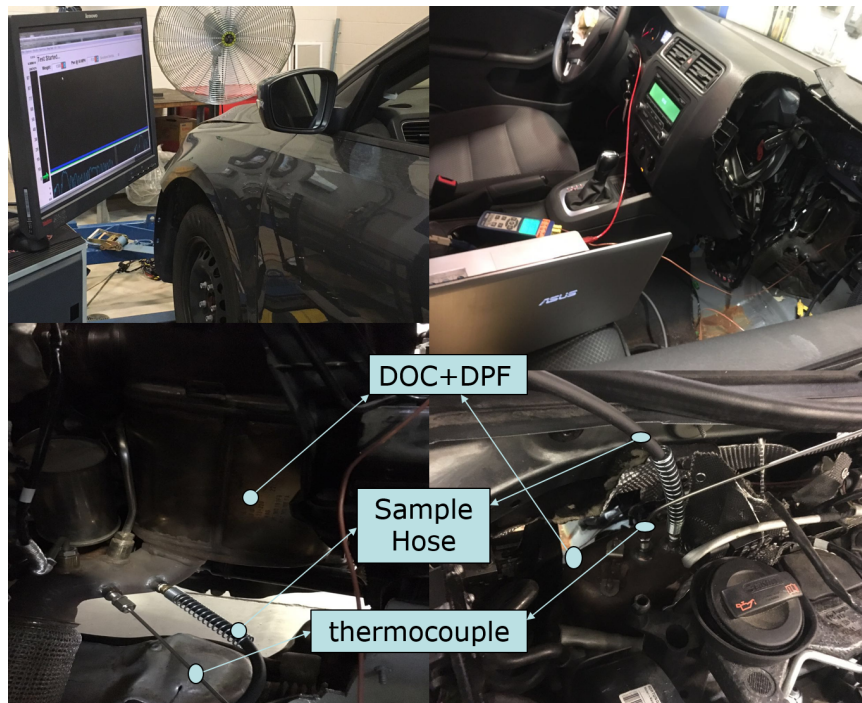
Figure 5.2: Chassis dyno test platform

DOC are demonstrated in table 1.

Table 1: Specifications of the DOC

Attributes	Values
Channel Geometry	square
Frontal Area (mm^2)	7693
Cell Density ($1/in^2$)	400
Length (mm)	90
Wall Thickness (mm)	0.05
Density of the substrate (kg/m^3)	7900

5.5 The Thermal Dynamic and Modelling of a DOC

To understand the complex thermal dynamics of a DOC and design mean temperature estimators, this section introduces the principle of a DOC and a reduced order model presented in [2].

5.5.1 Thermal Dynamic of DOC

The DOC is a flow-through honeycomb monolith structure composed of inner layer (substrate layer) and outer layer, as can be seen in Figure 5.3. The substrate layer divides into the washcoat and the substrate wall. The washcoat lay is a catalytic lay consisted of alumina and precious pltinum group metals (PGM) such as Platinum (Pt), Palladium (Pd) and Rhodium (Rh). The exhaust gases flow through the honeycomb monolith structure and oxidation reactions occur on the washcoat layer. Therefore, the thermal dynamic of DOC is complicated since it has thermal

conduction, convection and chemical reactions.
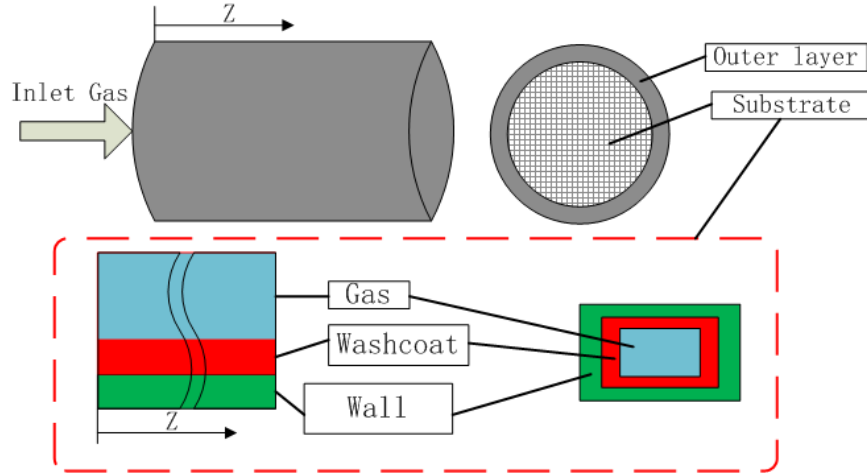
Figure 5.3: Schematic diagram of DOC

5.5.2 Main Reactions in DOC

The chemical reactions in DOC are complex and more details can be seen in [4–6]. The main reactions in DOC include oxidation reactions [5] and hydrocarbon storage [4], as demonstrated in table 2. Although there are about 80 hydrocarbon species, C_3H_6 and DF (DF_1 and DF_2) represent the partially reacted fuel hydrocarbons and unburned fuel, respectively. In table 2, DF_1 and DF_2 represent adsorbable slow oxidizing hydrocarbon and non-adsorbable slow oxidizing hydrocarbon, respectively. Z represents Zeolite.

Table 2: Main Reactions in DOC

	Oxidation Reactions
	Oxidation Reactions
1	$CO + 0.5O_2 \rightarrow CO_2$
2	$C_3H_6 + 4.5O_2 \rightarrow 3CO_2 + 3H_2O$
3	$H_2 + 0.5O_2 \rightarrow H_2O$
4	$NO + 0.5O_2 \rightarrow NO_2$
5	$DF_1 + 19.4O_2 \rightarrow 13.5CO_2 + 11.8H_2O$
6	$DF_2 + 19.4O_2 \rightarrow 13.5CO_2 + 11.8H_2O$
	Hydrocarbon Storage Reactions
7	$Z + DF_1 \rightarrow ZDF_1$
8	$ZDF_1 \rightarrow Z + DF_1$

The reaction rate of reactions (1)-(6) can be expressed:

$$R_i = \frac{k_i C_m C_n \exp(-\frac{E_i}{R_g T})}{G} \tag{5.1}$$

where i is from 1 to 6. m can be CO, C_3H_6, H_2, NO depending on the reactions, k_i is the pre-exponent multiplier, n is the O_2, R_i is the reaction rate in the DOC, E is the activation energy of reactions, R_g is a constant, C is the concentration, G is the inhibition factor, T is the solid phase temperature.

5.5.3   Reduced Order Model of DOC

Several DOC models have been presented in literature. To reduce the computational load and achieve sufficient accuracy of thermal dynamics, a reduced order model

proposed in [2] is adopted to design the SVSF based mean temperature estimator. Several assumptions are made for the reduced order model: 1) the surface phase and gas phase are considered as one phase so they have the same temperature and concentration; 2) the reactions are instantaneous; 3) three reactions (Reaction 1, 2 and 4 in table 2) are considered in this reduced order model. More details about the reduced order model can be referenced in [2]. The reduced order model of a DOC can be expressed bellow [2],

$$
\begin{cases}
\varepsilon u \frac{dC_i}{dx} = -R_i \\[2mm]
((1-\varepsilon)\rho_s c_{p,s} + \varepsilon \rho c_v)\frac{\partial T}{\partial t} = -\varepsilon \rho u c_p \frac{\partial T}{\partial x} - \sum \Delta h_i R_i - h_a S(T-Ta)/V \\[2mm]
y = T_{out}
\end{cases}
\tag{5.2}
$$

where $i = CO, NO, C_3H_6$, R_i represents the reaction rate, Ta is ambient temperature, u is velocity of the exhaust gas, ε is the void fraction of the DOC, ρ_s and $c_{p,s}$ are the density and specific heat of solid phase, ρ is the density of the exhaust gas, c_p and c_v are specific heat of exhaust gas, Δh_i is the enthalpy of the oxidation reaction, h_a is the external convection coefficient, S is the outer surface of the DOC, V is the volume of the DOC, y is the measurement DOC outlet temperature. The discretized form of the reduced order model of a DOC is expressed by the following equation [2],

$$
\begin{cases}
C_{i,r} = C_{i,r-1} - \dfrac{\Delta z}{\varepsilon u} R_i \\[3mm]
(T_{r,k} - T_{r,k-1}) = \dfrac{1}{\Delta z((1-\varepsilon)\rho_s c_{p,s} + \varepsilon \rho c_v)} \\[3mm]
(-\Delta t \varepsilon \rho u c_p (T_{r,k} - T_{r-1,k}) \\[2mm]
- \Delta t \Delta z \sum \Delta h_i R_i - \Delta t \Delta z h_a S(T_{r,k} - Ta)/V) \\[3mm]
y = T_{r\,\text{max},k-1}
\end{cases}
\tag{5.3}
$$

where Δt is time interval, Δz is discretization length, $T_{r,k}$ is DOC temperature, r represents the axial elements $1, ..., N$, k represents the index of integration in time. To be noted, total hydrocarbons for DOC model is represented by the C_3H_6 only, causing uncertainties between reduced order model and real DOC system. Therefore, the above discretization and nonlinear reduced order model can be transformed into the standard nonlinear model in the following,

$$x_k = \begin{bmatrix} T_{1,k} \\ T_{2,k} \\ \vdots \\ T_{r-1,k} \\ T_{r,k} \end{bmatrix} = f(x_{k-1}, C_{i,k-1}) + w_{k-1} \tag{5.4}$$

$$y_k = h(x_k) + v_k$$

where $i = CO, NO, C_3H_6$, r represents the axial elements $1, ..., N$, k represents the index of integration in time, f represents the reduced order model (5.3), w_k is the unknown system dynamics including model uncertainties and disturbances, v_k is the measurement noise.

5.6 SVSF based Design for Mean Temperature of a DOC

Figure 5.4 demonstrates the estimation scheme of the DOC mean temperature. Two SVSF based temperature estimators are designed to estimate the internal temperature of the DOC and the mean temperature is calculated based on the internal temperature

of DOC. The mean temperature of DOC can be expressed by the equation: $T_{mean} = \frac{1}{N}\sum\limits_{r=1}^{N} T_r$.
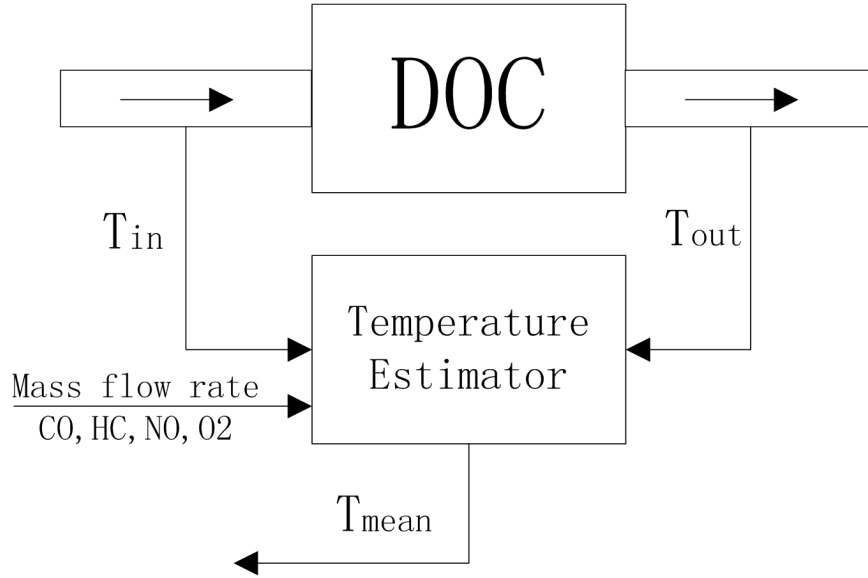
Figure 5.4: The mean temperature estimation scheme of a DOC

5.6.1 Regular SVSF Design with Reduced Order Model

Figure 5.5 depicts the concept of Smooth Variable Structure Filter (SVSF). The estimated state trajectory converges to a bounded region of the system state trajectory. The bounded region of the system state trajectory is also called existence subspace (β). A smooth subspace (also called smooth boundary lay Ψ) is used in SVSF to reduce or remove the chattering effect and improve the robustness [27]. As demonstrated in the reference [27], the SVSF for nonlinear model can be designed by the linearized strategy like extended Kalman Filter. Thus, two steps are required to design the SVSF:1) model linearization, 2) SVSF design based on the linear model.
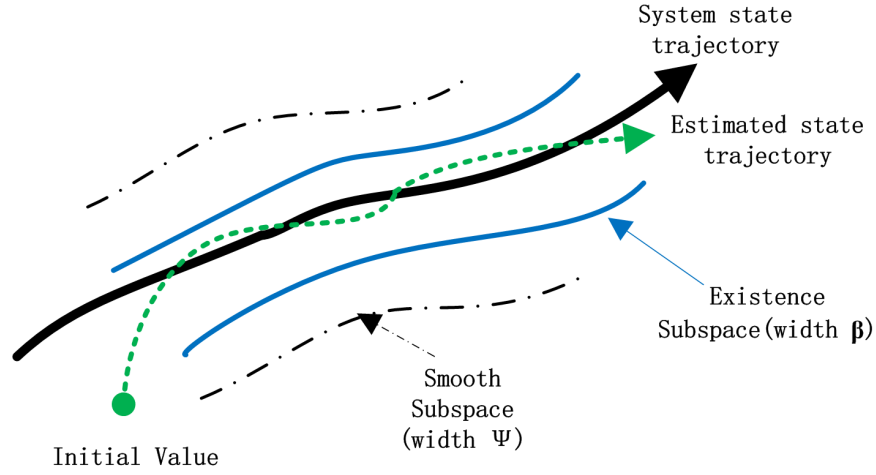
Figure 5.5: The concept of Smooth Variable Structure Filter [27]

Linearization of the Reduced Order Model

The linear model of the reduced order model (5.4) can be expressed by the following equation,

$$x_{k+1} = Fx_k + w_k$$
$$y_k = Hx_k + v_k$$

(5.5)

where x_k is the DOC temperature, w_k is process noise, y_k is the measurement output, v_k is the measurement noise. F and H can be expressed by the following equation,

$$F = \frac{df}{dx}\Big|_{x_{k-1}} = \begin{bmatrix} \frac{\partial T_{1,k}}{\partial T_{1,k-1}} & \frac{\partial T_{1,k}}{\partial T_{2,k-1}} & \cdots & \frac{\partial T_{1,k}}{\partial T_{r,k-1}} \\ \frac{\partial T_{2,k}}{\partial T_{1,k-1}} & \frac{\partial T_{2,k}}{\partial T_{2,k-1}} & \cdots & \frac{\partial T_{2,k}}{\partial T_{r,k-1}} \\ \vdots & \vdots & \cdots & \vdots \\ \frac{\partial T_{r,k}}{\partial T_{1,k-1}} & \frac{\partial T_{r,k}}{\partial T_{2,k-1}} & \cdots & \frac{\partial T_{r,k}}{\partial T_{r,k-1}} \end{bmatrix}$$

$$H = \frac{dh}{dx} = [0 \cdots 1]$$

(5.6)

Regular SVSF design

Based on the linear model (5.5) and the reference [27], the regular SVSF can be designed in the following steps,

1) A priori state estimation

$$
\begin{aligned}
\hat{x}_{k|k-1} &= f(\hat{x}_{k-1|k-1}, C_{i,k-1}) \\
\hat{y}_{k|k-1} &= H\hat{x}_{k|k-1} \\
e_{y_{k|k-1}} &= y_k - \hat{y}_{k|k-1}
\end{aligned}
\tag{5.7}
$$

2) A correction term K_k is derived from the error in the predictive output.

3) Posteriori state correction

$$
\begin{aligned}
\hat{x}_{k|k} &= \hat{x}_{k|k-1} + K_k \\
\hat{y}_{k|k} &= H\hat{x}_{k|k} \\
e_{y_{k|k}} &= y_k - \hat{y}_{k|k}
\end{aligned}
\tag{5.8}
$$

4) Steps 1 to 4 are iteratively repeated.

The calculation of the correction term is different for different systems. For the DOC system with fewer measurements than state variables, it requires to transform the

model (5.5) to a new form as follow,

$$
x_k = \begin{bmatrix} x_{uk} \\ x_{lk} \end{bmatrix}
$$
$$
H = \begin{bmatrix} H_1 \\ H_2 \end{bmatrix}
\tag{5.9}
$$

Therefor, the correction term K_k is required to divided into the upper and lower term, $K_k = \begin{bmatrix} K_k^u \\ K_k^l \end{bmatrix}$. The upper correction term can be expressed in the following form,

$$
K_k^u = H_1^{+1} \left(\left| e_{y_{k|k-1}} \right| + \gamma \left| e_{y_{k-1|k-1}} \right| \right) \circ sat(e_{y_{k|k-1}}, \Psi)
\tag{5.10}
$$

where γ is a tuning parameter and $0 < \gamma < 1$.

To calculate the lower correction term, it requires to transform the model (5.5) to a new form by the transformation matrix $Tx_k = \begin{bmatrix} y_{uk} \\ y_{lk} \end{bmatrix}$. The new form of the model can be expressed as follow,

$$
\begin{bmatrix} y_{u_{k+1}} \\ y_{l_{k+1}} \end{bmatrix} = \begin{bmatrix} \Phi_{11} & \Phi_{12} \\ \Phi_{21} & \Phi_{22} \end{bmatrix} \begin{bmatrix} y_{u_k} \\ y_{l_k} \end{bmatrix} + \begin{bmatrix} \bar{w}_{1_k} \\ \bar{w}_{2_k} \end{bmatrix}
\tag{5.11}
$$

where y_{u_k} is measurement variables and $y_{l_{k+1}}$ is estimated states, T is a transformation matrix, $\Phi = T^{-1}FT = \begin{bmatrix} \Phi_{11} & \Phi_{12} \\ \Phi_{21} & \Phi_{22} \end{bmatrix}$, $\bar{w} = T^{-1}w_k - \begin{bmatrix} \Phi_{11} \\ \Phi_{21} \end{bmatrix} v_k = \begin{bmatrix} \bar{w}_{1_k} \\ \bar{w}_{2_k} \end{bmatrix}$. Based on the nominal model (5.5), the filter gain for the estimated states $y_{l_{k+1}}$ can be expressed

by the following equations,

$$K_{l_k} = \left(\left| \Phi_{22} \Phi_{12}^{-1} e_{y_{k|k-1}} \right|_{ABS} + \gamma \left| \Phi_{12}^{-1} e_{y_{k|k-1}} \right|_{ABS} \right)$$
$$\circ sat(\Phi_{22} \Phi_{12}^{-1} e_{y_{k|k-1}}, \Psi)$$

(5.12)

More details and the convergence of regular SVSF can be reference from [27].

5.6.2   Robust SVSF Design with Augmented Reduced Order Model

The regular SVSF obtains the robustness at the cost of estimation accuracy since the existence subspace (β) and smooth subspace (Ψ) have significant effect on the estimation accuracy. The DOC system may have large unknown system dynamics including input disturbance and model uncertainties, leading to large existence subspace. The design of robust SVSF is motivated by the idea of augmented states [11–13] or extended states [14–19] to achieve better robustness and estimation precision. Figure (5.6) demonstrates the idea of robust SVSF: the augmented states timely estimate the unknown system dynamics including disturbances and model uncertainties, no matter how large the unknown system dynamics is, and force the existence subspace (β) into the smooth subspace (Ψ) to improve the accuracy and remove chatting. As the existence subspace (β) is forced to be small, the smooth subspace (Ψ) also can be set small to get better estimation precision. Two steps are required for the robust SVSF design: 1) the reduced order model of DOC is augmented with disturbance states; 2) the robust SVSF is designed based on the augmented state model.
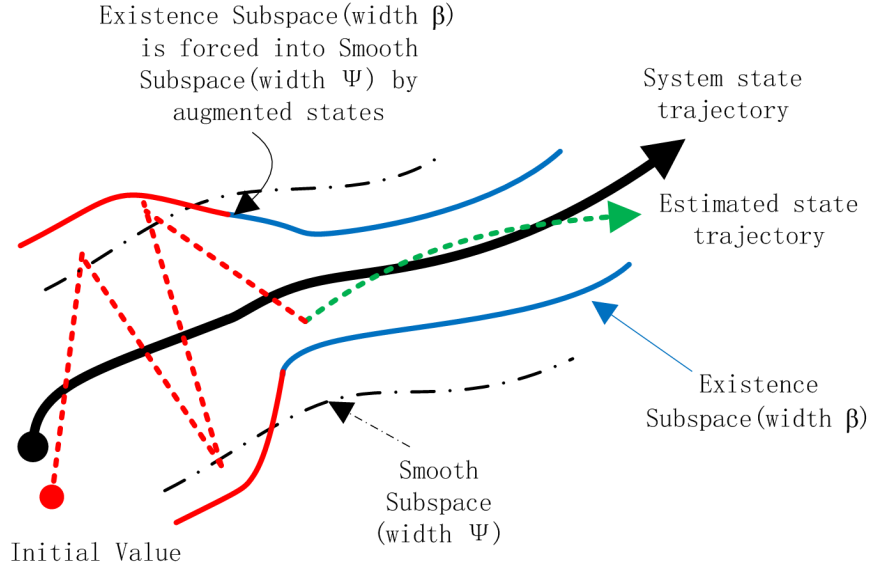
Figure 5.6: The idea of robust Smooth Variable Structure Filter

Augmented Reduced Order Model

Different from the regular SVSF design, the unknown system dynamic w_k in the reduced order model of DOC (5.4) is treated as a new state for the robust SVSF design. Thus, the augmented reduced order model of DOC can be expressed by the following equation,

$$x_k = f(x_{k-1}, C_{i,k-1}) + Dx_{d,k-1}$$
$$y_k = h(x_k) + v_k$$

(5.13)

where $x_{d,k}$ represents the unknown system dynamics, D is the matrix of the dynamic of $x_{d,k}$ for augmented states. Here, $x_{d,k}$ is assumed to be bounded and its dynamic is assumed to be $x_{d,k+1} = x_{d,k} + Eh(k)$. $h(k)$ is unknown but is assumed to be bounded. In fact, unknown system dynamic $x_{d,k}$ and its dynamic $h(k)$ are bounded in DOC system. Therefore, the augmented linear model can be expressed in the following

equation,

$$
\begin{cases}
\bar{x}_{k+1} = \bar{F}\bar{x}_k + Gh_k \\[2mm]
y_k = \bar{H}\bar{x}_k + v_k \\[2mm]
\bar{x}_k = [x_k, x_{d,k}]^T \\[2mm]
\bar{F} = \begin{bmatrix} F & D \\ 0 & E \end{bmatrix} \\[4mm]
G = \begin{bmatrix} 0 & E \end{bmatrix} \\[4mm]
\bar{H} = \begin{bmatrix} H & 0 \end{bmatrix}
\end{cases}
\tag{5.14}
$$

Based on equation (5.14), the a priori estimate of the augmented linear model can be expressed in the following equation,

$$
\begin{cases}
\hat{\bar{x}}_{k+1} = \hat{\bar{F}}\hat{\bar{x}}_k \\[2mm]
y_k = \bar{H}\hat{\bar{x}}_k + v_k \\[2mm]
\hat{\bar{x}}_k = [\hat{x}_k, \hat{x}_{d,k}]^T \\[2mm]
\hat{\bar{F}} = \begin{bmatrix} F & \hat{D} \\ 0 & E \end{bmatrix} \\[4mm]
\bar{H} = \begin{bmatrix} H & 0 \end{bmatrix}
\end{cases}
\tag{5.15}
$$

where $\hat{x}_{d,k}$ represents the estimated unknown system dynamics. For the augmented model, the number of estimated augmented disturbance states should not exceed the number of the measurement variables [11, 12]. More details about the number of augmented disturbance states can be referenced from [11, 12]. For the DOC model, there is one measurement output only, so that there can be only one augmented disturbance $\hat{x}_{d,k}$. Therefore, the matrix $\hat{D}$ is very critical for the estimation. Based on the DOC system, heat release from chemical reactions is difficult to be accurate,

especially when HC is not accurate. To effectively estimate the mean temperature of DOC even in the case where HC is not accurate for the filter, the disturbance state is expressed by $\hat{x}_{d,r} = \Delta t \Delta z h_{HC} R_{HC,r}$. Based on reduced order model of DOC, the concentration and reaction rate can be expressed as follow,

$$
\begin{cases}
C_{HC,r} = C_{HC,r-1}/(1+d) = C_{HC,1}/(1+d)^{r-1} \\
d = \frac{k_{HC}C_{O_2}\exp(-E_{HC}/R_gT)\Delta z}{\varepsilon u} \\
R_{HC,r} = k_{HC}C_{O_2}\exp(-E_{HC}/R_gT)C_{HC,1}/(1+d)^{r-1}
\end{cases}
\tag{5.16}
$$

Thus, the unknown system dynamic can be expressed by the following equation,

$$
\begin{cases}
\hat{x}_{d,r} = \hat{x}_{d,1}\frac{1}{(1+d)^{r-1}} \\
\hat{x}_{d,1} = \Delta t \Delta z \Delta h_{HC}k_{HC}C_{O_2}\exp(-E_{HC}/R_gT)C_{HC,1}
\end{cases}
\tag{5.17}
$$

Therefore, motivated from equation (5.17), $\hat{D}$ can be expressed by the following matrix, $\hat{D} = \begin{bmatrix} 1 & \frac{1}{(1+d_f)^1} & \cdots & \frac{1}{(1+d_f)^{r-1}} \end{bmatrix}^T$ and d_f is a tuning parameter.

Robust SVSF Design

Design steps of robust SVSF are the same as the regular SVSF but the robust SVSF design is based on the augmented reduced order model. The design steps of robust SVSF are summarized as following,

1) A priori state estimation

$$
\hat{\bar{x}}_{k|k-1} =
\begin{bmatrix}
\hat{x}_{k|k-1} \\
\hat{x}_{d,k|k-1}
\end{bmatrix}
=
\begin{bmatrix}
f(\hat{x}_{k-1|k-1}, C_{i,k-1}) + \hat{D}\hat{x}_{d,k-1|k-1} \\
\hat{x}_{d,k-1|k-1}
\end{bmatrix}
$$

$$\hat{y}_{k|k-1} = \bar{H}\hat{\bar{x}}_{k|k-1}$$

$$e_{y_{k|k-1}} = y_k - \hat{y}_{k|k-1}$$

(5.18)

2) A correction term K_k is derived from the error in the predictive output.

3) Posteriori state correction

$$\hat{\bar{x}}_{k|k} = \hat{\bar{x}}_{k|k-1} + K_k$$

$$\hat{y}_{k|k} = \bar{H}\hat{\bar{x}}_{k|k}$$

(5.19)

$$e_{y_{k|k}} = y_k - \hat{y}_{k|k}$$

4) Steps 1 to 4 are iteratively repeated.

The upper correction term (K_{u_k}) of robust SVSF is the same as equation (5.10) of regular SVSF. To calculate the lower correction term (K_{l_k}) of the robust SVSF based on the augmented model, it is required to transform the augmented model (5.15) to a new form as follow,

$$
\begin{bmatrix}
\hat{y}_{u_{k+1}} \\
\hat{y}_{l_{k+1}}
\end{bmatrix}
=
\begin{bmatrix}
\hat{\Phi}_{11} & \hat{\Phi}_{12} \\
\hat{\Phi}_{21} & \hat{\Phi}_{22}
\end{bmatrix}
\begin{bmatrix}
y_{u_k} \\
\hat{y}_{l_k}
\end{bmatrix}
$$

(5.20)

where $\begin{bmatrix} \hat{y}_{u_{k+1}} \\ \hat{y}_{l_{k+1}} \end{bmatrix} = T\hat{\bar{x}}(k)$, y_{u_k} is measurement variables and $\hat{y}_{l_{k+1}}$ is system states,

T is a transformation matrix, $\hat{\Phi} = T^{-1}\hat{\bar{F}}T = \begin{bmatrix} \hat{\Phi}_{11} & \hat{\Phi}_{12} \\ \hat{\Phi}_{21} & \hat{\Phi}_{22} \end{bmatrix}$. Based on equation

(5.20), the filter gain for the estimated states $\hat{y}_{l_{k+1}}$ can be expressed by the following

equations,

$$
\begin{aligned}
K_{l_k} = (\left| \hat{\Phi}_{22}\hat{\Phi}_{12}^{-1} e_{y_{u_{k|k-1}}} \right|_{ABS} + \gamma \left| \hat{\Phi}_{12}^{-1} e_{y_{u_{k|k-1}}} \right|_{ABS}) \\
\circ sat(\hat{\Phi}_{22}\hat{\Phi}_{12}^{-1} e_{y_{u_{k|k-1}}}, \Psi)
\end{aligned}
\tag{5.21}
$$

where γ is a tuning parameter and $0 < \gamma < 1$.

The Convergence of Robust SVSF

Similar to equation (5.20), the augmented reduced order model (5.13) can be transformed to a new form as follow,

$$
\begin{bmatrix} y_{u_{k+1}} \\ y_{l_{k+1}} \end{bmatrix} = \begin{bmatrix} \Phi_{11} & \Phi_{12} \\ \Phi_{21} & \Phi_{22} \end{bmatrix} \begin{bmatrix} y_{u_k} \\ y_{l_k} \end{bmatrix} + \begin{bmatrix} \bar{w}_{1_k} \\ \bar{w}_{2_k} \end{bmatrix}
\tag{5.22}
$$

where $\begin{bmatrix} y_{u_{k+1}} \\ y_{l_{k+1}} \end{bmatrix} = T\bar{x}(k)$, y_{u_k} is measurement variables and $y_{l_{k+1}}$ is system states, T is

a transformation matrix, $\Phi = T^{-1}\bar{F}T = \begin{bmatrix} \Phi_{11} & \Phi_{12} \\ \Phi_{21} & \Phi_{22} \end{bmatrix}$, $\bar{w} = T^{-1}Gh_k - \begin{bmatrix} \Phi_{11} \\ \Phi_{21} \end{bmatrix} v_k =$

$\begin{bmatrix} \bar{w}_{1_k} \\ \bar{w}_{2_k} \end{bmatrix}$ is bounded. Subtracting (5.20) from (5.22), the following error dynamics is

achieved,

$$
\begin{bmatrix} e_{y_{u_{k+1|k}}} \\ e_{y_{l_{k+1|k}}} \end{bmatrix} = \begin{bmatrix} \hat{\Phi}_{11} & \hat{\Phi}_{12} \\ \hat{\Phi}_{21} & \hat{\Phi}_{22} \end{bmatrix} \begin{bmatrix} 0 \\ e_{y_{l_{k|k}}} \end{bmatrix} + \bar{d}(k) \tag{5.23}
$$

where $\hat{\Phi} = \Phi - \tilde{\Phi}$, and $\bar{d}(k) = \begin{pmatrix} d_{1_k} \\ d_{2_k} \end{pmatrix} = \left(\tilde{\Phi} \begin{bmatrix} y_{u_k} \\ y_{l_k} \end{bmatrix} + \begin{bmatrix} \overline{w}_{1_k} \\ \overline{w}_{2_k} \end{bmatrix} \right)$ is bounded.

Equation (5.23) can be transformed into the following expression,

$$
\begin{cases} e_{y_{l_{k|k}}} = \hat{\Phi}_{12}^{-1} e_{y_{u_{k+1|k}}} - \hat{\Phi}_{12}^{-1} d_{1_k} \\ e_{y_{l_{k+1|k}}} = \hat{\Phi}_{22} \hat{\Phi}_{12}^{-1} e_{y_{u_{k+1|k}}} - \hat{\Phi}_{22} \hat{\Phi}_{12}^{-1} d_{1_k} + d_{2_k} \end{cases} \tag{5.24}
$$

The literature [27] demonstrated that the estimated lower partition of the state vector $\hat{y}_{l_k}$ is convergent if

$$
\left| e_{y_{l_{k|k-1}}} \right|_{ABS} \leq |K_k|_{ABS} \leq \left| e_{y_{l_{k|k-1}}} \right|_{ABS} + \left| e_{y_{l_{k-1|k-1}}} \right|_{ABS} \tag{5.25}
$$
$$
\mathrm{sgn}(K_k) = sgn(e_{y_{l_{k|k-1}}})
$$

Expand (5.25) with (5.21) and (5.24), the condition satisfies (5.25) can be found as follow,

$$
\left\| e_{y_{u_{k|k-1}}} \right\| \geq
$$
$$
\max \left(\frac{\left\| \hat{\Phi}_{22} \hat{\Phi}_{12}^{-1} d_{1_{k-1}} - d_{2_{k-1}} \right\| + \left\| \hat{\Phi}_{12}^{-1} d_{1_{k-1}} \right\|}{(1-\gamma) \left\| \hat{\Phi}_{12}^{-1} \right\|}, \frac{\left\| \hat{\Phi}_{22} \hat{\Phi}_{12}^{-1} d_{1_{k-1}} - d_{2_{k-1}} \right\|}{\gamma \left\| \hat{\Phi}_{12}^{-1} \right\|} \right)
$$

5.7   Experimental and Simulation Results

To validate the proposed Smooth Variable Structure Filter based filtering strategies, this section presents the calibration and validation of the high-fidelity GT-power DOC model and the simulation results of the proposed filtering methods. The simulation

results were obtained by the co-simulation between GT-Power and Matlab/Simulink environment.

5.7.1 Calibration and Validation of High-fidelity GT-power DOC Model

To test the proposed mean temperature estimation algorithms, a 1-D high-fidelity Diesel Oxidation Catalyst model built in GT-power environment is calibrated and validated by the experimental data. The GT-power DOC model is showed in Figure 5.7. The high-fidelity DOC model is a modified version referenced from [4] and [5], which considers thermal dynamics including thermal conduction, heat convection, and chemical reactions. Figure 5.11 demonstrates that the GT-power DOC model fits the data well. The component of the DOC model includes inlet and outlet variables, Diesel Oxidation Catalyst and exhaust pipes. The measurement DOC inlet temperature, exhaust gas mass flow rate (see Figure 5.8), the concentration of O_2, CO_2, CO (see Figure 5.9), NO and C_3H_6 (see Figure 5.10) are used for the inlet variables of high-fidelity DOC model in GT-power environment.

The Methodology of Model Calibration

The parameters of the DOC model can divide into two diffrent categories: physical parameters and chemical parameters. The physical parameters can be measured directly and used for the DOC GT-power model. Main physical parameters are demonstrated in table 1. The chemical parameters are demonstrated in equation (5.1). The initial chemical reaction parameters are inherited from [4] and [5] and manual tuning was performed to fit the data based on the evolution of the kinetics

of the DOC system reference from [4] and [5].
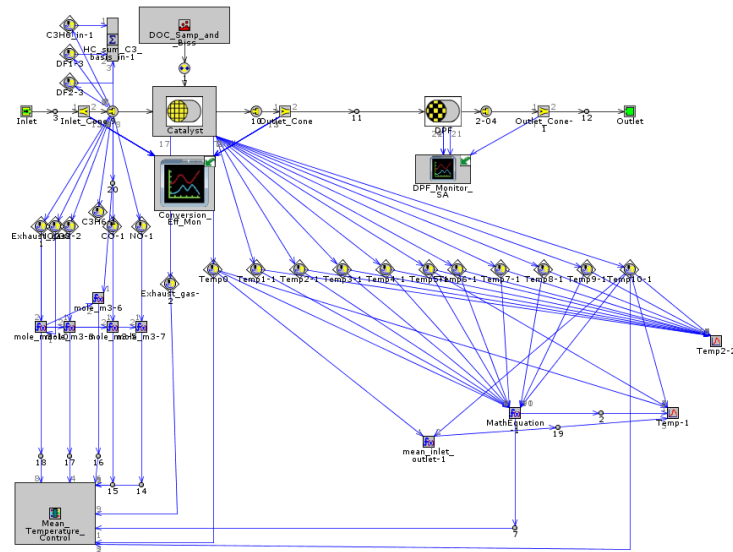
Figure 5.7: The co-simulation between GT-Power and Matlab/Simulink
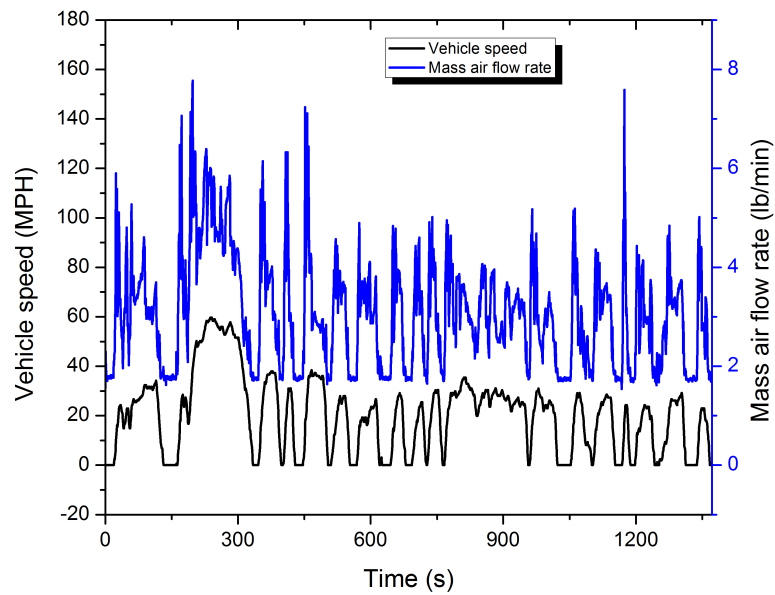
Figure 5.8: Vehicle speed and exhaust gas mass flow rate under FTP-72 test
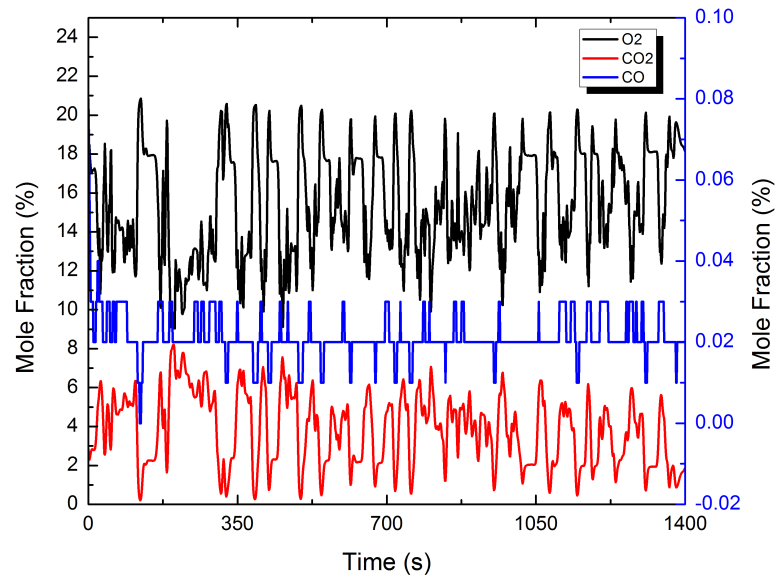
Figure 5.9: DOC inlet O_2, CO_2 and CO concentration under FTP-72 test
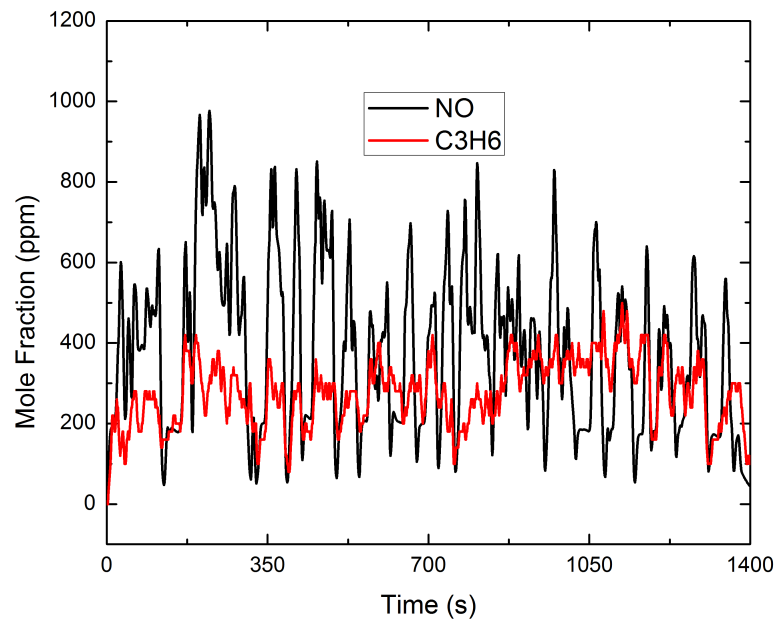
Figure 5.10: DOC inlet NO and C_3H_6 concentration under FTP-72 test

148
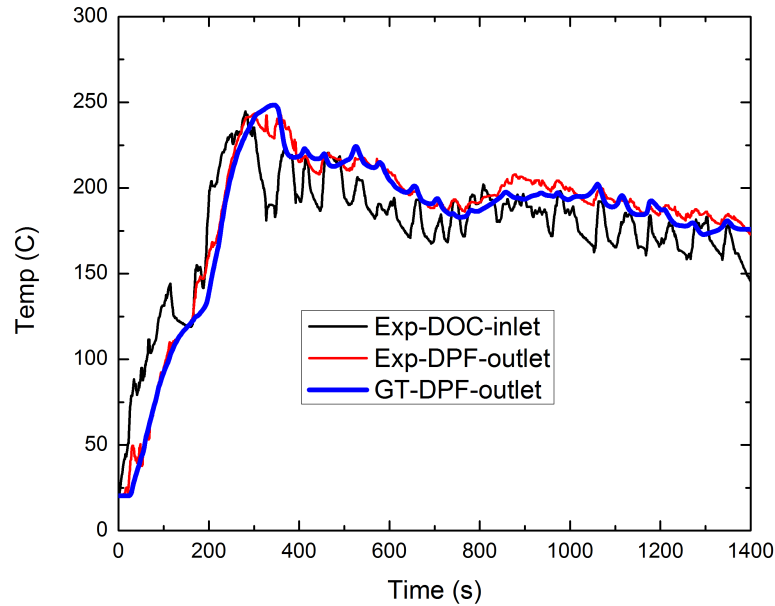
Figure 5.11: The comparison between GT-Power and experimental data

5.7.2   Estimation Performance under Steady State

The reduced order model of DOC was calibrated and validated based on the GT-power model. The physical parameters and chemical parameters are the same as the high-fidelity GT-power model. Three different test cases are used to validate the estimation performance of the proposed SVSF based methods. In all the three cases, the GT-power model simulates the engine on steady state and therefore the engine-out (DOC-inlet) mass flow rate, velocity of exhasut gas, the concentration of CO,NO,HC are constant. In the following figures, the "GT" means the mean temperature from GT-power model, the "reduced order model" means mean temperature estimated by the reduced order model only, the "SVSF" means the mean temperature estimated by the regular SVSF, and the "SVSF-aug" means the mean temperature estimated by the robust SVSF. The γ of both regular SVSF and robust SVSF were set to 0.5.

$fd = 0.3$ was selected for the robust SVSF.

Case 1: The velocity of exhaust gas, the concentration of CO, NO, HC for the mean temperature filter are the same with that of GT-power model. In this case, both regular SVSF and robust SVSF can accurately estimate the mean temperature, as can be seen in Figure 5.12. In addition, the estimated mean temperature by the reduced order model is close to real mean temperature in GT-power model, which means that the reduced order model is sufficient accurate.
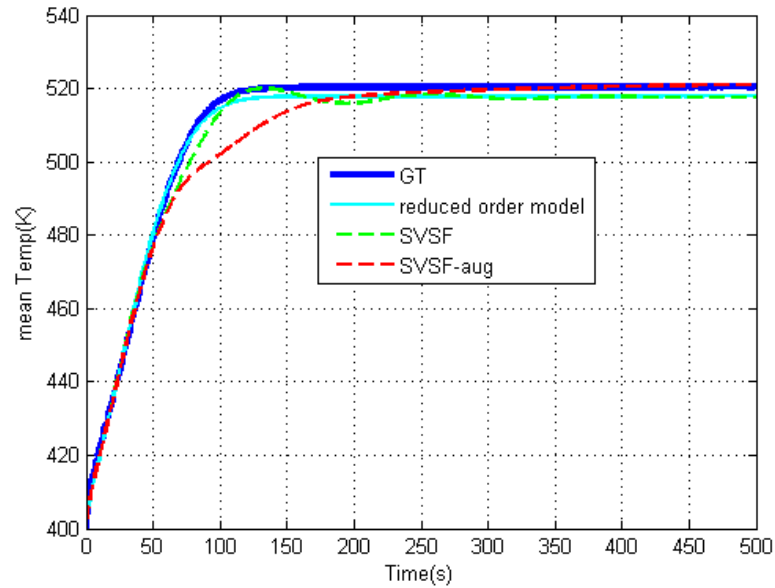
Figure 5.12: The mean temperature estimation in Case 1

Case 2: The velocity of exhaust gas, the concentration of CO, NO for the mean temperature filter are the same with that of GT-power model. But the concentration of HC for the mean temperature filter is smaller than real HC in GT-power model. In this case, the mean temperature estimated by the reduced order model and regular SVSF are smaller that the real mean temperature from GT-power model. However,

the robust SVSF can accurately estimate the mean temperature at steady state, as can be seen in Figure 5.13.
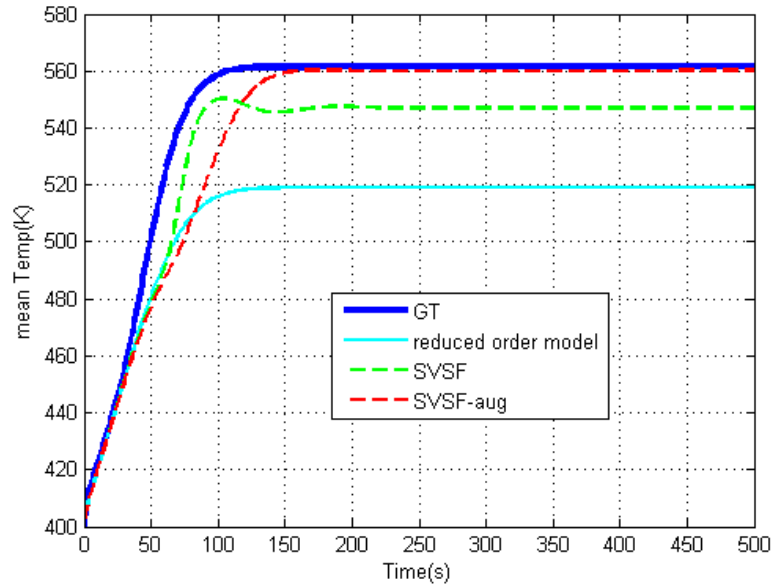
Figure 5.13: The mean temperature estimation in Case 2

Case 3: The velocity of exhaust gas, the concentration of CO, NO for the mean temperature filter are the same with that of GT-power model. But the concentration of HC for the mean temperature filter is larger than real HC in GT-power model. In this case, the mean temperature estimated by the reduced order model and regular SVSF are larger that the real mean temperature from GT-power model. However, the robust SVSF can accurately estimate the mean temperature at steady state, as can be seen in Figure 5.13.
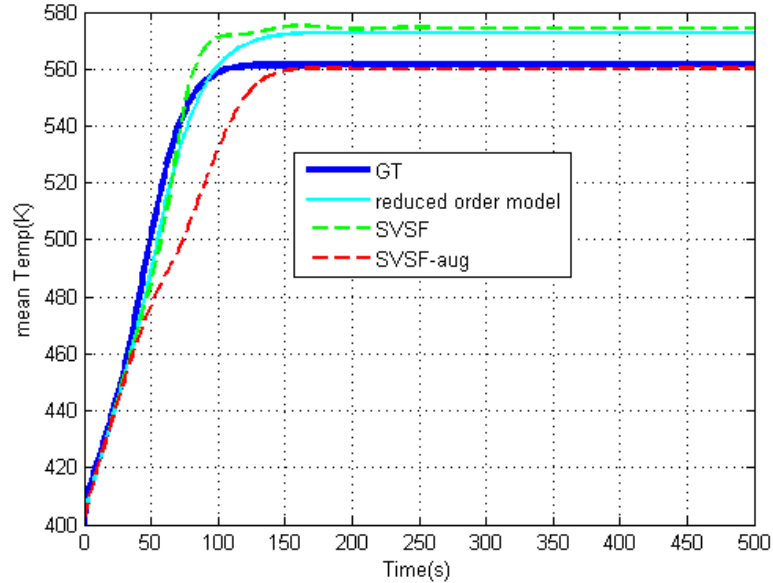
Figure 5.14: The mean temperature estimation in Case 3

5.7.3   Estimation Performance under Transient States

In this scenario, the regular SVSF and robust SVSF are validated under highly transient new European dynamic cycle (NEDC). The GT-power model simulates the vehicle under highly transient state so that the engine-out (DOC-inlet) mass flow rate, velocity of exhasut gas, the concentration of CO,NO,HC highly vary.

Case 4: The velocity of exhaust gas, the concentration of CO, NO, HC for the mean temperature filter and GT-power model are the same. In this case, both regular SVSF and robust SVSF can accurately estimate the mean temperature, as can be seen in Figure 5.15.
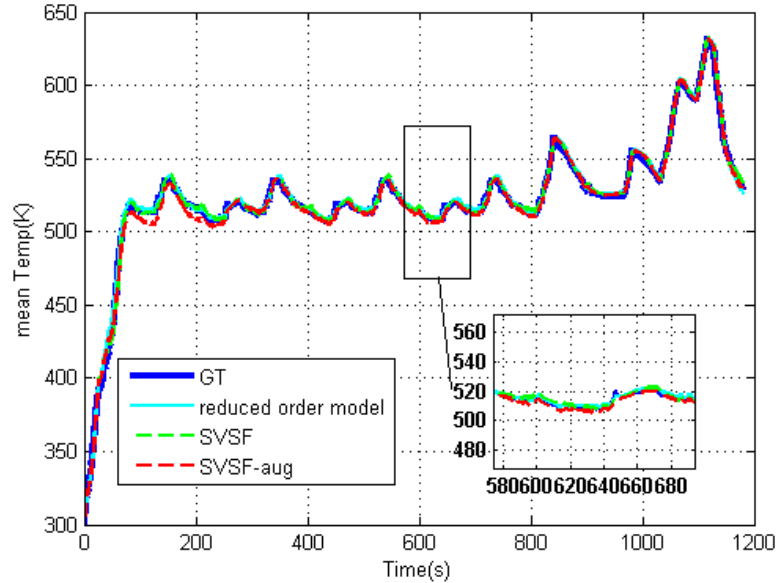
Figure 5.15: The mean temperature estimation and control of a DOC when HC is same as GT-power model under NEDC

Case 5: The velocity of exhaust gas, the concentration of CO, NO for the mean temperature filter and GT-power model are the same. But the concentration of HC for the mean temperature filter is smaller than real HC in GT-power model. In this case, the mean temperature estimated by the reduced order model and regular SVSF are smaller that the real mean temperature from GT-power model. However, the robust SVSF can accurately estimate the mean temperature at steady state, as can be seen in Figure 5.16.
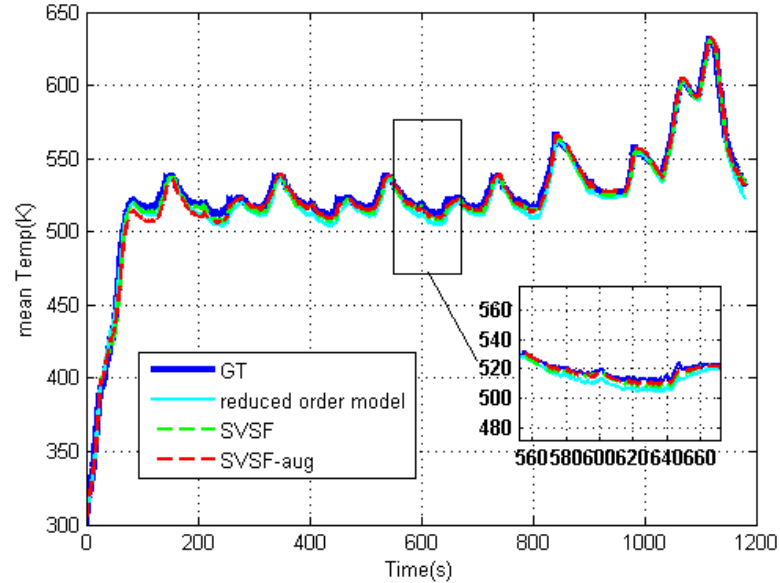
Figure 5.16: The mean temperature estimation and control of a DOC when HC is smaller than GT-power model under NEDC

Case 6: The velocity of exhaust gas, the concentration of CO, NO for the mean temperature filter and GT-power model are the same. But the concentration of HC for the mean temperature filter is larger than real HC in GT-power model. As can been seen in Figure 5.17, the mean temperature estimated by the reduced order model and regular SVSF are a little larger that the real mean temperature from GT-power model. Figure 5.17 also demonstrates that the estimation results of robust SVSF is better than regular SVSF in this case where the concentration of the HC for the mean temperature filter is larger than real HC in GT-power model.
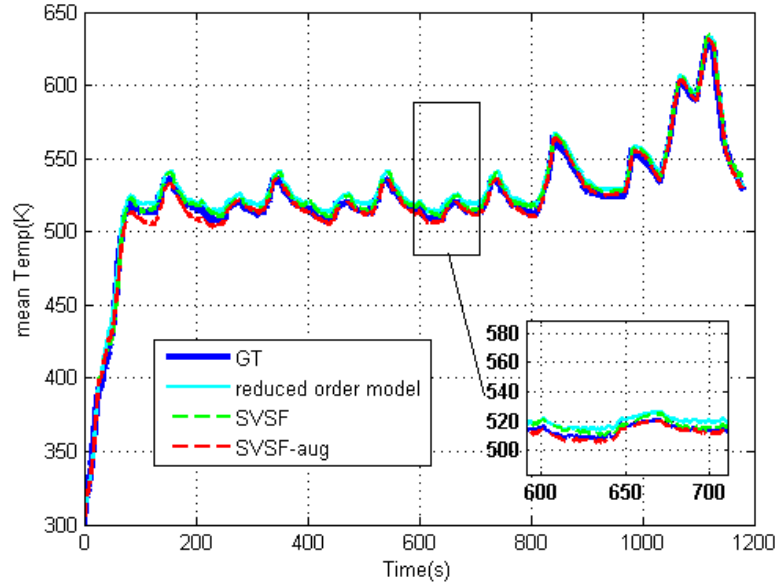
Figure 5.17: The mean temperature estimation and control of a DOC when HC is larger than GT-power model under NEDC

5.8 Conclusions

In this paper, two different Smooth Variable Structure Filter based methods are proposed to estimate the mean temperature of a Diesel Oxidation Catalyst. The reduced order model of a DOC was adopted to design the SVSF based filtering strategies. To improve the performance of the regular SVSF against to highly inaccurate HC concentration, a robust SVSF was designed for the estimation of mean temperature based on augmented reduced order model of a DOC. Furthermore, the convergence of robust SVSF is theoretically analysed. Experiments based on chassis dyno were conducted for calibration and validation of the high-fidelity GT-power DOC model. The simulation results based on the high-fidelity GT-power DOC model demonstrated

that the proposed methods have good performances in terms of disturbance rejection. However, the robust SVSF has better estimation performance in the case where the concentration of HC is inaccurate by comparing with the regular SVSF.

Reference

[1] Christopher Depcik, and Dennis Assanis. "One-dimensional automotive catalyst modeling." Progress in energy and combustion science 31, no. 4 (2005): 308-369.

[2] Harsha Shankar Surenahalli, Gordon Parker, and John H. Johnson. "Extended Kalman Filter to Estimate NO, NO_2, Hydrocarbon and Temperatures in a DOC during Active Regeneration and Under Steady State Conditions." No. 2015-01-1059. SAE Technical Paper, 2015.

[3] K. Hauff, U. Tuttlies, G. Eigenberger, and U. Nieken. "A global description of DOC kinetics for catalysts with different platinum loadings and aging status." Applied Catalysis B: Environmental 100, no. 1 (2010): 10-18.

[4] Chaitanya S. Sampara, Edward J. Bissett, and Dennis Assanis. "Hydrocarbon storage modeling for diesel oxidation catalysts." Chemical Engineering Science 63, no. 21 (2008): 5179-5192.

[5] Chaitanya S. Sampara, Edward J. Bissett, and Matthew Chmielewski. "Global kinetics for a commercial diesel oxidation catalyst with two exhaust hydrocarbons." Industrial & Engineering Chemistry Research 47, no. 2 (2008): 311-322.

[6] Chaitanya S. Sampara, Edward J. Bissett, Matthew Chmielewski, and Dennis

Assanis. "Global kinetics for platinum diesel oxidation catalysts." Industrial & Engineering Chemistry Research 46, no. 24 (2007): 7993-8003.

[7] Pingen Chen, and Junmin Wang. "Control-oriented modeling of thermal behaviors for a diesel oxidation catalyst." In American Control Conference (ACC), 2012, pp. 4987-4992. IEEE, 2012.

[8] Pingen Chen, and Junmin Wang. "Control-oriented modeling and observer-based estimation of solid and gas temperatures for a diesel engine aftertreatment system." Journal of Dynamic Systems, Measurement, and Control 134, no. 6 (2012): 061011.

[9] C. Guardiola, B. Pla, J. Mora, and D. Lefebvre. "Control oriented model for diesel oxidation catalyst diagnosis." IFAC-PapersOnLine 48, no. 15 (2015): 427-433.

[10] Stanislav V. Bohac, Manbae Han, Timothy J. Jacobs, Alberto J. López, Dennis N. Assanis, and Patrick G. Szymkowicz. "Speciated hydrocarbon emissions from an automotive diesel engine and DOC utilizing conventional and PCI combustion." No. 2006-01-0201. SAE Technical Paper, 2006.

[11] Kenneth R. Muske, and Thomas A. Badgwell. "Disturbance modeling for offset-free linear model predictive control." Journal of Process Control 12, no. 5 (2002): 617-632.

[12] Matt Wallace, Buddhadeva Das, Prashant Mhaskar, John House, and Tim Salsbury. "Offset-free model predictive control of a vapor compression cycle." Journal of Process Control 22, no. 7 (2012): 1374-1386.

[13] Urban Maeder, Francesco Borrelli, and Manfred Morari. "Linear offset-free model predictive control." Automatica 45, no. 10 (2009): 2214-2222.

[14] Zhiqiang Gao, Yi Huang, and Jingqing Han. "An alternative paradigm for control system design." In Decision and Control, 2001. Proceedings of the 40th IEEE Conference on, vol. 5, pp. 4578-4585. IEEE, 2001.

[15] Jingqing Han. "From PID to active disturbance rejection control." IEEE transactions on Industrial Electronics 56, no. 3 (2009): 900-906.

[16] Zhiqiang Gao. "Active disturbance rejection control: a paradigm shift in feedback control system design." In American Control Conference, 2006, pp. 7-pp. IEEE, 2006.

[17] Qing Zheng, Zhongzhou Chen, and Zhiqiang Gao. "A practical approach to disturbance decoupling control." Control Engineering Practice 17, no. 9 (2009): 1016-1025.

[18] Jinbiao Ning, and Fengjun Yan. "Compound Control Strategy Based on Active Disturbance Rejection for Selected Catalytic Reduction systems." Journal of Dynamic Systems, Measurement, and Control 137, no. 5 (2015): 051008.

[19] Jinbiao Ning, and Fengjun Yan. "Disturbance rejection in DOC-out temperature control for DPF regeneration." Proceedings of the Institution of Mechanical Engineers, Part D: Journal of Automobile Engineering (2016): 0954407016650782.

[20] Song Chen, and Fengjun Yan. "Trapped Unburned Fuel Estimation and Robustness Analysis for a Turbocharged Diesel Engine With Negative Valve Overlap

Strategy." Journal of Dynamic Systems, Measurement, and Control 137, no. 6 (2015): 061004.

[21] Mohammed Sayed Farag, Ryan Ahmed, S. A. Gadsden, S. R. Habibi, and J. Tjong. "A comparative study of Li-ion battery models and nonlinear dual estimation strategies." In Transportation Electrification Conference and Expo (ITEC), 2012 IEEE, pp. 1-8. IEEE, 2012. 2012.

[22] Hui Zhang, Junmin Wang, and Yue-Yun Wang. "Robust filtering for ammonia coverage estimation in diesel engine selective catalytic reduction systems." Journal of Dynamic Systems, Measurement, and Control 135, no. 6 (2013): 064504.

[23] Ryan Ahmed. "Training of Neural Networks Using the Smooth Variable Structure Filter with Application to Fault Detection." PhD diss., 2011.

[24] R. M. Ahmed, S. A. Gadsden, M. El Sayed, and S. R. Habibi. "Fault Detection and Classification of an Electrohydrostatic Actuator Using a Neural Network Trained by the Smooth Variable Structure Filter." In 23rd Canadian Congress of Applied Mechanics (CANCAM). 2011.

[25] Ryan M. Ahmed, Mohammed A. El Sayed, S. Andrew Gadsden, and Saeid R. Habibi. "Fault detection of an engine using a neural network trained by the smooth variable structure filter." In Control Applications (CCA), 2011 IEEE International Conference on, pp. 1190-1196. IEEE, 2011.

[26] S. Andrew Gadsden, Yu Song, and Saeid R. Habibi. "Novel model-based estimators for the purposes of fault detection and diagnosis." IEEE/ASME Transactions on Mechatronics 18, no. 4 (2013): 1237-1249.

[27] Saeid Habibi. "The smooth variable structure filter." Proceedings of the IEEE 95, no. 5 (2007): 1026-1059.

Chapter 6

Disturbance Rejection in DOC-out Temperature control for DPF Regeneration

6.1 Citation and Main Contributor

Jinbiao Ning, and Fengjun Yan. "Disturbance rejection in DOC-out temperature control for DPF regeneration." Proceedings of the Institution of Mechanical Engineers, Part D: Journal of Automobile Engineering (2016): 0954407016650782.

The main contributor to this paper is the first author-Jinbiao Ning (contributes more than 70%).

6.2   Abstract

Control of Diesel Oxidation Catalyst (DOC) outlet temperature is critical for the downstream Diesel Particulate Filter (DPF) regeneration, but is challenging to control due to the non-minimum phase behavior and varying time delay. To effectively address this issue, a novel and time-efficient Composite Controller (CC) based on modified Active Disturbance Rejection Control (mADRC) was proposed for DOC-out temperature control in this paper. The proposed mADRC-based CC is a new combination of a model-based Feedforward controller (FF) and a mADRC with time delay compensation through the mass flow rate of exhaust gas. The model-based FF is designed to partially compensate the variations of DOC inlet temperature and mass flow rate, while the mADRC is proposed to address the remain disturbances and model uncertainties including time delay uncertainties. Simulation and test results through high-fidelity GT-Power model demonstrate the effectiveness and robustness of the proposed composite controller in the DOC-out temperature control under steady state and highly transient new European dynamic cycle (NEDC).

6.3   Introduction

Advanced Diesel after-treatment systems consists of DOC, DPF and SCR (Selective Catalytic Reduction), as can be seen in Figure 6.1. The use of DPF is considered to be the only feasible Diesel after-treatment technology that can effectively reduce particulate matter (PM) and meet the increasingly stringent regulations such as US2010, Low Emission Vehicle (LEV III), and Euro VI [1]. The composition of PM is extremely complex including solid (e.g. inorganic carbon and metal ashes) and condensate (e.g.

high boiling hydrocarbons, water, and sulfuric acid) material [2, 3]. The PM emission is accumulated and burned in the DPF. The process of burning the accumulated PM is called DPF regeneration.

Passive regeneration and active regeneration are two different ways for DPF regeneration. Since passive regeneration is limited and not enough to keep the filter clean in long-term, the active regeneration of DPF is necessary [5]. The active regeneration of DPF divides into two stages [6]: 1) close post injection is used to drive the DOC temperature up to light-off temperature for high hydrocarbons (HC) conversion efficiency. 2) far post injection in cylinder or downstream injection in the exhaust pipe is adopted to boost the DOC outlet temperature to satisfy the DPF regeneration temperature.

The DOC-out temperature is critical for DPF periodical regeneration as the DPF inlet temperature should be high enough to effectively burn the accumulated soot in the DPF and should be kept below a certain threshold to prevent damage to the DPF. The control of DOC-out temperature is challenging due to several factors including wide-range engine operations, DOC thermal inertia, the complexities of the reactions in DOC, and the physical saturation of the fuel injectors.

Several model-based control strategies [4, 6, 20] were proposed to address this issue. Linear Parameters Varying (LPV) controller was demonstrated in [4] to have better tracking performance for the Diesel Particulate Filter Thermal Management by comparing with model-based PID controller. Model-based temperature control with parameter adaptation by exhaust gas velocity is proposed in [20]. Model Predictive Control (MPC) was proposed in [6] for DOC-out temperature control during DPF regeneration and achieved small temperature error in general but more overshoots

than the production controller. There exist several drawbacks in the aforementioned model-based controllers. First of all, these model-based control methods are designed deeply relying on accurate DOC model. However, it is difficult to achieve precise model for DOC system since the chemical reactions and thermal dynamics in DOC are complex. Second drawbacks lies in the complexity in design (e.g. LPV) and the high computational load (e.g. MPC). Furthermore, the above controllers still have nontrivial overshoots that are harmful for the DPF regeneration. Therefore, more efforts are required to get better tracking performance of the DOC-out temperature for better DPF regeneration, avoiding the aforementioned drawbacks.
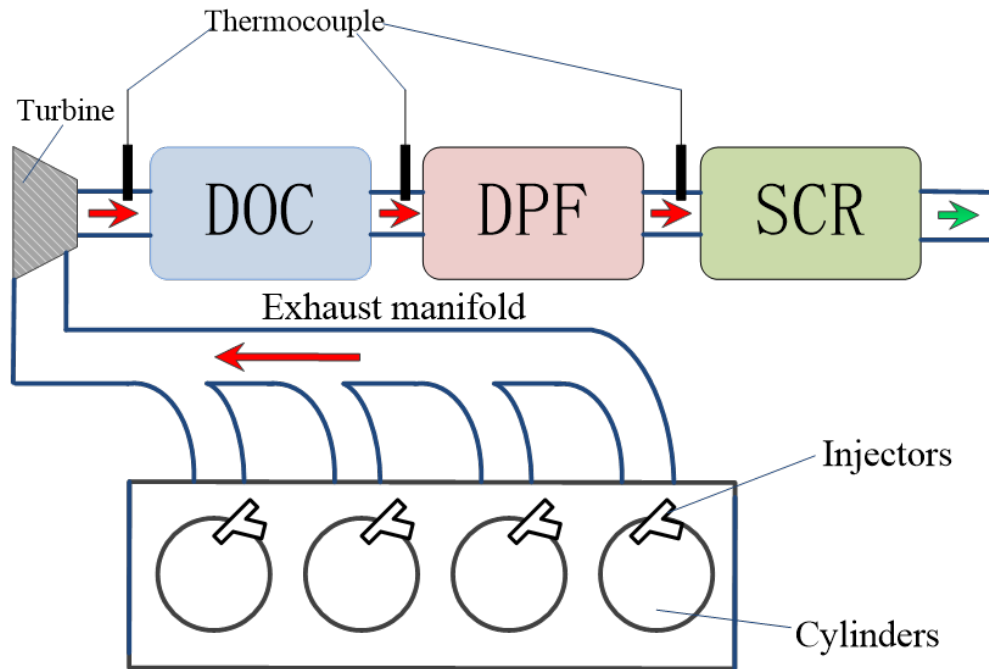
Figure 6.1: Aftertreatment system configuration

In this paper, a novel Composite Control (CC) based on modified Active Disturbance Rejection Control with time delay compensation (mADRC-based CC) is

proposed for the DOC-out temperature control. The Active Disturbance Rejection Control (ADRC) concept [14–16] has been widely used in many fields to actively deal with disturbances and model uncertainties [17–19].

The main contributions of this paper are: 1) A DOC-out temperature model is identified as a process model with variable time delay and derived in state space form. 2) A Composite Control based on modified Active Disturbance Rejection Control is proposed for DOC-out temperature control. 3) A Feedforward controller is used based on the the relation among the inlet temperature, the mass flow rate of inlet exhaust gas and the fuel injection. 4) The relation between the delay time and mass flow rate was fitted based on the data from high-fidelity DOC model and used for the time delay compensation.

The rest of the paper is organized as follows. A brief introduction of the control problem, system dynamics and modeling of DOC is demonstrated in section 6.4. The design of Composite Control based on modified Active Disturbance Rejection Control with time delay compensation is presented in section 6.5. Simulation results based on 1-D high-fidelity DOC model are introduced to verify the proposed approach in section 6.6. At the end of the chapter, conclusions are given.

6.4   System Dynamics and Modeling of DOC

As mentioned in Section 6.3, DPF active regeneration consists of two stages. The first stage (close post injection) is out of the scope of this paper. The second stage is achieved by bringing the DOC-out temperature up to the regeneration temperature ($650°C$ is used as the regeneration temperature in this paper) by far post injections in cylinder or downstream injections in the exhaust pipe after the temperature condition

satisfies the requirement of first process. To understand the control problem and the dynamics of the DOC system, this section describes the control problem, the principle of DOC system, and modeling of DOC.

6.4.1   Control Problem

The DOC is a single-input-single-output system (see Figure 6.2) with disturbances (DOC inlet temperature T_{in}, mass flow rate of inlet exhaust gas $\dot{m}_{ex}$ and reductants (THC, NO and CO) from pilot and main injections), input saturation ($0 < U_{inj} < U_{max}$), and output measurement noise (measurement noise from temperature sensor). The output (T) of the system is the DOC-out temperature. The inlet temperature, mass flow rate and system output can be measured directly. Main control issues of the DOC system are listed in the following items,

  a) Measurement noise from temperature sensor.

  b) Input Saturation: the Diesel injector as the actuator of the control input has input saturation.

  c) Asymmetric control: the control of DOC-out temperature is asymmetric due to the input saturation, which means that the DOC can be heated up by adding fuel injections but only can be cooled by the natural cooling.

  d) Disturbances and Uncertainties: there exist disturbances due to different engine operations and model uncertainties including time delay uncertainties due to the complexity of thermal dynamic and chemical reactions. The disturbances (i.e. DOC inlet temperature, mass flow rate of inlet exhaust gas and reductants

(THC,NO and CO) from pilot and main injections) vary significantly with different engine operations.

e) Time delay: the thermal response time of DOC is long and variable, from several seconds to hundred seconds since DOC is a heat distributed reservoir. On the control point of view, the dynamic of DOC system has a time delay due to the long response of the DOC-out temperature. Time delay of DOC outlet temperature change significantly while mass flow rate change significantly over transient conditions (e.g. FTP 75 or NEDC test cycle). There exist time delay uncertainties since the delay time is difficult to be precisely determined.

f) Non-minimum phase behavior: there exist undershoot under a step decrease of the mass flow rate and overshoot under a step increase of the mass flow rate. This is the most challenging issue due to time delay in input-to-output loop.
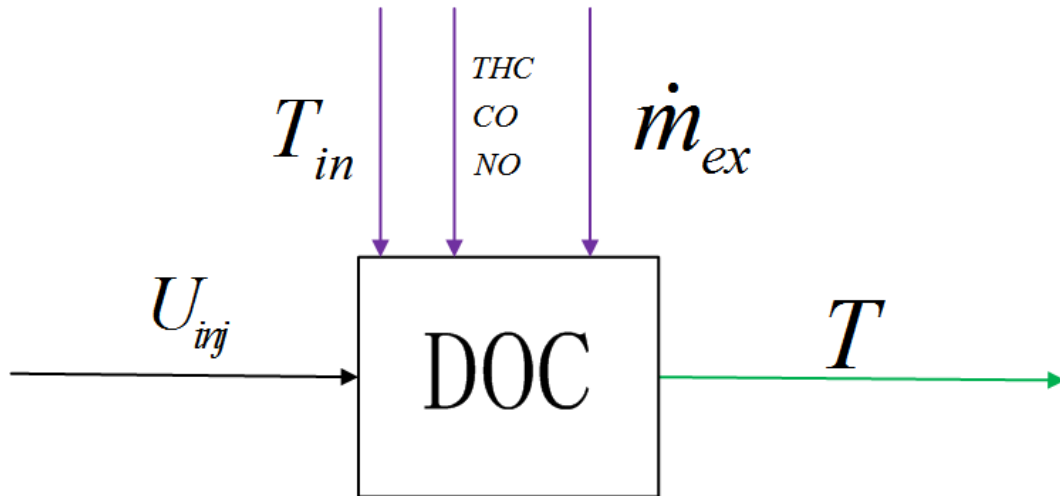
Figure 6.2: The control system of DOC including input (U_{inj}), output (T) and disturbances (T_{in}, $\dot{m}_{ex}$, and reductants)

6.4.2   The Principle of DOC

The DOC is composed of inner layer (substrate layer) and outer layer, as can be seen in Figure 6.3. The substrate layer divides into the washcoat and the substrate wall. The exhaust gas goes through the substrate and oxidation reactions occur on the substrate. The thermal dynamic of DOC is complicated since it has thermal conduction, convection and chemical reactions.
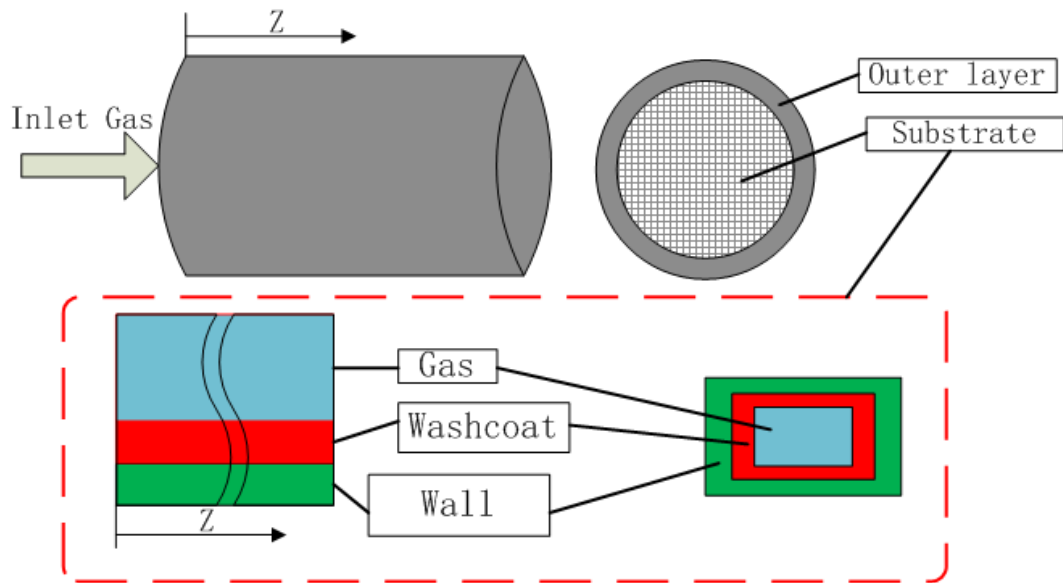
Figure 6.3: Schematic diagram of DOC

The chemical reactions in DOC are complex and more details can be seen in [7–11]. The main reactions in DOC include oxidation reactions [7] and Hydrocarbon storage [8], as demonstrated in table 1.

Table 1: Main Reactions in DOC

	Oxidation Reactions
1	$CO + 0.5O_2 \rightarrow CO_2$
2	$C_3H_6 + 4.5O_2 \rightarrow 3CO_2 + 3H_2O$
3	$H_2 + 0.5O_2 \rightarrow H_2O$
4	$NO + 0.5O_2 \rightarrow NO_2$
5	$DF_1 + 19.4O_2 \rightarrow 13.5CO_2 + 11.8H_2O$
6	$DF_2 + 19.4O_2 \rightarrow 13.5CO_2 + 11.8H_2O$
	Hydrocarbon Storage Reactions
7	$Z + DF_1 \rightarrow ZDF_1$
8	$ZDF_1 \rightarrow Z + DF_1$

6.4.3   The Control Input

To generate sufficient Hydrocarbon into the exhaust gas for heating up the DOC-out Temperature, far post injection in cylinder or downstream injection in the exhaust pipe is adopted to inject the Diesel fuel. The influence of far post injection in cylinder or downstream injection in the exhaust pipe on the DOC inlet temperature can be negligible [12]. Diesel fuel divides into Diesel vapor ($Fuel_1$) and Diesel liquid ($Fuel_2$) after injected into the exhaust pipe and converted into fast oxidizing Hydrocarbon especially propylene (C_3H_6), adsorbable slow oxidizing Hydrocarbon (DF_1), non-adsorbable slow oxidizing Hydrocarbon (DF_2), and Oxygen (O_2) due to high temperature, as expressed in table 2.

Table 2: Reactions for Diesel Fuel to Hydrocarbon

1	$Fuel_1 + 0.309091H_2O = 0.818182C_3H_6 + 0.409091DF_1$ $+ 0.409091DF_2 + 0.154545O_2$
2	$Fuel_2 + 0.309091H_2O = 0.818182C_3H_6 + 0.409091DF_1$ $+ 0.409091DF_2 + 0.154545O_2$

6.4.4   Time Delay and Non-minimum Phase Behavior of DOC

To intuitively understand the main system dynamics and their causes, the step response of input-to-output loop, inlet-temperature-to-output loop and mass-flow-rate-to-output loop are demonstrated in this section, based on a high-fidelity DOC model in GT-power referenced from [7] and [8]. Specifications of the high-fidelity DOC model in GT-power are listed in table 3.

Table 3: Specifications of the high-fidelity DOC model in GT-power

Attributes	Values
Channel Geometry	square
Frontal Area (mm^2)	20000
Cell Density ($1/in^2$)	400
Length (mm)	260
Wall Thickness (mm)	0.15
Density of the substrate (kg/m^3)	1720
Ambient heat transfer coefficient (w/m^2K)	15

In the input-to-output loop, there exists a time delay in the system response under the step increase and decrease of the input, as can be seen in Figure 6.4. In fact, the time delay varies depending on the mass flow rate (see Figure 6.7).
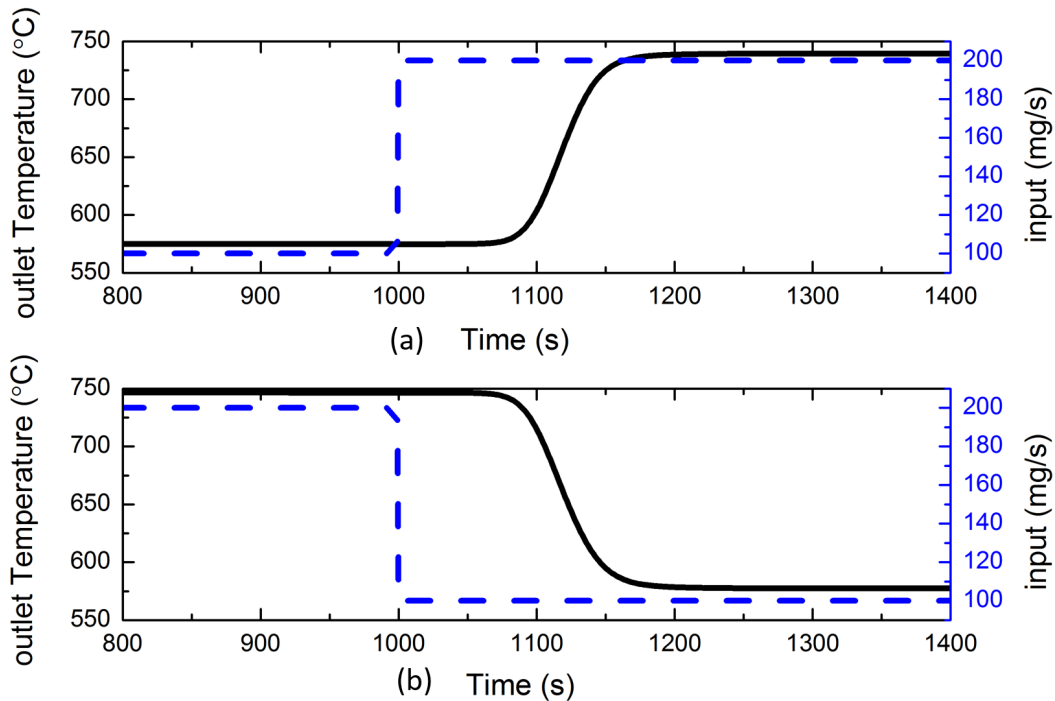
Figure 6.4: (a) is system response under a step increase of input from 100 mg/s to 200 mg/s, (b) is system response under a step decrease of input (far post fuel injection) from 200 mg/s to 100 mg/s, both inlet temperature are 400 $°C$, both mass flow rates are 0.02 kg/s

Likewise, Figure 6.5 shows a time delay in the system response under the step increase and decrease of inlet temperature with or without input in the inlet-temperature-to-output loop. There is no non-minimum phase behavior since both directions in system output response of inlet temperature step change and input step change are the same.
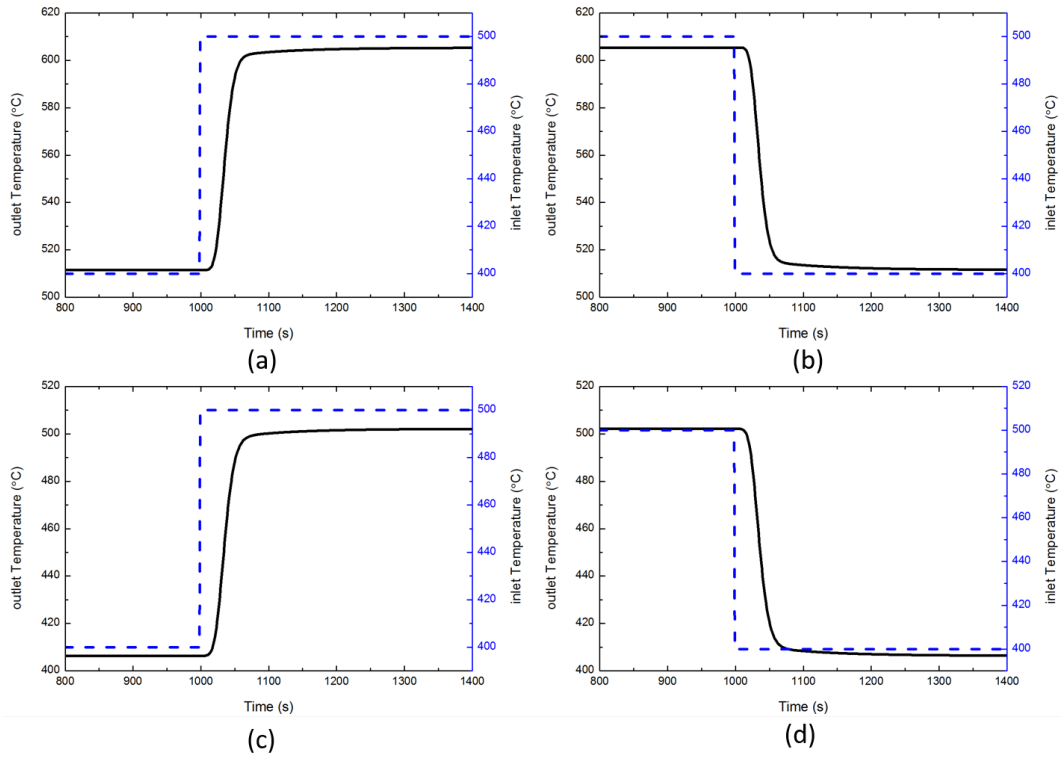
Figure 6.5: (a) and (c) are system response under a step increase of inlet temperature from 400 °C to 500 °C, (b) and (d) are system response under a step decrease of inlet temperature from 500 °C to 400 °C, the input (far post fuel injection) of (a) and (b) are 50 mg/s, the input (far post fuel injection) of (c) and (d) are 0 mg/s, all mass flow rates are the same (i.e.0.07 kg/s)

Similarly, Figure 6.6 demonstrates a time delay in the system response under the step increase and decrease of mass flow rate in inlet-mass-flow-to-output loop. It is worth noting that there is an undershoot before the output rises under a decrease of mass flow rate (see subplot (a) in Figure 6.6) and an overshoot before the output decreases under a step increase of mass flow rate (see subplot (b) in Figure 6.6) with constant input, while there is no undershoot and overshoot phenomena without input

(see subplot (c) and (d) in Figure 6.6). The undershoot and overshoot phenomena is the accumulated result of the system response to the mass flow rate and the input since they have different directions in system output response and it has faster response under the the step change of mass flow rate than that of step change of input. More Importantly, the undershoot and overshoot phenomena is a non-minimum phase behavior (NMP), which has challenging impact on the control of DOC-out temperature. Due to the input time delay, the undershoot and overshoot phenomena is difficult to compensate and has side effects with compensations, as demonstrated in [20, 21].
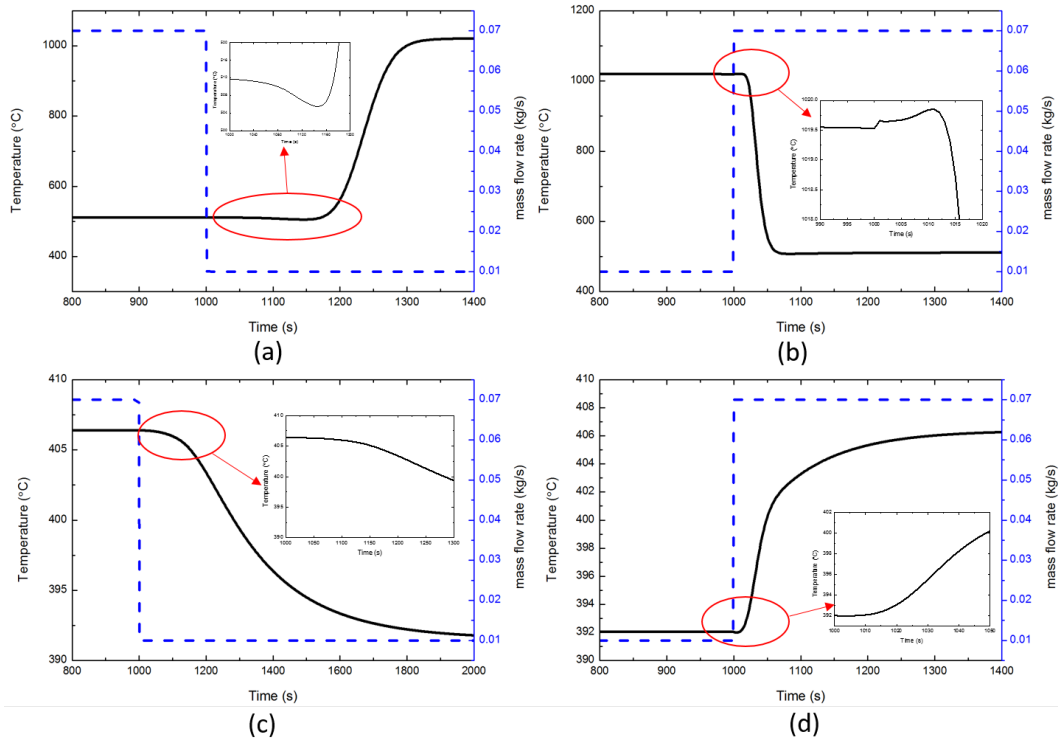
Figure 6.6: (a) and (c) are system response under a step decrease of mass flow rate from 0.07 kg/s to 0.01 kg/s, (b) and (d) are system response under a step increase of mass flow rate 0.01 kg/s to 0.07 kg/s, the input (far post fuel injection) of (a) and (b) are 200 mg/s, the input (far post fuel injection) of (c) and (d) are 0 mg/s, all inlet temperatures are the same (i.e.400 $^{\circ}C$)

6.4.5   Linear Model of DOC

Although a detail 1-D thermal dynamic model of DOC is proposed in [7], the parameters for thermal dynamic and reactions are difficult to be precisely determined since the thermal dynamics and reactions are too complex. Also, the concentration and the reaction rate are difficult to be accurately measured [7]. The detail 1-D model

not only increases the complexity in modeling the DOC thermal dynamics, but also increases the difficulty in designing robust model-based controller. However, the proposed mADRC-based CC is not a model-based design. Therefore, the linear model of DOC thermal dynamics is sufficient for the proposed controller design.
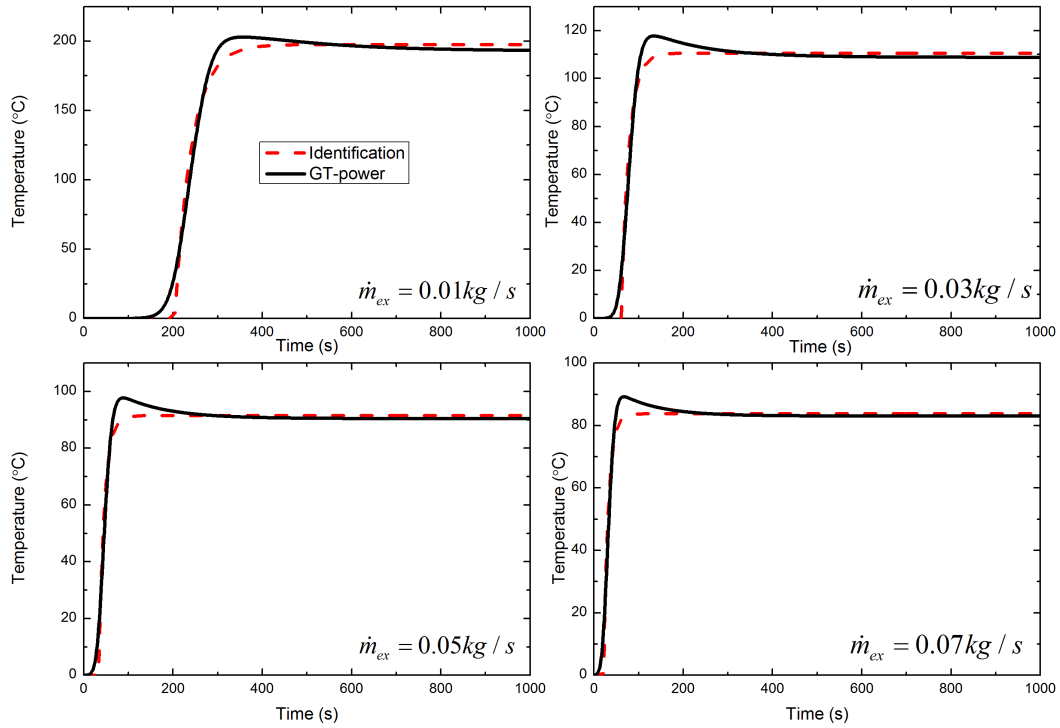
Figure 6.7: Step increase from Comparison between GT-Power model and identified process model

To achieve the linear model of DOC thermal dynamics, the step response of the DOC-out temperature is achieved under different conditions. The step response of DOC-out temperature can be acquired by injecting constant amount (i.e. 50 mg/s) of Diesel fuel into the exhaust pipe upstream of the DOC during different steady states (i.e. constant inlet temperature and mass flow rate of exhaust gas). Figure 6.7 demonstrates the step response under different mass flow rate from 0.01 kg/s to

0.07 kg/s. Based on the step response of the DOC, the process model is achieved by using the identification tool of the Matlab. Both Figure 6.7 and the identified models show that the time delay varies significantly ranging from 21.59 seconds at 0.07 kg/s to 203.76 seconds at 0.01 kg/s. Furthermore, identified models are first-order linear process model with time delay. The first-order linear process model with time delay is expressed in the following equation,

$$G(s) = \frac{k}{\delta s + 1} e^{-\tau s} \tag{6.1}$$

where k, δ, τ are parameters. The Fitting Accuracy of identified models to the GT-power data and the parameters of identified models are demonstrated in table 4. Let $y(t)$ equal to the DOC-out temperature and the first-order transfer function (6.1) can be rewritten in the state space form,

$$\begin{cases} \dot{x}(t) = -\dfrac{1}{\delta}x(t) + \dfrac{k}{\delta}u(t - \tau) \\ y(t) = x(t) \end{cases} \tag{6.2}$$

The thermal dynamics of DOC can be expressed by the following equation,

$$\begin{cases} \dot{x}(t) = -\dfrac{1}{\delta}x(t) + \omega + \dfrac{k}{\delta}u(t - \tau) \\ y(t) = x(t) \end{cases} \tag{6.3}$$

where ω presents the unknown disturbances and model uncertainties between the linear model (6.2) and real DOC thermal dynamics.

Table 4: Fitting Accuracy and parameters for identified models

Mass Flow Rate (kg/s)	k	δ	τ	Fitting Accuracy (%)
0.01	3.955	38.151	203.76	92.3
0.03	2.2113	17.101	60.856	87.9
0.05	1.8305	12.435	33.411	86.2
0.07	1.6765	10.55	21.58	85.4

6.5 mADRC-based Composite Controller Design

The objective of the controller design is to track the desired DOC-out temperature trajectory for safe and effective DPF regeneration in spite of the disturbances, model uncertainties including time delay uncertainties, and non-minimum phase behavior. The non-minimum phase property is not desired due to its limitation on the achievable feedback performance. The control issues of non-minimum behavior have long been recognized [22–24] and feedforward control is required to effectively compensate the feedback control [25–28]. To deal with the aforementioned control issues in Section 6.4 and achieve the control target, the mADRC-based Composite Controller is designed by combining modified Active Disturbance Rejection Control (mADRC) with time delay compensation and feedforward control. Figure 6.8 is the scheme of the mADRC-based Composite Controller for DOC-out temperature control.
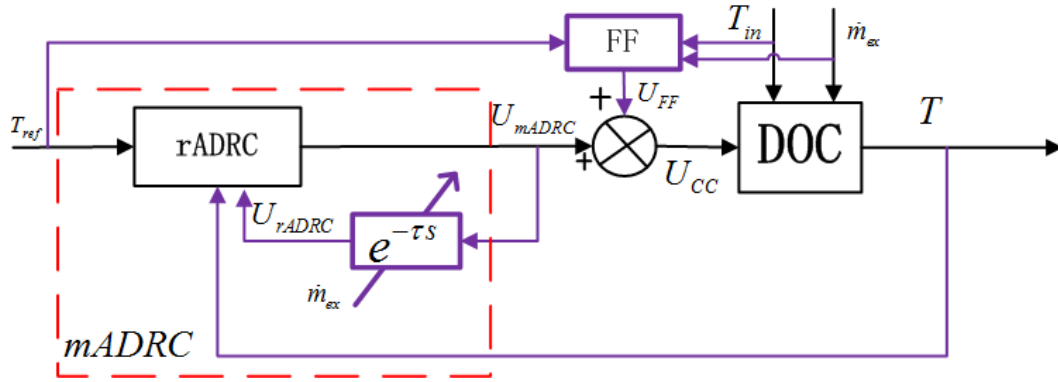
Figure 6.8: Scheme of Composite Controller for DOC outlet temperature

In Figure 6.8, T_{ref} is the desired trajectory, T_{in} and $\dot{m}_{ex}$ is inlet temperature and mass flow rate of inlet exhaust gas, respectively, the diagram of FF represents Feedforward controller, U_{FF} is the control rate of Feedforward controller, mADRC is the modified active disturbance rejection control with time delay compensation, rADRC is the regular active disturbance rejection control, U_{mADRC} and U_{rADRC} is the control law of mADRC and the input of rADRC, respectively, U_{CC} is the control law of the Composite Controller. U_{CC} and U_{rADRC} can be expressed in the following equation,

$$\begin{cases} U_{CC} = U_{FF} + U_{mADRC} \\ U_{rADRC} = U_{mADRC}(t - \tau) \end{cases} \tag{6.4}$$

The design of Feedforward controller, time delay compensation, and mADRC are given in the following subsections.

6.5.1   Feedforward Controller

The objective of Feedforward Controller is to partially compensate the disturbances including the inlet temperature, mass flow rate, and reductants (THC,NO and CO)

from pilot and main injections. The remain disturbances and model uncertainties are rejected by the feedback control loop. The control law of the Feedforward controller can be expressed below,

$$U_{FF} = \dot{m}_{ff} \tag{6.5}$$

where $\dot{m}_{ff}$ is the mass flow rate of far post injection. To achieve the mass flow rate of the post fuel injection, some assumptions are required to make. It is assumed that the temperature of DOC is uniform along the axial length and constant at steady state so that the total heat release from post injection is used to rise the exhaust gas temperature from inlet temperature to outlet temperature. The THC from post injection is assumed to be completely combusted inside the DOC [12]. However, there exist other reductants including NO, CO and THC generated by pilot and main injections in the exhaust gas. These reductants of NO, CO and THC plays an important role in the heat release. To attenuate the effect of these reductants, a lookup table is calibrated to estimate these reductants under steady state. Therefore, the Feedforward controller is calculated based on the aforementioned assumptions when the system is on steady state. Figure 6.9 describes the energy balance of the DOC system. Based on the assumptions, the energy balance can be expressed in the following equation,

$$\dot{Q} = \dot{m}_{ff}LHV_{THC} + \dot{m}_{THC}LHV_{THC} + \dot{m}_{CO}LHV_{CO} + \dot{m}_{NO}LHV_{NO} = c_g\dot{m}_{ex}(T_{out} - T_{in})$$

$$\tag{6.6}$$

where the LHV_{THC}, LHV_{CO} and LHV_{NO} denotes the lower heating value of THC, CO and NO, $\dot{m}_{CO}$, $\dot{m}_{NO}$ and $\dot{m}_{THC}$ represent the mass flow rate of CO, NO and THC from pilot and main injections, c_g is the specific heat of exhaust gas. Therefore, the

fuel injection rate $\dot{m}_{ff}$ is calculated by equation (6.6).
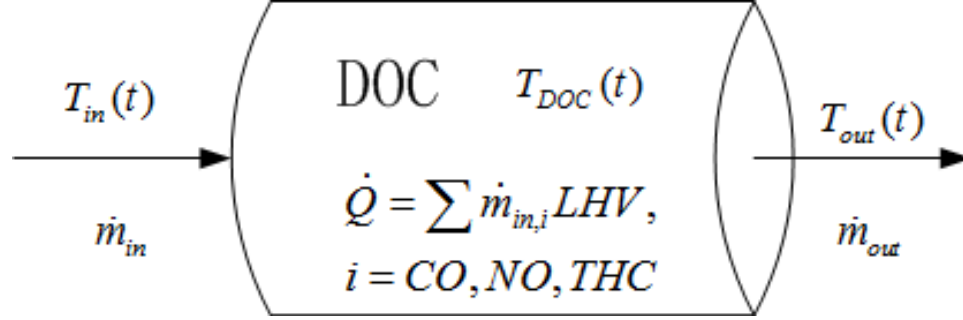
Figure 6.9: DOC energy balance schematic diagram

6.5.2 Time Delay Compensation

Figure 6.10 demonstrates that the delay time significantly varies from about 338 seconds to 12 seconds at different mass flow rate from 0.005 kg/s to 0.1 kg/s. Delay time is small after the mass flow rate is greater than 0.1 kg/s. Based on Figure 6.10, the relation between delay time and the mass flow rate can be expressed by the following equation,

$$\tau = a\dot{m}_{ex}^{b} \tag{6.7}$$

where a and b are parameters. $a = 2.235$ and $b = -0.953$ are given after fitting and the regular residual is demonstrated in Figure 6.11. Therefore, the delay time in mADRC-based CC is compensated by equation (6.7). Figure 6.11 demonstrates time delay uncertainties in the controller. However, achieving accurate delay time is impossible and unnecessary since the proposed mADRC-based CC can deal with disturbances and model uncertainties including time delay uncertainties.
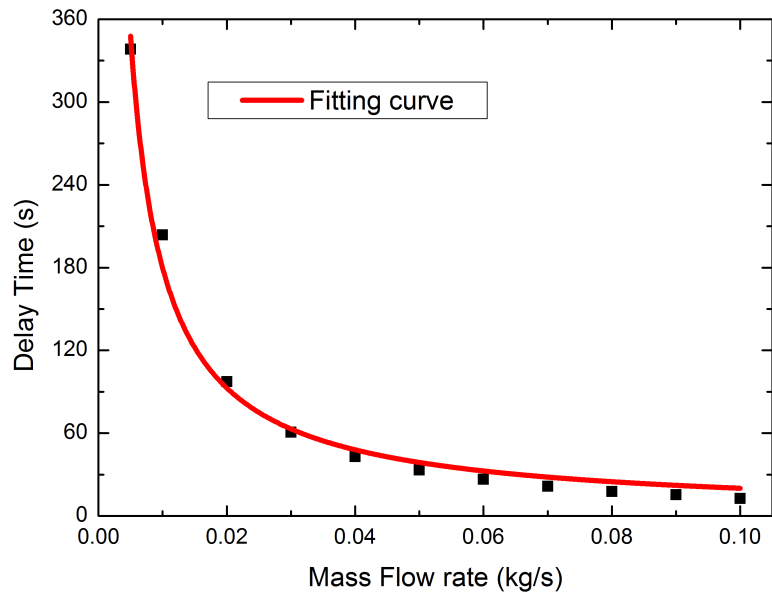
Figure 6.10: Time Delay at different mass flow rate
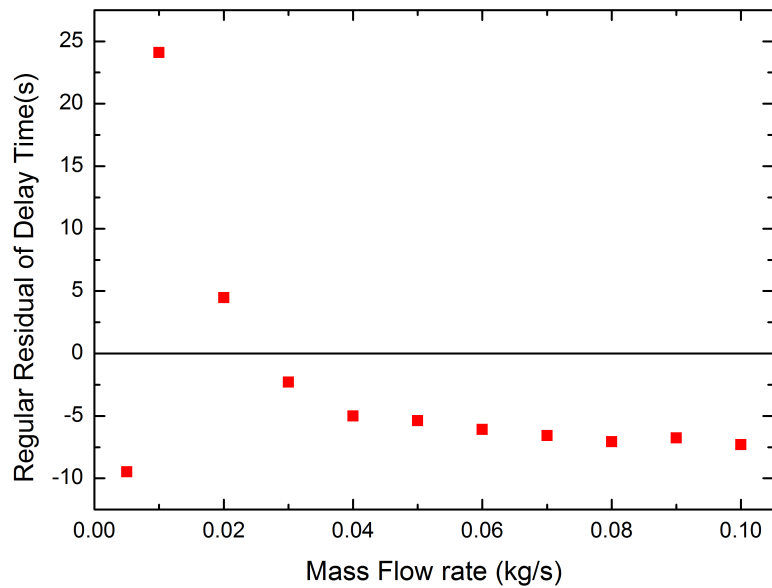
Figure 6.11: Regular Residual of Time Delay at different mass flow rate

6.5.3   Modified Active Disturbance Rejection Controller Design

The mADRC modified from regular Active Disturbance Rejection Contoller (rADRC) consists of a time delay, an Extended State Observer (ESO) and a Disturbance Rejection Controller. Figure 6.12 is the structure of mADRC for DOC-out temperature control.
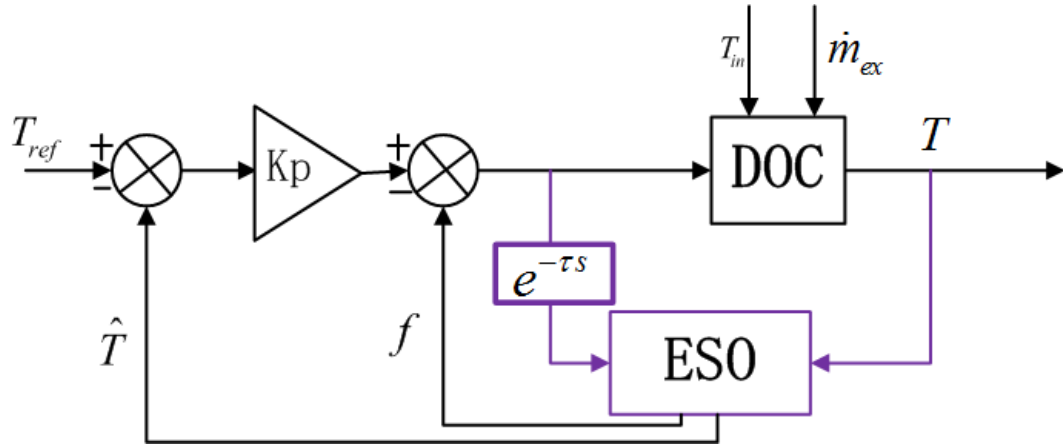
Figure 6.12: mADRC design for DOC system

Extended state observer (ESO) design

Based on the design of mADRC referenced from [13], the linear model (6.1) can be rewritten in the following state space form:

$$
\begin{cases}
\dot{x}_1(t) = x_2(t) + b_0 u(t - \tau) \\
\dot{x}_2(t) = \dot{f}(t) = h \\
y(t) = x_1(t)
\end{cases} \tag{6.8}
$$

where the state is augmented with

$$x_2(t) = f(t) = -\frac{1}{\delta}x(t) + \omega + \frac{k}{\delta}u(t - \tau) - b_0 u(t - \tau), \tag{6.9}$$

where $f(t)$ is the total disturbance including external disturbances and internal distur-bances of DOC system and rejected in the controller, assuming that $\dot{x}_2(t) = \dot{f}(t) = h$ is bounded. The ESO is designed to estimate $f(t)$ by the following equations:

$$\begin{cases} \dot{\hat{x}}_1(t) = \hat{x}_2(t) + b_0 u(t - \tau) + l_1(y(t) - \hat{y}(t)) \\ \dot{\hat{x}}_2(t) = l_2(y(t) - \hat{y}(t)) \\ \hat{y}(t) = \hat{x}_1(t) \end{cases} \tag{6.10}$$

In equation (6.10), $L = \begin{bmatrix} l_1 & l_2 \end{bmatrix}^T$ is the observer gain vector, which can be determined by the pole-placement technique. According to [18], the observer gain vector can be easily tuned after parameterization $L = \begin{bmatrix} l_1 & l_2 \end{bmatrix}^T = \begin{bmatrix} 2\omega_0 & \omega_0^2 \end{bmatrix}^T$. Therefore, the ESO has only one parameter to specify: ω_0. The ω_0 is a tuning parameter which amounts to the bandwidth of the observer.

Disturbance Rejection controller design

With the extended state observer, the augmented state $x_2(t)$ can be estimated in real-time. Based on the estimated state $\hat{x}_2(t)$, the Disturbance Rejection controller is designed to cancel the total disturbance, which transforms the model (6.1) to 1st Order Integrate Cascade form. A Proportion controller is designed to control the 1st Order Integrate Cascade form. Therefore, the Disturbance Rejection controller is

designed as expressed below,

$$U_{mADRC} = \frac{k_c(T_{ref} - \hat{x}_1(t)) - \hat{x}_2(t)}{b_0} \qquad (6.11)$$

where k_c is a tuning parameter amounting to the bandwidth of the Disturbance Rejection controller. With this control raw, the system (6.8) can be turned into the following form,

$$\dot{x}_1(t) = f(t) - \hat{x}_2(t) + k_c(T_{ref} - \hat{x}_1(t)) \qquad (6.12)$$

For a well-turned ESO, $\hat{x}_2(t)$ tracks $f(t)$ closely and turns the term $f(t) - \hat{x}_2(t)$ in equation (6.12) into a little bounded error, which makes equation (6.12) become a bounded input and bounded output (BIBO) stable by tuning the parameter k_c.

Tuning rule for mADRC

There are three different tuning parameters for the proposed controller: i.e. the controller bandwidth k_c, the observer bandwidth ω_0, and b_0. Adjusting ω_0, the trade-off can be easily made between performance and noise-sensitivity. The controller bandwidth should be high enough to meet the desire of the designed transient response. b_0 should be determined by the system. More details about mADRC tuning rule can be seen in [13, 16].

6.6 Simulation Results

To validate the proposed controller, in this section, the operating conditions and the simulation results of the composite controller are presented. The simulation result is obtained in co-simulation between GT-Power and Matlab/Simulink environment.

$\omega_0 = 0.5$ and $k_c = 0.16$ are taken for the simulation. The period of DPF regeneration is assumed to be 1000 seconds.

6.6.1   Operating Conditions

To validate the proposed controller, the light-duty vehicle model is used. Figure 6.13 shows a 1-D vehicle model built in GT-power environment with 5 different components: Driver, ECU, Engine, Vehicle and After-treatment systems. Driver Model is to track the test cycle to make the Engine and After-treatment system operate in different operating conditions. This particular Engine is based on a 3-liter turbo-charged Diesel engine. The engine model is a map-based model and the Diesel Oxidation Catalyst model is a modified version referenced from [7] and [8].
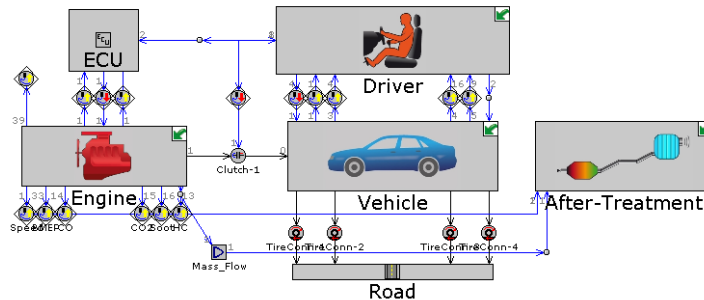
Figure 6.13: The light-duty vehicle model built in GT-POWER

6.6.2   Effectiveness of mADRC-based CC under Temperature Step Change

In this scenario, the reference temperature steps from 500 $^\circ C$ to 650 $^\circ C$. In Figure 6.14 and other figures in this paper, the legend 'with FF' means the controller is

mADRC-based CC and 'without FF' means that the controller is mADRC only. As can be seen from Figure 6.14, both mADRC-based CC and mADRC can converge to the reference temperature without overshoot. However, mADRC-based CC with FF compensation has faster tracking performance than that of mADRC only.
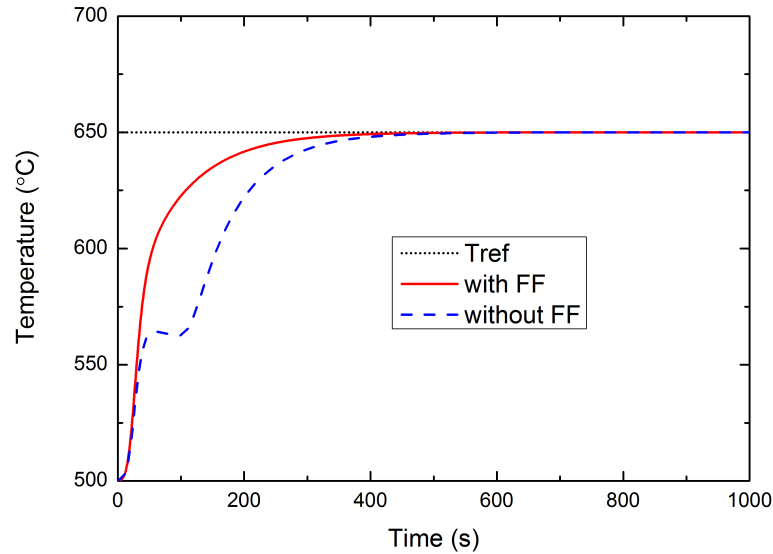
Figure 6.14: Comparison between with and without FF under temperature step change

6.6.3 Effectiveness of mADRC-based CC under Measurement Noise

To validate the robustness of the proposed mADRC-based CC against measurement noise, high frequency white noise is added to the measurement temperature. The measurement noise is uniformly distributed in the range [-10 10] based on the temperature sensor (Thermocouple) characteristics. From Figure 6.15, the proposed controller is stable and get robust tracking performance even when the temperature sensor has

measurement noise.
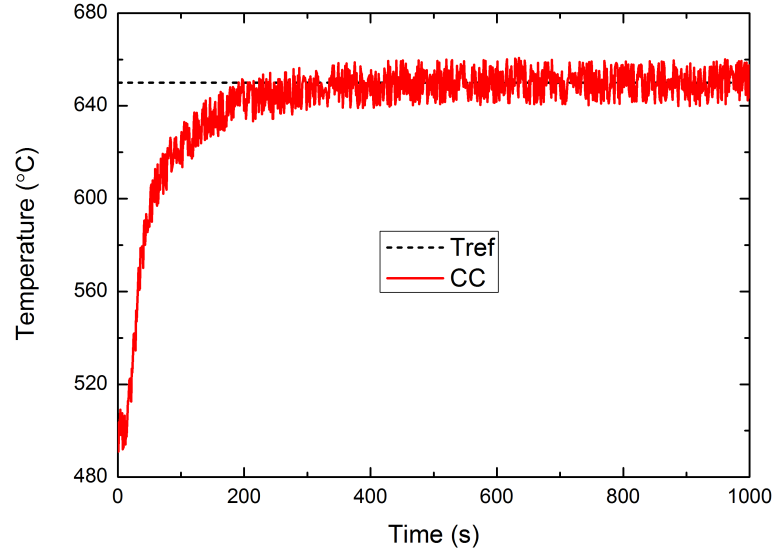
Figure 6.15: Control Performance with measurement noise

6.6.4   Effectiveness of Time Delay Compensation

In this scenario, the proposed controller is compared between with and without time delay compensation. In Figure 6.16, the legend 'with time delay compensation' means that the delay time of mADRC-based CC is compensated by the mass flow rate while 'without time delay compensation' in Figure 6.17 means that the delay time of mADRC-based CC is a constant value. Figure 6.16 is the temperature tracking under different mass flow rate from 0.04 kg/s to 0.1 kg/s by mADRC-based CC with time delay compensation, while Figure 6.17 is the result of mADRC-based CC with a constant delay time. The comparison between both figures shows that mADRC-based CC with time delay compensation obtains better performance on temperature tracking, while mADRC-based CC with constant delay time is almost unstable under mass flow rate of 0.06 kg/s and 0.08 kg/s.

188
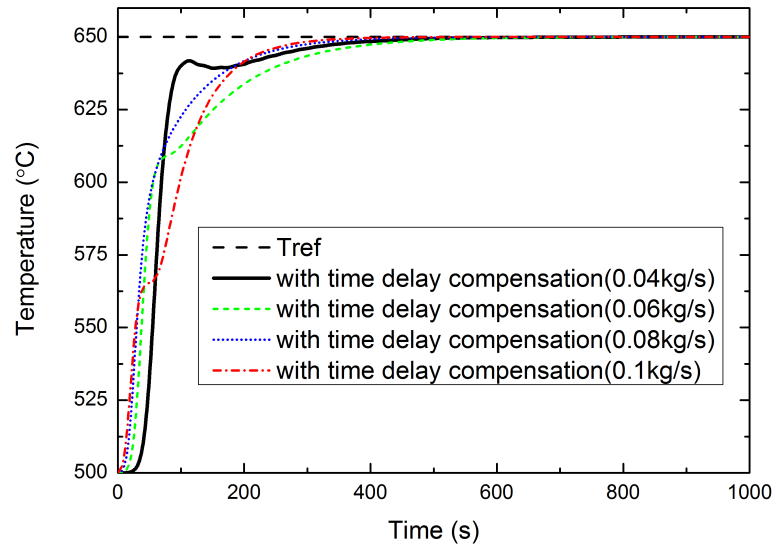
Figure 6.16: Control Performance with time delay compensation
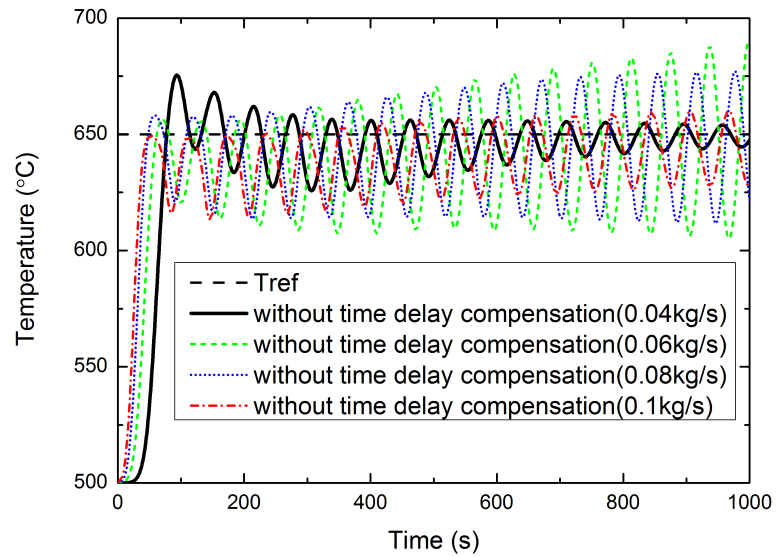
Figure 6.17: Control Performance without time delay compensation

6.6.5   Effectiveness of mADRC-based CC under Mass Flow Step Change

The proposed controller is validated under the condition that the mass flow rate of exhaust gas suddenly changes from one state to another. Figure 6.18 demonstrates the control performance between mADRC-based CC and mADRC when the mass flow rate suddenly rises from 0.04 kg/s to 0.08 kg/s at 200 second and Figure 6.19 is their control inputs. Figure 6.20 and Figure 6.21 is the control performance when the mass flow rate suddenly decreases from 0.08 kg/s to 0.04 kg/s and control inputs, respectively. Both Figure 6.18 and Figure 6.20 show that the mADRC-based CC achieves smaller variation during the step change of the mass flow rate than that of mADRC. The control inputs in both Figure 6.19 and Figure 6.21 demonstrate that mADRC-based CC has faster response to the variation of the mass flow rate than that of mADRC, resulting in lower temperature variations. The reason that the control input of mADRC has slower response to the mass flow variations is that DOC outlet temperature has undergoes when mass flow rate suddenly rises (see Figure 6.18) and overgoes when mass flow rate suddenly decreases (see Figure 6.20). The mADRC responses to the undergoes and overgoes first, resulting in larger temperature variations due to the input time delay.
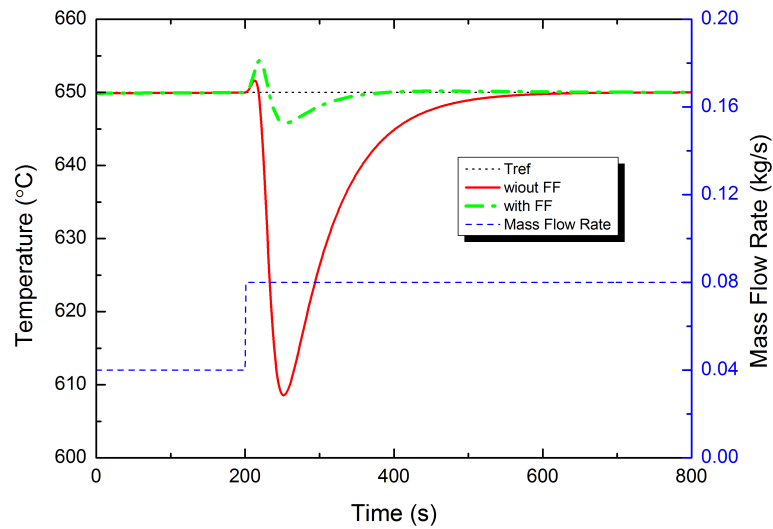
Figure 6.18: Control Performance between with and without FF under mass flow rate suddenly rises
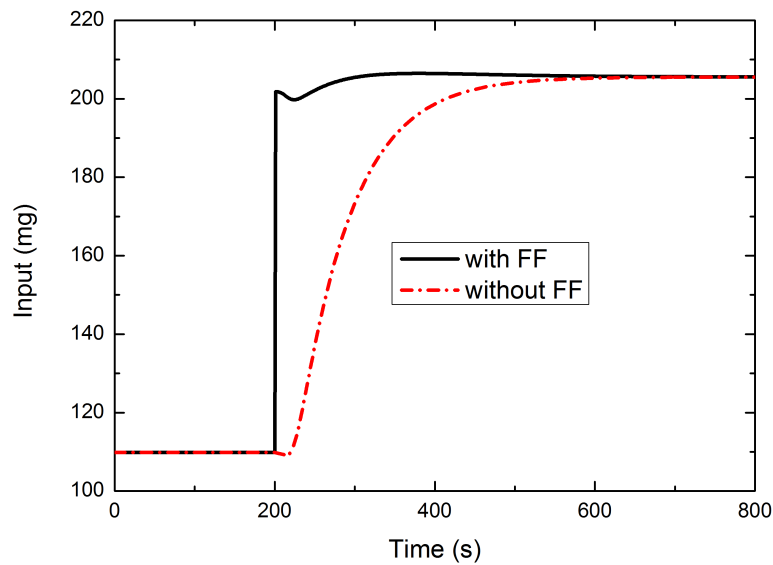
Figure 6.19: Control Input between with and without FF under mass flow rate suddenly rises
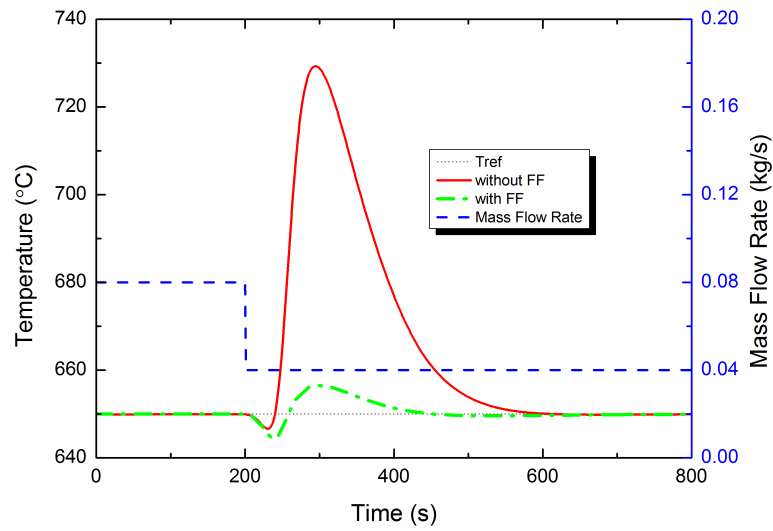
Figure 6.20: Control Performance between with and without FF under mass flow rate suddenly decreases
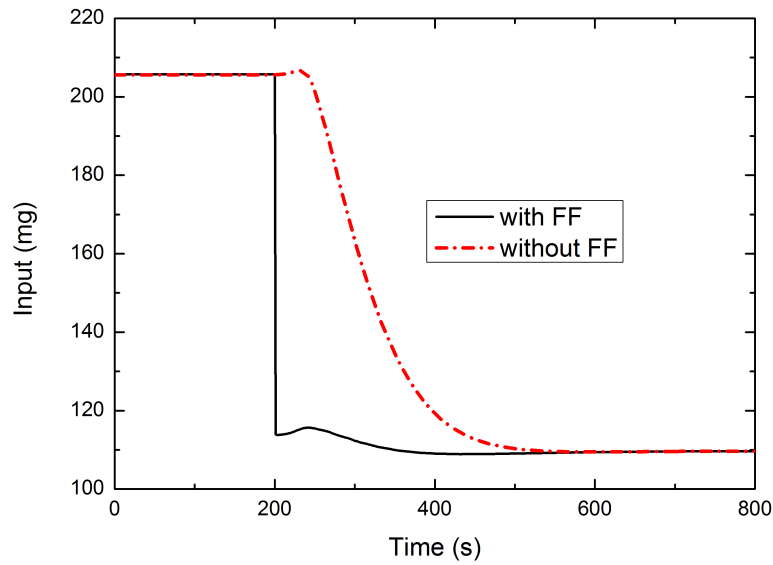
Figure 6.21: Control Input between with and without FF under mass flow rate suddenly decreases

6.6.6   Control Performance of mADRC-based CC under Drop-to-idle Condition

The scenario is to simulate a drop-to-idle condition, which is the most challenging situation for DOC-out temperature control since the mass flow rate of exhaust gas suddenly and significantly drop from 0.08 kg/s to 0.01 kg/s, as can be seen from Figure 6.22. The control performance of mADRC-based CC is compared with IMC-based CC. The control scheme of Internal Model Control (IMC)-based CC is the same as mADRC-based CC (see Figure 6.8) but the mADRC is replaced by IMC. IMC is designed by using equation (6.1). More details about IMC design can be seen in [29]. Figure 6.22 shows the effectiveness of both controllers that the undershoot and overshoot of DOC outlet temperature is within an acceptable range (i.e. $\pm20^\circ C$) under drop-to-idle condition. However, the IMC-based CC has higher overshoot than that of mADRC-based CC. Therefore, mADRC-based CC has better performance by comparing with IMC-based CC since too much overshoot is harmful to DPF.
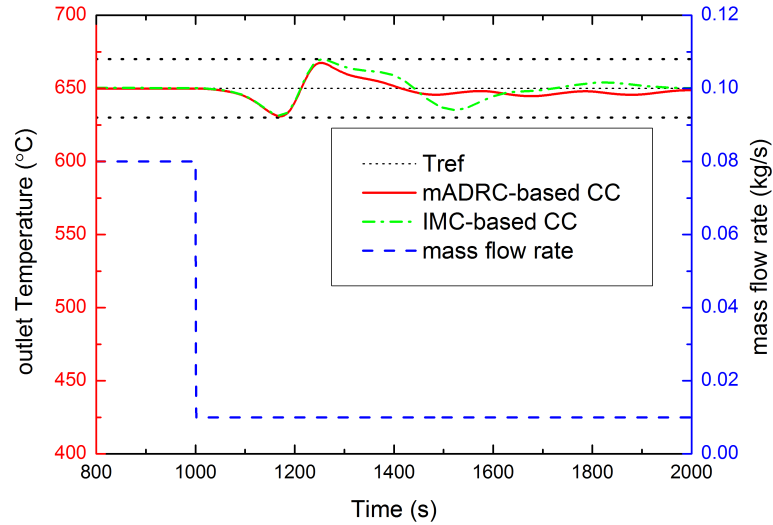
Figure 6.22: DOC-out temperature under Drop to idle state,inlet temperature is 400 $^{\circ}C$

6.6.7 Control Performance of mADRC-based CC under NEDC test cycle

In this scenario, the control performance of the proposed mADRC-based CC is validated under NEDC by comparing with IMC-based CC. Figure 6.23 demonstrates the variations of both DOC inlet temperature and mass flow rate of inlet exhaust gas under NEDC test cycle. The continuous and significant variations of both inlet temperature and mass flow rate make it difficult to control the DOC-out temperature due to the time delay, NMP behavior. Figure 6.24 shows the control performance of both controllers. The DOC-out temperature of mADRC-based CC rises from 400 $^{\circ}C$ to 650 $^{\circ}C$ with smaller overshoot and maintains at 650 $^{\circ}C$ with smaller errors (i.e. $\pm15^{\circ}C$) than that of IMC-based CC, which is the best practically achievable results [20, 21].
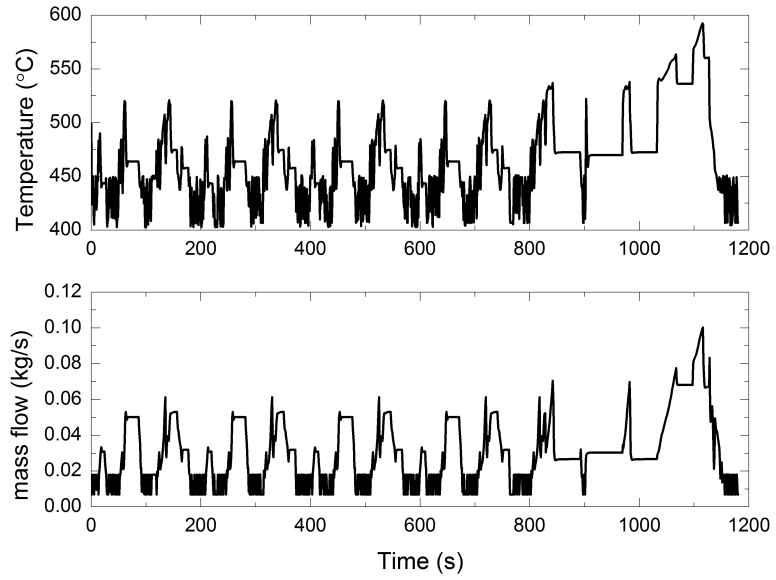
Figure 6.23: DOC inlet temperature and mass flow rate of NEDC
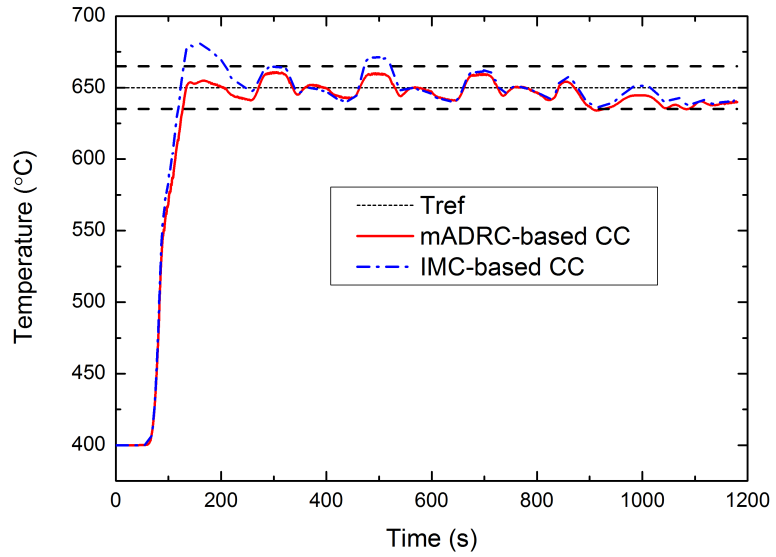
Figure 6.24: DOC-out temperature over NEDC test cycle

6.7 Conclusion

To achieve safe and effective DPF regeneration, a novel Composite Controller based on a Feedforward controller and a mADRC was proposed for DOC-out temperature control. The model-based FF was designed based on the relation between the reference temperature, inlet temperature, mass flow rate and the far post fuel injection, while the mADRC was modified from regular Active Disturbance Rejection Contoller with input time delay compensation through the mass flow rate of exhaust gas. The control performance of the proposed controller was validated under steady state and highly transient states (e.g. NEDC test cycle) through the high-fidelity GT-Power model. Simulation results demonstrate the effectiveness of the proposed controller that it achieves fast and no-overshoot tracking performance under steady states and significant robustness under the most challenging transient states (i.e. $\pm 20°C$ under drop-to-idle state and $\pm 15°C$ under NEDC test cycle).

Reference

[1] Guan B, Zhan R, Lin H, Huang Z. Review of the state-of-the-art of exhaust particulate filter technology in internal combustion engines. *Journal of Environmental Management*. 2015 May 1;154:225-58.

[2] Vouitsis E, Ntziachristos L, Samaras Z. Particulate matter mass measurements for low emitting Diesel powered vehicles: what's next?. *Progress in Energy and Combustion Science*. 2003 Dec 31;29(6):635-72.

[3] Burtscher H. Physical characterization of particulate emissions from Diesel engines: a review. *Journal of Aerosol Science*. 2005 Jul 31;36(7):896-932.

[4] Bencherif K, Benaicha F, Sadaï S, Sorine M. Diesel Particulate Filter Thermal Management Using Model-Based Design. SAE Technical Paper; 2009 Apr 20.

[5] Johnson T. Diesel engine emissions and their control. *Platinum Metals Review*. 2008 Jan 1;52(1):23-37.

[6] Kim YW, Van Nieuwstadt M, Stewart G, Pekar J. Model Predictive Control of DOC Temperature during DPF Regeneration. SAE Technical Paper; 2014 Apr 1.

[7] Sampara CS, Bissett EJ, Chmielewski M. Global kinetics for a commercial Diesel

oxidation catalyst with two exhaust hydrocarbons. *Industrial & Engineering Chemistry Research*. 2008 Jan 16;47(2):311-22.

[8] Sampara CS, Bissett EJ, Assanis D. Hydrocarbon storage modeling for Diesel oxidation catalysts. *Chemical Engineering Science*. 2008 Nov 30;63(21):5179-92.

[9] Wang TJ, Baek SW, Lee JH. Kinetic parameter estimation of a Diesel oxidation catalyst under actual vehicle operating conditions. *Industrial & Engineering Chemistry Research*. 2008 Apr 16;47(8):2528-37.

[10] Voltz SE, Morgan CR, Liederman D, Jacob SM. Kinetic study of carbon monoxide and propylene oxidation on platinum catalysts. *Industrial & Engineering Chemistry Product Research and Development*. 1973 Dec;12(4):294-301.

[11] Song X, Surenahalli H, Naber J, Parker G, Johnson JH. Experimental and Modeling Study of a Diesel Oxidation Catalyst (DOC) under Transient and CPF Active Regeneration Conditions. SAE Technical Paper; 2013 Apr 8.

[12] Chen P, Wang J. Control-oriented model for integrated Diesel engine and aftertreatment systems thermal management. *Control Engineering Practice*. 2014 Jan 31;22:81-93.

[13] Zhao S, Gao Z. Modified active disturbance rejection control for time-delay systems. *ISA transactions*. 2014 Jul 31;53(4):882-8.

[14] Gao Z, Huang Y, Han J. An alternative paradigm for control system design. In Decision and Control, 2001. *Proceedings of the 40th IEEE Conference on 2001* (Vol. 5, pp. 4578-4585). IEEE.

[15] Han J. From PID to active disturbance rejection control. *IEEE transactions on Industrial Electronics.* 2009 Mar;56(3):900-6.

[16] Gao Z. Active disturbance rejection control: a paradigm shift in feedback control system design. In American Control Conference, 2006 Jun 14; (pp. 7-pp). IEEE.

[17] Zheng Q, Chen Z, Gao Z. A practical approach to disturbance decoupling control. *Control Engineering Practice.* 2009 Sep 30;17(9):1016-25.

[18] Gao Z. Scaling and bandwidth-parameterization based controller tuning. In Proceedings of the American Control Conference 2006 (Vol. 6, pp. 4989-4996).

[19] Ning J, Yan F. Compound Control Strategy Based on Active Disturbance Rejection for Selected Catalytic Reduction systems. *Journal of Dynamic Systems, Measurement, and Control.* 2015 May 1;137(5):051008.

[20] Lepreux O, Creff Y, Petit N. Model-based temperature control of a Diesel oxidation catalyst. *Journal of Process Control.* 2012 Jan 31;22(1):41-50.

[21] Lepreux O, Creff Y, Petit N. Practical achievable performance in Diesel oxidation catalyst temperature control. *Oil & Gas Science and TechnologyRevue dIFP Energies nouvelles.* 2011 Jul 1;66(4):693-704.

[22] Middleton RH. Trade-offs in linear control system design. *Automatica.* 1991 Mar 31;27(2):281-92.

[23] Skogestad S, Postlethwaite I. Multivariable feedback control: analysis and design. New York: Wiley; 2007 Feb.

[24] Middleton RH, Freudenberg JS, McClamroch NH. Sensitivity and robustness properties in the preview control of linear non-minimum phase plants. In American Control Conference, 2001. *Proceedings of the 2001*, 2001 (Vol. 4, pp. 2957-2962). IEEE.

[25] Al-Hiddabi S, Shen J, McClamroch NH. A study of flight manoeuvres for the PVTOL aircraft model. In American Control Conference, 1999. *Proceedings of the 1999*, 1999 (Vol. 4, pp. 2727-2731). IEEE.

[26] Vipperman JS, Burdisso RA. Adaptive feedforward control of non-minimum phase structural systems. *Journal of sound and vibration*. 1995 Jun 8;183(3):369-82.

[27] Fujimoto H, Yao B. Multirate adaptive robust control for discrete-time non-minimum phase systems and application to linear motors. *IEEE/ASME Transactions on Mechatronics*. 2005 Aug;10(4):371-7.

[28] Chen D, Peng H. Nonminimum-Phase Phenomenon of PEM Fuel Cell Membrane Humidifiers. *Journal of Dynamic Systems, Measurement, and Control*. 2008 Jul 1;130(4):044501.

[29] Morari M, Zafiriou E. Robust process control. Prentice Hall, Englewood Cliffs, New Jersey, 1989.

Chapter 7

Conclusions and Future Work

In this chapter, Contributions, conclusions of the thesis and some potential research directions are demonstrated.

7.1 Contributions

The contributions of this thesis are explained in the following aspects.

1) A novel correction factor is defined to actively detect overdosing or underdosing urea injection and accurately compensate for the urea dosing control. The identification of the correction factor is explored by using either pump frequency extracted from line pressure signals or effective motor voltage.

2) The ammonia storage ratio is treated as an external disturbance and estimated by a novel, cost-effective, and robust Nonlinear Disturbance Observer (robust NDO) based on part of the three-state SCR model.

3) A novel and model-free compound control strategy consisted of an Active Disturbance Rejection Controller (ADRC), a zero-input controller and a switching

mechanism is proposed for ammonia feedback control to achieve high NO_x reduction efficiency and low ammonia slip simultaneously.

4) The DOC mean temperature is estimated by a novel and robust Smooth Variable Structure Filter (robust SVSF) based on an augmented reduced order model of a DOC.

5) A novel and robust composite controller based on modified Active Disturbance Rejection Controller (mADRC) with time delay compensation and feedforward controller is proposed for DOC-out temperature control during DPF regeneration.

7.2   Conclusions

In this thesis, several strategies based on active disturbance estimation and compensation were proposed to improve the aftertreatment performance of NO_x and PM reduction. Chapter 1 presents the historical view of emission regulations, the brief introduction of the principle and control reviews of diesel aftertreatment systems, and contributions and the outline of this study.

Accurate urea injections play important role in achieving low ammonia slip and high NO_x reduction efficiency. Therefore, in chapter 2, a correction factor was defined and identified for the detection of overdosing or under-dosing and correction for accurate urea injections. Two different methods were proposed to identify the correction factor. The first method is to identify the correction factor by comparing the pump frequency extracted from frequency analysis of line pressure by FFT method under normal injector and partially blocked injector. The second method is to identify the correction factor by comparing the effective voltage of motor under normal injector and partially blocked injector. The effectiveness of both methods are experimentally

validated.

The ammonia storage ratio is critical for achieving low ammonia slip and high NO_x reduction efficiency. Thus, in chapter 3, the ammonia storage ratio was treated as an external disturbance and estimated by a robust Nonlinear Disturbance Observer (robust NDO) and a regular Nonlinear Disturbance Observer (regular NDO). Both observers were designed based on parts of the three-state SCR model. The stabilities and noise attenuation abilities of both NDOs were discussed to guarantee the convergence of ammonia storage ratio estimation. Both NDOs can effectively estimate the ammonia storage ratio while the robust NDO has better noise attenuation performance than the regular NDO.

The SCR outlet ammonia concentration based feedback control is needed for achieving low ammonia slip and high NO_x reduction efficiency. Hence, in chapter 4, a novel compound control strategy was proposed for ammonia feedback control. The compound control strategy consists of a switching mechanism, an Active Disturbance Rejection Controller and a zero-input controller. The results under steady-state and FTP-75 test show that the compound control strategy can keep the ammonia slip under 10 ppm on average and 25 ppm at peak. The proposed compound control strategy obtains significant robustness even in the case of transient operation states and ageing conditions.

The mean temperature of DOC is critical for DOC light-off management and DPF active regeneration. For this reason, in chapter 5, two different Smooth Variable Structure Filter based methods were proposed to estimate the DOC mean temperature. To improve the robustness of regular SVSF against to large model uncertainties and disturbances, a robust SVSF was designed based on the augmented reduced order

model of a DOC while the regular SVSF was designed based on the reduced order model. Experiments based on chassis dyno were conducted for calibration and validation of the high-fidelity GT-power DOC model. The simulation results demonstrate that the proposed SVSF based methods have good performance in terms of disturbance rejection and the robust SVSF has better performance than the regular SVSF in the case where the inlet HC is inaccurate.

DOC outlet temperature is critical for safe and effective DPF active regeneration. Consequently, in chapter 6, a novel composite controller composed of a feedforward controller and a modified Active Disturbance Rejection Control (mADRC) with time delay compensation was proposed for DOC-out temperature control. The model-based Feedforward controller was designed based on the reference temperature, inlet temperature, mass flow rate and the far post injection. The mADRC was modified from regular ADRC with a time delay compensation through the mass flow rate of exhaust gas. The effectiveness of the proposed control strategy was validated by the experimentally calibrated GT-power model.

7.3   Future Work

Based on the studies conducted in this thesis, several potential directions can be further investigated for future work as follow,

7.3.1 Ageing Detection and Compensation for Aftertreatment Systems

The ageing phenomena of Diesel aftertreatment systems may reduce the conversion efficiency and affect the light-off management. The ageing of DOC may have a light off temperature drift and affect the light off management and NO/NO_2 conversion. Also, the NO/NO_2 ratio affects the DPF regeneration and SCR NO_x reduction efficiency. In addition, the ageing of SCR system may reduce the ammonia storage capacity and NO_x reduction efficiency. Therefore, ageing level should be detected and compensated for estimations and controls of aftertreatment systems to meet increasingly stringent regulation and in-use compliance.

7.3.2 Optimization of Integrated Diesel Engine and Aftertreatment Systems

Engine-based technologies (e.g. EGR,VGT, Multiple fuel injections) and after-treatment systems (e.g. DOC, DPF and SCR/LNT) are adopted to regulate both engine-out emissions and exhaust pipe-out emissions. These technologies consume more fuel to achieve low emission. Especially in cold-start and warm-up phase, extra fuel is required to heat up the engine and after-treatment systems. However, the control of engine-based technologies and after-treatment systems are separated and optimization research on integrated Diesel engine and after-treatment systems is rarely proposed due to their complexities. To effectively address these issues, optimization of integrated Diesel engine and aftertreatment systems is a potential direction to boost the fuel efficiency and keep the emissions (e.g. CO, HC, NOx, PM) low.

205

Appendix A

Proof of Lemma 2

Let $V = \eta^T P \eta$ be a Lyapunov function where P satisfies the equation $A^T P + PA = -Q$ and Q is a positive definite matrix. Then the deviation of the Lyapunov function is expressed in the following equations,

$$\dot{V} = -\eta^T Q \eta + 2h_D P \eta$$
$$= (-\eta^T Q + 2h_D P)\eta$$

Furthermore, it implies that $\dot{V} < 0$ if

$$\|\eta\| > \left\| \frac{2h_D P}{Q} \right\|$$

which means that $\|\eta\|$ decrease for any $\|\eta\|$ is greater than $\left\| \frac{2h_D P}{Q} \right\|$. Hence the observer error of the robust NDO is bounded. In other words, the robust NDO is Bounded Input Bounded Output (BIBO) stable.